EFFECT OF CO-DOPING ON THE MULTIFERROIC PROPERTIES OF $BiFeO_3$

BY
Takian Fakhrul
STUDENT NUMBER 0412112014
April 23, 2014

THIS THESIS PAPER IS SUBMITTED TO THE DEPARTMENT OF MATERIALS AND METALLURGICAL ENGINEERING IN PARTIAL FULFILLMENT OF THE REQUIREMENTS FOR THE DEGREE OF MASTER OF SCIENCE IN MATERIALS AND METALLURGICAL ENGINEERING

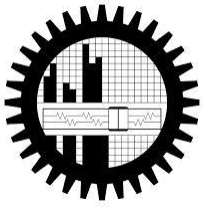

DEPARTMENT OF MATERIALS AND METALLURGICAL ENGINEERING
BANGLADESH UNIVERSITY OF ENGINEERING AND TECHNOLOGY

CANDIDATES' DECLARATION

IT IS HEREBY DECLARED THAT THIS THESIS PAPER OR ANY PART OF IT HAS NOT BEEN SUBMITTED ANYWHERE ELSE FOR THE AWARD OF ANY DEGREE

.....

Takian Fakhrul
M.Sc. Engg., MME, BUET

DEDICATION

To the people who made me believe in my dreams,

Ammu & Abbu.

ACKNOWLEDGEMENTS

I would like to start by thanking the Almighty for blessing me with the means, courage and guidance for performing this research study, despite all odds.

First of all, I express my profound gratitude to Prof. Dr. Ahmed Sharif, my supervisor and revered mentor, for his constant direction and inspiration in pursuing the whole investigation of this research project and for correcting my mistakes whenever necessary. I thank him from the bottom of my heart for his sincere cooperation, precious advice and consistent encouragement and motivation. Had he not been there, the research could not have been completed.

I specially thank the Department of Glass and Ceramic Engineering (GCE) and all of its members who have worked day and night to make my research project successful. Without the facilities, equipment and raw materials provided by GCE my research project would have remained a dream. I particularly thank Rubayyat Mahbub, Lecturer, GCE, for his constant assistance with the FESEM and impedance analyzer.

I am eternally grateful to my father for his constructive criticism, advice and his yearning to make me achieve perfection that has helped me deeply and allowed me to meticulously correct my mistakes during working on this research project.

I convey my heartiest regards to Prof. Dr. A.K.M Akhter Hossain, Department of Physics, BUET, for his help, co-operation and valuable advice during this research project that has helped me immensely. I am extremely grateful to him for sharing his wisdom and for generously letting me use his lab on such short notice.

I also express my sincere gratitude to Dr. Abdul Hakim for sharing his vast pool of knowledge and for his invaluable technical advice which helped me greatly while working on this research project.

I am grateful to Dr. Gafur, Senior Scientific Officer, BCSIR and Mr. Rakib, Engineer, BCSIR for their support with the XRD and DTA.

I would also like to pay my utmost gratitude to the Department of Materials and Metallurgical and all of its teachers for their support and motivation throughout this research project, specially Head of the Department Prof. Dr. Md. Mohar Ali for his constant encouragement.

I am forever in debt to my sister for making me a better, more God conscious and humble person than I have been in the past. I cannot put into words how grateful I am to have her in my life.

Last but not the least, I express my undying love and gratitude for my mother, the person who is behind all my successes in life, no matter how small or big, and who has been my mental and moral support through thick and thin, my pillar of strength and undoubtedly is the greatest blessing of the Almighty. Words fall short to express how much indebted I am to her for everything she has unconditionally given me and for all her sacrifices. I end by thanking the Almighty once again for giving me the best mother one could possibly ask for.

ABSTRACT

The role of codoping with La in Bi-site and Ta in Fe-site on the multiferroic properties of $BiFeO_3$ ceramic has been investigated in this research. Single phase $Bi_{0.8}La_{0.2}Fe_{1-x}Ta_xO_3$ (BLFTO) ceramics with x = 0.0, 0.01, 0.03 and 0.05 were synthesized by the conventional solid-state reaction method. The BLFTO dried pellets were calcined at 800^oC for 2 hours and then sintered at temperatures in the range of 850-1000^oC for holding times of 1 and 2 hours. Phase analysis by X–ray diffraction (XRD) indicated formation of single phase distorted R3c structure. Percentage theoretical density as high as 98% was achieved for $Bi_{0.8}La_{0.2}FeO_3$ ceramics although this was associated with excessive grain growth. Microstructural investigation using the field emission scanning electron microscope (FESEM) showed that addition of Ta dramatically reduced the average grain size of $Bi_{0.8}La_{0.2}FeO_3$ due to its strong pinning effect from 10.6 μm in $Bi_{0.8}La_{0.2}FeO_3$ to 0.92μm in $Bi_{0.8}La_{0.2}Fe_{0.95}Ta_{0.05}O_3$ at a sintering temperature of 1000^oC for a holding time of 2 hours. A combination of good theoretical density, average grain size and optimum multiferroic properties were obtained at a sintering temperature of 1000^oC for 2 hours. La and Ta codoped BFO showed superior values of dielectric constant and magnetic permeability. The best values of dielectric constant (> 2000) at room temperature were attained for the Ta doped ceramics at average grain sizes in the range of 0.92-0.98 μm. At higher temperature a considerable increase in the dielectric constant of $Bi_{0.8}La_{0.2}FeO_3$ samples occurred due to space charge polarization. However, in Ta-substituted ceramics the stability of dielectric constant with temperature considerably improved. DTA analysis revealed that the peak for ferroelectric transition (T_C) shifted towards higher temperatures for the Ta-substituted ceramics and reached 870^oC for x=0.05. The real part of initial permeability, μ_i', was found to decrease with increasing Ta substitution due to decrease in grain size. Moreover it was observed that μ_i' increased with sintering temperature. For samples sintered at 1000^oC for 2 hours, μ_i' of $Bi_{0.8}La_{0.2}Fe_{0.97}Ta_{0.03}O_3$ and $Bi_{0.8}La_{0.2}Fe_{0.95}Ta_{0.05}O_3$ ceramics remained almost constant with increase in frequency up to 15MHz. However, for $Bi_{0.8}La_{0.2}FeO_3$ and $Bi_{0.8}La_{0.2}Fe_{.99}Ta_{.01}O_3$, μ_i' remained constant up to the resonance frequency, fr, i.e. 10 MHz and 14MHz respectively after which there was a sharp decrease in μ_i' and increase in the imaginary part of permeability, μ_i'', due to domain wall relaxation.

Table of Contents

List of Figures

List of Tables

CHAPTER 1
INTRODUCTION

1.1 Scope for Bismuth Ferrite

Multiferroics are multifunctional materials that exhibit more than one ferroic order in the same phase. In recent years, multiferroics have been drawing the attention of researchers due to their unique behaviour of coupling between two or more properties of ferroelectricity, ferromagnetism and ferroelasticity and also because of their potential technological applications in devices in spintronics, information storage, sensing and actuation [1-3]. However, ferroelectricity and ferromagnetism tend to be mutually exclusive and attaining both orders in a single compound is a rare phenomenon because the requirement of transition metal ions with partially filled d electrons for magnetism is not compatible with the requirement of empty d orbitals for ferroelectricity [4, 5]. Consequently, although there are many magnetic and ferroelectric materials, there are relatively few multiferroic materials. $BiFeO_3$ (BFO) is perhaps the only material that is both magnetic and a strong ferroelectric at room temperature. As a result, it has had an impact on the field of multiferroics that is comparable to that of yttrium barium copper oxide (YBCO) on superconductors, with hundreds of publications devoted to it in the past few years.

Bismuth ferrite is one of the most promising multiferroics and at room temperature, bulk $BiFeO_3$ presents a rhombohedrally distorted perovskite structure belonging to the space group R3c. The primitive unit cell contains two formula units (10 atoms) as shown in figure 1.1. Compared to other multiferroics, BFO exhibits a higher ferroelectric Curie temperature (T_C ~830^oC) and a high G-type antiferromagnetic ordering (T_N ~370^oC) temperature [6-7]. The Fe magnetic moments are coupled ferromagnetically within the pseudocubic (111) planes and antiferromagnetically between the near planes; this is called the *G*-type antiferromagnetic order. If the magnetic moments are oriented perpendicular to the [111] direction, the symmetry also permits a canting of the antiferromagnetic sublattices resulting in a macroscopic magnetization called weak magnetism. The R3c symmetry permits the development of a spontaneous polarization along [111], and Bi, Fe, and O are displaced relative to one another along this 3-fold axis. The largest relative displacements are those of Bi relative to O, consistent with a stereochemically active Bi lone pair. The polar displacements (relative to cubic perovskite) are noticeably extreme when compared with those in non-lone-pair-active perovskite ferroelectrics such as $BaTiO_3$ or $KNbO_3$, but are consistent with those observed in other Bi-based perovskites.

Thus BFO is one of the most popular objects in modern material science and an excellent candidate for use in ferroelectric non-volatile memories and high performance electronics.

But unfortunately, BFO has some inherent problems. In BFO, magnetic ordering is of antiferromagnetic type, having a spatially modulated spin structure with an incommensurate long-wavelength period of 62 nm which cancels the macroscopic magnetization and also inhibits the observation of the linear magnetoelectric effect [8–11]. In addition, the bulk BFO is characterized by serious current leakage problems due to the existence of a large number of charge centres caused by oxygen ion vacancies and Bi_2O_3 evaporation during sintering process which makes it difficult to achieve high resistivity. These problems limit the use of BFO for fabrication of multifunctional devices. The mechanism inducing resistivity in BFO films can be attributed to the variable oxidation states of Fe ions (Fe^{3+} to Fe^{2+}), which requires oxygen vacancies (Vo^{2+}) for charge compensation and produces electron hopping in films. Another mechanism is due to high volatility of atom Bi which generates V_{Bi}^{3-} vacancies in lattice accompanied by the emergence of the second-phase (such as $Bi_2Fe_4O_9$). The Vo^{2+} and V_{Bi}^{3-} vacancies are highly mobile and inclined to reduce resistivity on the application of electric field. Therefore of late, there has been considerable interest in the design of magnetoelectric materials and finding ways to improve the magnetic and ferroelectric properties of BFO.

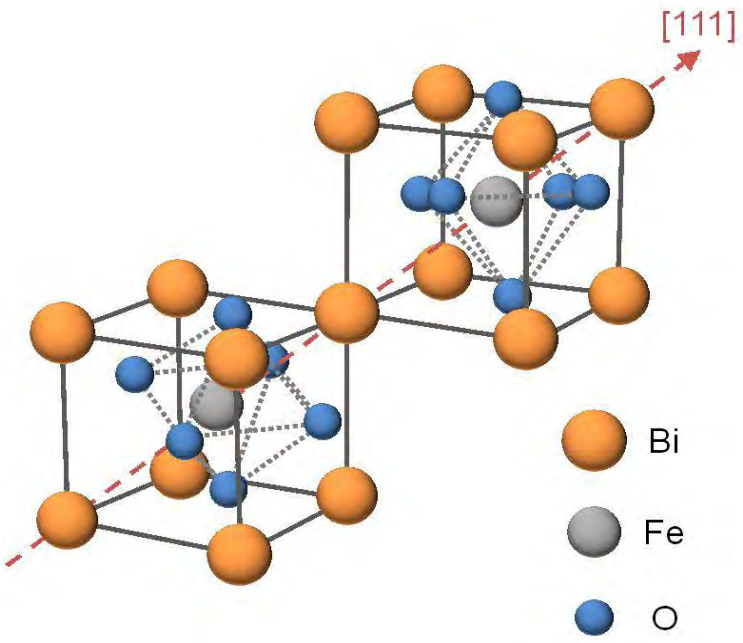

Figure 1.1: Schematic view of the R3c structure built up from two cubic perovskite $BiFeO_3$ unit cells. The cations are displaced along the [111] direction relative to the anions, and the oxygen octahedral rotate with alternating sense around the [111] axis. In the ideal cubic perovskite structure the oxygen ions would occupy the face-centered sites.

1.2 Need for modification of BFO

In order to overcome the problems associated with BFO, many attempts have been made recently, which include:

(i) Doping rare earth lanthanide ions (La^{3+}, Nd^{3+}or Sm^{3+}) or divalent ions (Ca^{2+}, Sr^{2+}, Ba^{2+}, Pb^{2+}) at the A site of BFO for substituting part of Bi^{3+} or with ions of Nb^{5+}, Mn^{4+}, Cr^{3+}, Ti^{4+} at the B site for substituting part of Fe^{3+}; [12-15] .

(ii) Fabricating a solid solution of BFO with other ABO_3 perovskite materials, such as $BaTiO_3$.

(iii) Synthesizing $BiFeO_3$ nano particles with grain size below 62 nm to achieve ferromagnetism by destroying spiral spin structure [16].

(iv) Depositing ultra-thin $BiFeO_3$ single layer or multilayer films to enhance ferroelectric property; [17, 18].

(v) Fabricating high quality single crystal of $BiFeO_3$ to solve non-stoichiometric problems [19].

Among these approaches, it has been proved that La substitution is an efficient way to improve the ferroelectric as well as ferromagnetic properties of BFO. Addition of La reduces significantly the volatilization of bismuth oxide and hence improves oxygen ion stability in the lattice [20, 21]. On the other hand, B-site (Fe-site) doping with high valence ions, such as Nb^{5+}, $Ti^{4+}$and Ta^{5+} can increase the resistivity of BFO, decrease leakage current significantly but also induce a remanent magnetization in BFO [22, 23] and allow the ferroelectricity to be determined at room temperature. Therefore, it is interesting to study the effect of co-substitution of La and Ta on BFO in order to have the combined advantages of the two.

1.3 Recent work on BFO

The current interest in bismuth ferrite was stimulated primarily by a 2003 paper from Ramesh's group,[24] which showed that it had unexpectedly large remnant polarization, P_r, 15 times larger than previously seen in bulk, together with very large ferromagnetism of ca. 1.0 Bohr magneton (μ_B) per unit cell. Single crystals grown more recently in France in 2006–7 have confirmed the large value of the polarization first observed in the films, showing also that it is intrinsic;[25-29] At any rate, the 2003 Science paper has proved enormously stimulating, and has inspired both new fundamental physics and exciting device applications.

In 2005 Xiaoding et al. [30] investigated the transport properties of aliovalent-ion-doped $BiFeO_3$ thin films in order to identify the cause of high leakage currents. Doping of 2 at. % Ti^{4+} ions increased the dc resistivity by more than three orders of magnitude. In contrast, doping of 2+ ions such as Ni^{2+} reduced the dc resistivity by two orders of magnitude. Current–voltage (I–V) characteristics indicated that the main conduction mechanism for pure and Ni^{2+} doped BFO was space charge limited, which was associated with the free-carriers trapped by the oxygen vacancies, whereas in the Ti^{4+} doped BFO, field-assisted ionic conduction was dominant.

In 2006 Wang et.al. [31] reported the effect of Ba doping on magnetic, ferroelectric, and magnetoelectric properties on $BiFeO_3$ at room temperature Ba doped $BiFeO_3$ compounds were prepared by a solid-state reaction. X-ray diffraction showed that $Bi_{1-x}Ba_xFeO_3$ was single phase up to x=0.25. These samples exhibited magnetism and ferroelectricity simultaneously at room temperature. The magnetoelectric coupling was evidenced by the increase of the dielectric constant with the increase of the applied magnetic field.

In 2007 Yuan-Hua et al. [32] studied the enhancement of ferromagnetic properties in $BiFeO_3$ polycrystalline ceramic by La doping. The authors present the structure transformation and magnetic properties of $Bi_{1-x}La_xFeO_3$(x=0.0–0.15) ceramics prepared by a conventional solid-state reaction processing. Magnetic measurements reveal that remnant magnetization of 15% La-doped $BiFeO_3$ has enhanced about 20 times as compared to pure $BiFeO_3$. It is the structural phase transition (R3c–C222) near x=0.15 that destructs the spin cycloid, and thus enhances the ferromagnetic properties significantly. In these $Bi_{1-x}La_xFeO_3$ ceramic samples, besides the known antiferromagnetic Néel temperature $T_{N1} \sim 615$ K, another Néel temperature $T_{N2} \sim 260$ K can be observed due to the trace impurity phase of $Bi_2Fe_4O_9$ in these ceramic samples.

In 2010 Cui et al. [33] reported the dielectric, magnetic, and magnetoelectric properties of La and Ti codoped $BiFeO_3$ (LBFTO). Codoping changes the structure of $BiFeO_3$ from rhombohedral to tetragonal and the ferromagnetic properties of LBFTO are remarkably improved. More interestingly, the dielectric constant of LBFTO shows a linear increase with magnetic field and the slope decreases linearly with increasing temperature. The electric polarization of LBFTO also increases upon applying a magnetic field. The ME coupling coefficients of different orders were obtained by analyzing these data. The results were discussed by considering the doping induced destruction of the cycloidal structure in LBFTO.

In 2010, Changyong et al. [34] reported the magnetic properties of La and (La, Zr) doped $BiFeO_3$ ceramics $Bi_{0.9}La_{0.1}FeO_3$ (BLF) and $B_{i0.9}La_{0.1}Fe_{0.98}Zr_{0.02}$ O_3 (BLFZ) ceramics were synthesized by conventional solid state reaction method. X-ray diffraction studies and Rietveld refinements indicated that both of the samples possessed rhombohedrally distorted perovskite structure. The average grain size of BLFZ (~700 μm) was greatly reduced in comparison with BLF (~6 μm).

The remanent magnetization of BLFZ was greatly enhanced compared with BLF. The enhancement of remanent magnetization was attributed to the collapse of the spiral spin structure. Both samples showed exchange bias. The possible reason for the appearance of exchange bias was attributed to the inhomogeneity in doping. The measurements of magnetization as a function of temperature indicated that BLF and BLFZ had almost the same magnetic transition temperature

In 2012 Reetu et al. [35] reported the structural transformation and improved dielectric and magnetic properties in $Bi_{0.8}La_{0.2}Fe_{1-x}Ti_xO_3$ (x = 0.0, 0.05, 0.1, 0.15) Powder x-ray diffraction investigations performed at room temperature show that the crystal structure was rhombohedral for x = 0.0, 0.05; tetragonal for x = 0.15; and a phase boundary occured at x = 0.1. In the Rietveld refinement good agreement between the observed and calculated pattern was observed. Dielectric response of these samples show a decrease in the values of real (ε′) and imaginary (ε′′) parts of dielectric constant with Ti substitution indicating reduced conductivity and hence enhanced resistivity in doped samples. Stability of dielectric constant and conductivity with temperature considerably improved with Ti substitution. Magnetic properties of $Bi_{0.8}La_{0.2}FeO_3$ ceramics are considerably improved on Ti substitution along with a significant opening in the room temperature M–H hysteresis loop.

In 2013, Anup et al. [36] reported the role of codoping (20% La in Bi-site and 10% Mn in Fe-site) on mutiferroic properties in insulating $BiFeO_3$ ceramic. The X-ray diffraction (XRD) with Rietveld refinement shows that the structure of $Bi_{0.8}La_{0.2}FeO_3$ is orthorhombic (Pnma). Furthermore,it shows that on substitution of 10% Mn- ions in Fe-site, no structural change occurs which has been supported by micro-Ramans tudy. DTA study shows that ferroelectric transition temperature (T_C) decreases very fast with La-doping and slowly with the Mn-doping. Measurement on magnetization vs. applied magnetic field (M–H) shows increase of magnetization due to codoping of La and Mn in $BiFeO_3$.

In 2013 Jin et al. [37] reported the effect of Mn doping on crystal structure, electric, magnetic and optical properties of $BiFeO_3$ thin films prepared via the sol-gel process on indium tin oxide/glass substrates X-ray diffraction analysis indicated that Mn-doped $BiFeO_3$ thin films

presented single tetragonal structure with P4mm symmetry. Compared with the pure $BiFeO_3$ film, the resistivity was found to increase while leakage current density and optical band gap decreased in low Mn content (≤ 7.5%) doped $BiFeO_3$ system. An evident magnetic hysteresis loop was observed for all the thin films at room temperature and Mn-doped $BiFeO_3$ films showed a larger saturated magnetization than pure $BiFeO_3$ film

From the work of previous researchers it is evident that A-site and B-site co-doping is a good way to improve the multiferroic properties of BFO, both in films and ceramics [38–40]. Till date, no investigations on La^{3+} and Ta^{5+} co-doped bulk materials were reported. Hence, in this work, I present the effect of co-doping with $La^{3+}$and Ta^{5+} on the multiferroic properties of BFO.

1.4 Targets and challenges of this thesis

The main objective of the research will be to reduce electrical leakage in BFO caused by oxygen vacancies by adding dopants La^{3+} and Ta^{5+} and thus to study the effect of this reduction on the magnetic and ferroelectric properties of BFO. Moreover, the research will focus on determining the optimum sintering condition of doped BFO samples that will increase both the ferromagnetic and ferroelectric properties of pure BFO at room temperature**.**

Recently, co-substitutions of Bi^{3+} ions by La^{3+} and Fe^{3+} ions partially by high valence like Ta^{5+} simultaneously has been proved to be effective for increasing the resistivity and, hence, improving the overall properties of BFO. The substitution of Bi^{3+} by La^{3+} is favorable for stabilizing the perovskite phase due to the similar radii values of Bi^{3+} (1.030) and La^{3+} (1.032), and La doping at the Bi site enhances the ferromagnetic property of BFO. On the other hand, partial substitution of Fe^{3+} by higher valence Ta^{5+} ions can decrease the charge defects and increase the electrical resistivity of BFO. So, it is interesting to investigate the effect of co-doping of La and Ta in order to combine the advantages of La doping and Ta doping. So far, there have been no reports on the codoping of La and Ta in BFO in the world. Moreover, no work based on BFO has been conducted previously in this department. On this point of view, this work imposes an entirely a new challenge. In addition the limitation of technical facilities further confines the scope of working. However the work, if carried out successfully, has the potential to

yield materials with superior ferroelectric and ferromagnetic properties, thereby offering the potential to revolutionize the application of electromagnetic materials. From this aspect the research is definitely exciting and commendable of being followed.

As the preparation of the compacts is simple, the biggest challenge is to achieve very fine grain structure with minimum porosity. On this occasion the toughest task is to find the optimum sintering temperature which will bring the desired microstructure. Control of the geometry of samples is another challenge to take over. Since this is attributed entirely on the rate of heating and cooling during sintering, the heating/cooling rate needs to be optimized as well.

One important thing here is the use of powder which has a size in nanometer range. Such powders possess very high surface energy and consequentially, are more reactive than coarser powders. Hence the sintering temperature needs to be modified accordingly.

CHAPTER 2
LITERATURE REVIEW

2.1 Primary ferroics

A primary ferroic material exhibits a spontaneous magnetization, a spontaneous polarization or a spontaneous stain. And these spontaneous orders can be reoriented by an external magnetic field, electric field, or mechanical stress below a characteristic temperature (Curie temperature).

There are four primary ferroic order parameters. They are described below.

- **Ferroelectricity:** It is the property due to which materials show spontaneous, stable polarization that can be switched hysteretically by an applied electric field; antiferroelectric materials have ordered dipole moments which cancel each other completely within each crystallographic unit cell resulting net polarization zero [41]. E.g. $BaTiO_3$.

- **Ferromagnetism:** It is the property due to which materials exhibit spontaneous, stable magnetization that can be switched hysteretically by an applied magnetic field; antiferromagnetic materials possess ordered magnetic moments which nullify each other completely within each magnetic unit cell resulting net magnetization zero [41]. E.g Fe_3O_4.

- **Ferroelasticity:** Materials display a spontaneous, stable deformation which if we apply a stress can be switched hysteretically [41]. E.g $Au_xCu_{1-x}Zn$.

- **Ferrotoroidicity:** Materials possess a stable and spontaneous order parameter that is taken to be the curl of a magnetization or polarization. By analogy with the above examples, it is anticipated that this order parameter may be switchable. Ferrotoroidic materials have evaded unambiguous observation.

Ferro- is a prefix which means iron in Latin, it is primitively used to describe materials exhibiting strong magnetic properties as iron does. Apart from iron, other elements like cobalt, nickel and rare earth elements also exhibit magnetic behavior called ferromagnetism, which enables materials made from the above-mentioned elements to form permanent magnets. Ferromagnetic materials were reported to have a long-range ordering phenomenon at the atomic

level. Many small domains can be found in a magnetic material with plenty of unpaired electrons inside. Microscopically, those unpaired electrons are not randomly alligned, they interact with others to make the alignment in the same direction within the same domain. However, these domains are randomly aligned so that on the whole, they cancel out to make zero magnetism.When an external magnetic field is applied, those domains with the magnetic field grow at the expense of their neighbouring domains, causing materials to be magnetized. This phenomenon is characterized by a hysteresis loop of magnetization M as a function of external magnetic field H, as illustrated in Figure 2.1 (a). It is obvious that the magnetization is saturated at high magnetic field and a remnant magnetization can still exist in the absence of the field. In addition, the direction of magnetization could be reversed provided that the external magnetic field is switched oppositely with quite strong field intensity.

However, the ferromagnetic material can lose its ferromagnetic properties under thermal agitation, the temperature that characterizes this phenomenon is known as the "Curie temperature (Tc)", above which spontaneous ferromagnetism becomes paramagnetism which owns a small, positive susceptibility to magnetic fields and can't keep this magnetic properties after removal of the external field. When such a material is cooled down and crosses the Curie temperature, it undergoes a phase transition from a non-ferroic to ferroic state. These transitions are generally accompanied with a lowering of the crystal symmetry. For example bulk $BaTiO_3$ an archetypal ferroelectric presents a transition from a cubic paraelectric structure to a tetragonal ferroelectric structure around 120°C.

Ferroelectricity and ferroelasticity are analogous to ferromagnetism. Polarization and strain are induced by externally applied electric field and mechanical stress respectively. They both show hysteresis loops with spontaneous electric polarization and strain, as depicted in Figure 2.1 (b) and (c**).** Figure 2.2 shows how ferroelectrics and ferromagnetics permit the orientations of electrical polarization and magnetization to be reversed by applying an electric field and magnetic field, respectively.

Actually, the discovery of ferroelectricity can date back to the early 20^{th} century when ferromagnetism had already been discovered. Since the appearance of hysteresis loops from

ferroelectricity and ferromagnetism look quite similar, the prefix ferro- was continuously carried forward to describe ferroelectricity, though many ferroelectric materials have nothing to do with iron either.

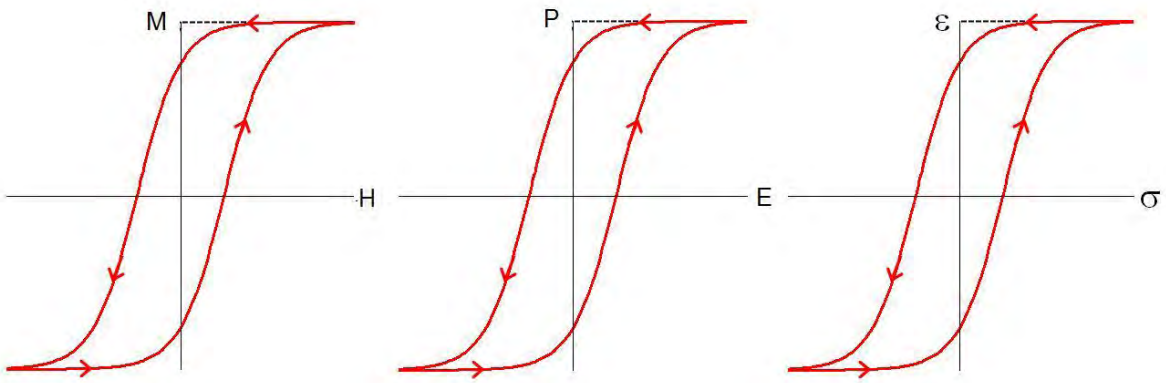

Figure 2.1: Hysteresis loops of (a) ferromagnetic, (b) ferroelectric and (c) ferroelastic materials.

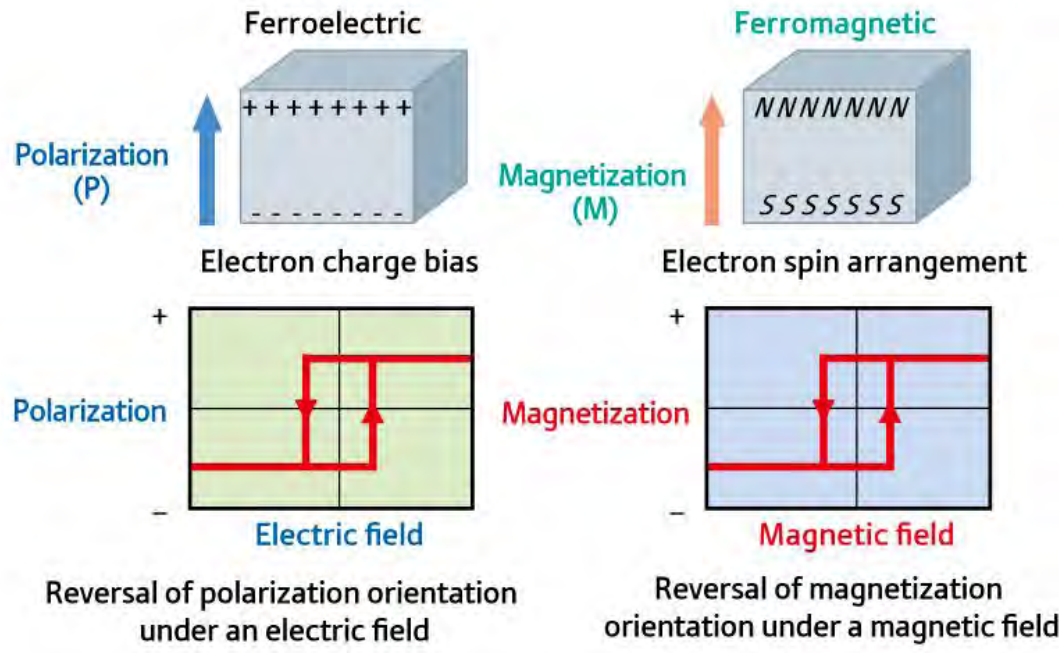

Figure 2.2: Schematic representation of ferroelectric and ferromagnetic characteristics. Ferroelectrics and ferromagnetics permit the orientations of electrical polarization and magnetization to be reversed by applying an electric field and magnetic field, respectively.

The strong interaction between electrical and magnetic dipoles results in small regions within thematerial in which the ferroic property is uniform, with the dipoles arranged parallel to each other.Such regions are known as domains and are separated by domain walls, whereby the dipoles undergo a coherent rotation from the direction in one domain to that in the adjacent domain. Due to the random orientation of the magnetic and electrical dipoles of different domains in the absence of an external stimulus, the total net polarization and magnetization is zero for ferroic materials. Ferroic properties depend on external conditions such as: magnetic field, electric field, pressure and temperature. The existence of domain structures is also responsible for the hysteretic response of the ferroic properties of the material when an external stress is applied. As a result, ferroic materials have the unique ability to store and release energy in the form of magnetic and electrical energy, an attribute which made them very attractive to different technologies1. Based on the above information, characteristics of ferroic materials are presented schematically in Figure 2.3 (a-c). In the following discussion, concepts of the ferroelectrics and ferro (ferri) magnetic materials will be discussed in detail.

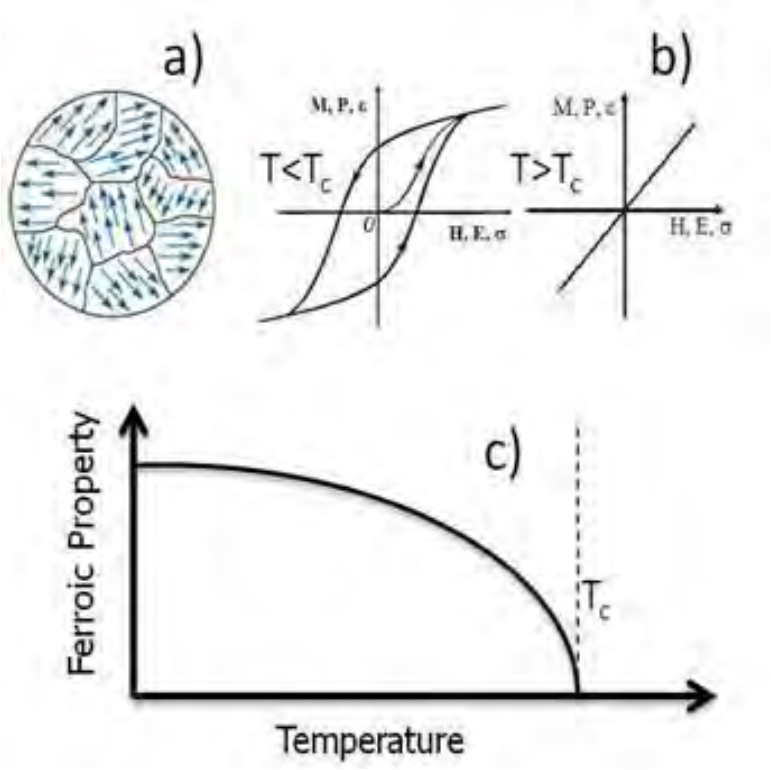

Figure 2.3: Characteristics of ferroic materials a) Ordering of physical properties, b) Hysteretic behavior and c) Existence of ferroic properties below a threshold temperature.

2.1.1 Ferroelectric materials

Ferroelectricity (FE) was first discovered in Rochelle salt in 1921. At that time, it was called Seignette-electricity, honoring its discoverer. For the past few decades, ferroelectric materials have received a great amount of interests because of their various uses in many applications such as nonvolatile ferroelectric random access memories (NVFRAM), dynamic random access memories, sensors and microactuators [42].

A crystal is said to be ferroelectric when it possesses at least two equilibrium orientations of the spontaneous polarization vector in the absence of an external electric field, and the spontaneous polarization can be switched between those orientations by an electric field. The polar character of the orientation states should represent an absolutely stable configuration in a null field [43].

Among the thirty-two crystal classes, eleven of them are characterized by the existence of a center of symmetry. The remaining twenty-one crystal classes do not have a center of symmetry. Thus, it is possible for the 21 groups to (i) have one or more polar axes, and (ii) possess odd-rank tensor properties. The only exception is the group 432, which lacks a center of symmetry, but has other symmetry operations that destroy polarity. All non-centrosymmetric point groups exhibit piezoelectric effect that is defined by a change in electric polarity under applied stress, and vice versa. Out of the twenty piezoelectric classes, ten possess a unique polar axis, the spontaneous polarization of which depends on temperature. This is called the pyroelectric effect. Ferroelectric crystals belong to the pyroelectric family, which in addition has a spontaneous polarization can be reversed by external electric field, i.e. more than one equivalent direction for Ps [44].

Among all ferroelectric materials, the most extensively studied and widely used are the perovskite. A perfect perovskite structure has a general formula of ABO_3, where A represents a divalent or trivalent cation, and B is typically a tetravalent or trivalent cation. The origin of ferroelectricity in this family of materials can be explained using the well-known example of barium titanate ($BaTiO_3$). As shown in Figure 1.2, the Ba^{2+} cations are located at the corners of the unit cell. A dipole moment occurs due to relative displacements of the Ti^{4+} and O^{2-} ions from their symmetrical positions.

A (proper) ferroelectric possesses a spontaneous polarisation of the electric dipole which can be switched by the application of an electric field. This polarisation is due to a lack of inversion symmetry within the crystal structure. For example, consider the most extensively studied and widely used classic perovskite of the form ABO_3, in which a central positive B-ion (a transition metal element) is surrounded by an octahedron of negatively charged oxygen ions (Figure 2.4). A shift in the position of the B-site ion would break the inversion symmetry and cause the induction of a dipole moment, giving rise to ferroelectric order. Such shifts can occur during structural phase transitions, in which the system moves from a high to low symmetry state (e.g. cubic to tetragonal). One of the best known examples of a proper ferroelectric is $BaTiO_3$. As shown in Figure 2.4, the Ba^{2+} cations are located at the corners of the unit cell. A dipole moment occurs due to relative displacements of the Ti^{4+} and O^{2-} ions from their symmetrical positions.

In the majority of ferroelectric perovskites, the B-site atom has an empty d electron shell, which allows covalent bonding with the full p orbitals of the the oxygen atoms. Ferroelectricity can also occur due to the existence of lone pairs of electrons on the outer shell of the A-site atom, which are highly susceptible to polarisation. This is the cause of ferroelectricity in $BiFeO_3$.

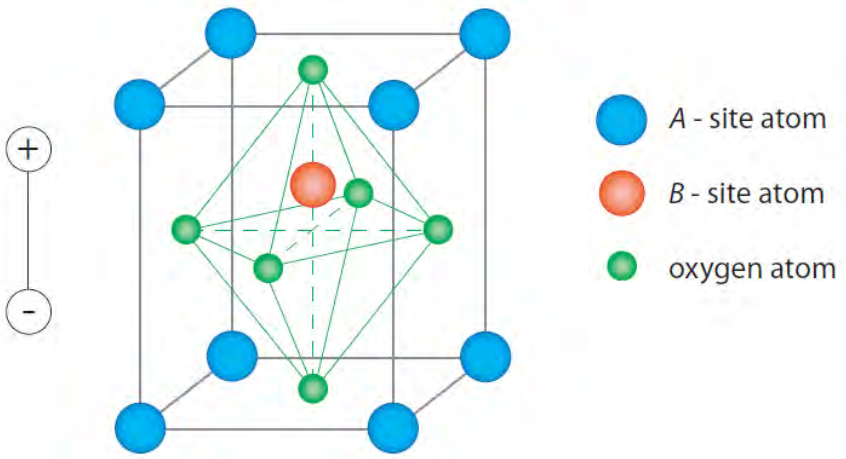

Figure 2.4: Perovskite crystal structure, showing a dipole moment generated by a displaced B-site atom.

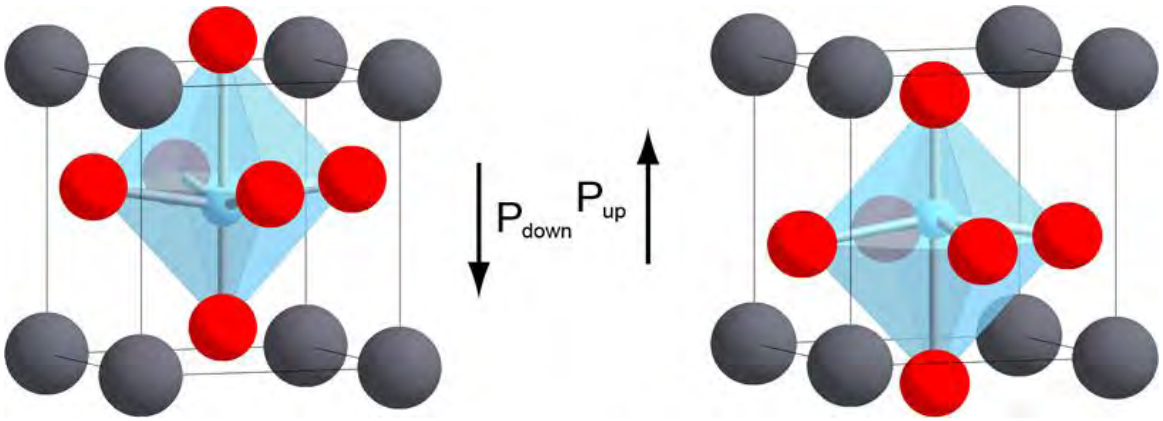

Figure 2.5: Elementary cell of $PbTiO_3$ in the ‗up' and ‗down' spontaneous polarization states.

In an improper ferroelectric, the spontaneous polarisation is not due to a polar displacement of the ions, but occurs as a result of some other effect within the material. In a geometric ferroelectric, the dipole moment occurs due to non-polar lattice distortions, due to e.g. electrostatic forces rather than changes in chemical bonding. An example of this is in $YMnO_3$, where a ferroelectric state is due to a buckling of the rigid MnO_5 bipyramids. In charge ordered ferroelectrics, the spontaneous polarisation is dependent on electron correlations in the material. Such charge ordered ferroelectricity is observed in $LuFe_2O_4$. Improper ferroelectricity can also occur due to magnetic order.

2.1.2 Ferro-, antiferro-, and ferri-magnetic materials

The phenomenon of magnetism has been known to mankind for many thousands of years. Lodestone (Fe_3O_4) was the first permanent magnetic material to be identified and studied. The magnetic moment of an atom/ion has three principal sources: (1) the spin of electrons; (2) electron orbital angular momentum about the nucleus; and (3) a change in the orbital moment induced by an applied magnetic field. The first two effects give paramagnetic contributions to the magnetization, and the third gives a diamagnetic contribution [45].

In a crystal, the overall magnetic property depends on two factors: (i) the magnetic response associated with each atom/ion, and (ii) the interactions between these magnetic moments. In the case that there are no unpaired electrons around each atom/ion, there will be no net magnetic

moments associated with them (bearing in mind that both orbital moments and electron spins cancel to zero in a fully filled orbital), the material will show diamagnetic behavior. When there are unpaired electrons, every atom/ion has a net magnetic moment. Depending on the interactions between the magnetic dipoles, the material may show (i) paramagnetism (PM); (ii) ferromagnetism (FM); (iii) antiferromagnetism (AFM) and (iv) ferrimagnetism (FIM). In a paramagnetic material, alignment of adjacent moments is not observed due to thermal fluctuation. Ferromagnetism consists of parallel aligned adjacent moments. Antiferromagnetic order consists of antiparallel aligned equal moments. And, ferrimagnetic order consists of antiparallel unequal moments, resulting in a non-zero net magnetization.

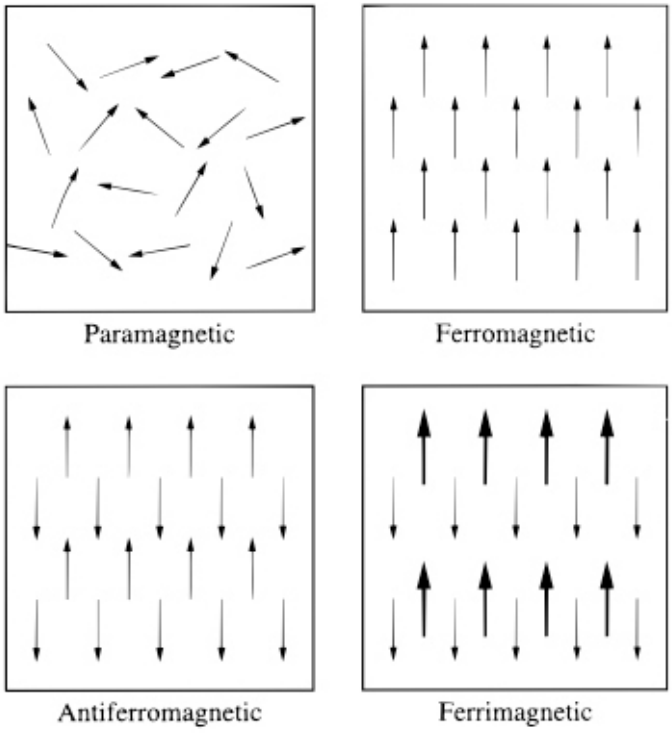

Figure 2.6: Common examples of magnetic dipole ordering, from [9].

Ferromagnetism is a very strong magnetic response compared with paramagnetic and diamagnetic behaviors. It is characterized by a transition temperature (Neel temperature, T_N). Above this temperature, the material is paramagnetic. Below this temperature, it is ferromagnetic. The magnetic susceptibility, $\chi = M/H$, which defines the degree of magnetization of a material in response to a magnetic field, is a good indication of their magnetic properties. If χ is positive the material is paramagnetic, and the magnetic field is strengthened by the presence of the material. If χ is negative then the material is diamagnetic and the magnetic field is weakened in the presence of the material. The magnetic susceptibility of a ferromagnetic substance is not linear.

2.1.3 Ferroelastic material

Ferroelastic materials develop a spontaneous strain below a phase transition temperature. From the symmetry point of view, the material undergo a structural phase transition from a high symmetry phase to a low symmetry phase, which is characterized by a _broken symmetry' of the high symmetry phase [46].

The phase transition mechanism results in a spontaneous strain. The spontaneous strain can be quite large. For example, the spontaneous strain of a typical ferroelastic material is >2%. The correlated changes in the enthalpy of the crystal related to this formation of spontaneous strain often reach some 6 KJ/mole, an energy which would reactive equivalent changes in thermochemical phase diagrams of some hundreds of degrees in temperature. In order to release the energy created by the phase transition, a twin domain structure is often created within a ferroelastic crystal, where the dominant twin planes are oriented approximately perpendicular to each other.

A wall between two adjacent domains can be envisaged as an internal surface of the crystal. The orientation of an individual twin wall is then determined by the condition that the crystal in the low-symmetry phase tends to maintain the total symmetry of the high-symmetry phase as an average. The domains are related equivalent to each other via the symmetry element lost at the phase transition that give rise to the long-range ordered state. It is commonly accepted that stress induced domain wall motion in ferroelastic materials yield hysteretic macroscopic behavior. Mueller et al. [47] showed that nonlinear effects in ferroelastic crystals are related to the

properties of ferroelastic domain walls pinned on defects, which became de-pined above a critical stress level. Additionally, Jian and Wayman [48] observed domain wall motion in single-crystal and polycrystalline $LaNbO_4$ ferroelastics under stress, and argued that the nonlinear elastic behavior is a direct result of domain wall motion, rather than the intrinsic properties of the crystal. In addition, Newnham [49] concluded that stress-induced movement of domain walls is the principle source of hysteresis in ferroelastics. A complete analysis of twin structure and domain wall can be seen in reference [47].

Figure 2.7 illustrates the stress-induced twin movement of a ferroelasteic $Pb_3(Pb_4)_2$ crystal [47].

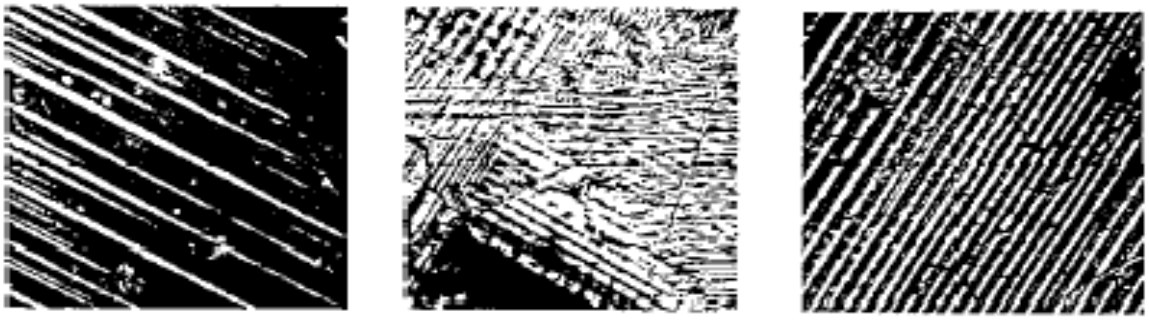

Figure 2.7: Experimentally observed microstructures of lead phosphate. The two fully „switched" crystals (a) and (c) display striped twin patterns whereas the crystal in the intermediate state (b) shows superposition of various twin orientations**.**

2.2 Order parameter couplings

There are four order parameters. The order parameter couplings are given below:

- **Piezoelectricity:** describes a change in strain as a linear function of applied electric field, or a change in polarization as a linear function of applied stress.

- **Piezomagnetism:** describes a change in strain as a linear function of applied magnetic field, or a change in magnetization as a linear function of applied stress.

- **Magnetoelectricity:** describes the influence of a magnetic (electric) field on the polarization (magnetization) of a material.

- **Electrostriction:** describes a change in strain as a quadratic function of applied electric field.

The effects of cross-coupling between ferroic orders is, represented in figure 2.8 Changes in strain as a function of an electric or magnetic field are shown by the black arrows, and the magnetoelectric coupling between the ferroelectric and ferromagnetic orders is shown by the green arrows.

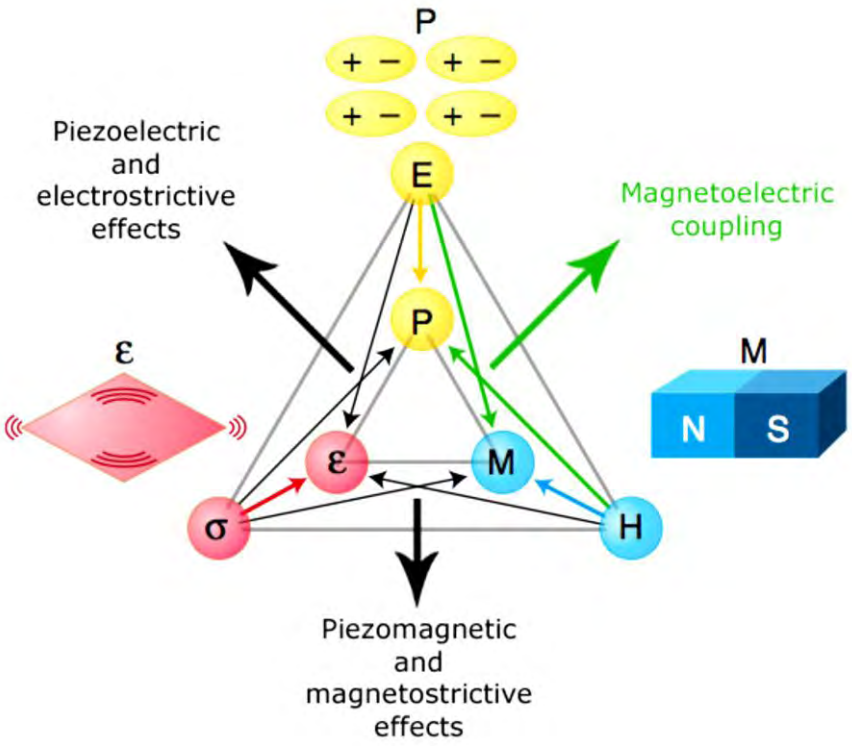

Figure 2.8: Ferroic orders and possible couplings between them.

2.3 Multiferroics

Multiferroic materials are single-component materials or composites exhibiting two or more ferroic properties such as ferromagnetism, ferroelectricity, or ferroelasticity, as shown in figure 2.9. In a broader definition, it also covers materials with ferro- and antiferro- orders. There are significant scientific and technological interests in these materials due to their unusual responses, including very large magneto-electric susceptibility, giant magnetostriction, and energy coupling coefficients [50, 51]. In addition, the ability to couple between the spontaneous order parameters offers extra degrees of freedom in the design of conventional devices. Examples of single component multiferroics are $BiFeO_3$ (a ferromagnetic/ferroelectric perovskite), and Fe-Ga (a ferromagnetic/ferroelastic alloy).

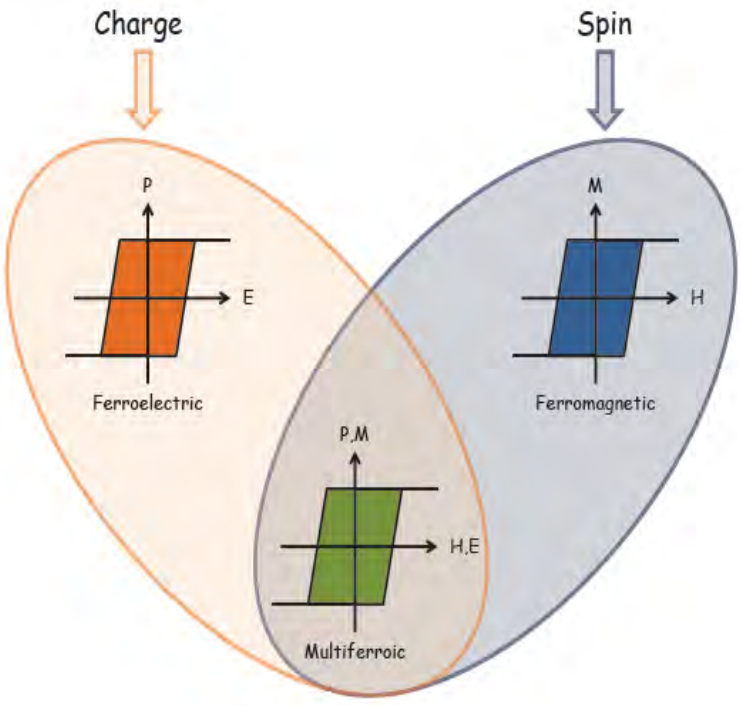

Figure 2.9: Multiferroics materials are those that present more than one ferroic order. Multiferroics combining ferroelectric (left-orange) and ferromagnetic (right- blue) properties are very appealing materials because the possible presence of magnetoelectric coupling (magnetic control of polarization or electric control of magnetization, bottom-green) can give rise to new technological functionalities.

The ability to combine magnetic and ferroelectic properties within one material and the potential functionality that can be achieved has resulted in much of the early work on multiferroics being concentrated within magnetic ferroelectrics [52]. Combining these two properties has, however, proven to be difficult. Normally, these two order parameters are mutually exclusive; yet a number of materials have simultaneously presented magnetic and ferroelectric properties. Coupling of the parameters within the multiferroic system tends to be weak. The microscopic mechanisms of magnetism and ferroelectricity are very different from each other therefore do not strongly interfere [4].

2.3.1 Classification of multiferroics

The microscopic origin of magnetism is basically the same in all magnets: it is the presence of localized electrons, mostly in the partially filled d or f shells of transition-metal or rare-earth ions, which have a corresponding localized spin, or magnetic moment. Exchange interactions between the localized moments lead to magnetic order. The situation with ferroelectrics is quite different. There are several different microscopic sources of ferroelectricity, and accordingly one can have different types of multiferroics.

Broadly, multiferroics can be classified as single-phase or composite multiferroics. Generally speaking, there are two groups of multiferroics. Single-phase multiferroics are those materials that show both ferroelectric and ferromagnetic order [53-58].Thus multiferroicity is intrinsic of the material. The scarcity of single phase multiferroic materials makes composite materials an interesting alternative. In opposition to single-phase multiferroics, multiferroic order is not intrinsic but results from the combination of two materials that are ferroelectric and ferromagnetic, separately. Therefore, the availability of ferromagnetic and ferroelectric materials at room temperature makes easy to obtain multiferroic composite materials at room temperature.

Single-phase multiferroics can be further classified into two groups. The first group, called type-I multiferroics, contains those materials in which ferroelectricity and magnetism have different sources and appear largely independently of one another, though there is some coupling between them. In these materials, ferroelectricity typically appears at higher temperatures than

magnetism, and the spontaneous polarization P is often rather large (of order 10 -100 μC/cm²). Examples are $BiFeO_3$ (T_{FE} ~ 1100K, T_N = 643 K, P ~90μC/cm²) and $YMnO_3$ (T_{FE} ~914K, T_N= 76 K, P ~ 6μC/cm²). The second group, which we can call type-II multiferroics, is the relatively recently discovered materials [59, 60], in which magnetism causes ferroelectricity, implying a strong coupling between the two. However, the polarization in these materials is usually much smaller (10^{-2}μC/cm^2). Many groups are also investigating composite multiferroics that consist of known magnets and ferroelectrics in the form of multilayers and self-organized nanostructures [53].

2.3.1.1 Type-I multiferroics

Type-I multiferroics are ―older" and more numerous. These are often good ferroelectrics, and the critical temperatures of the magnetic and ferroelectric transitions can be well above room temperature. Unfortunately, the coupling between magnetism and ferroelectricity in these materials is usually rather weak. The materials challenge for this group of multiferroics is to keep all their positive features, but enhance this coupling. As we will see later, the opposite problem exists for type-II multiferroics. One can single out several different subclasses of type-I multiferroics, depending on the mechanism of ferroelectricity in them. We will focus on four of the major subclasses, but there are certainly others.

Ferroelectricity due to lone pairs

In $BiFeO_3$, and probably in $BiMnO_3$ and $PbVO_3$, Bi^{3+} and Pb^{2+} play the major role in the origin of ferroelectricity. In these ions, there are two outer 6s electrons that do not participate in chemical bonds. They are called lone pairs, or sometimes dangling bonds. They have a high polarizability—the condition required for ferroelectricity in the classical description. These electrons generate an electric dipole, which is the origin of ferroelectric order. Other cations (i.e. Fe^{3+}, Mn^{3+}, Ni^{2+}) are responsible for magnetic properties. More microscopically one can explain the origin of ferroelectricity in these compounds by ordering of these lone pairs (with certain admixture of p orbitals) in one direction (Figure 2.10). Apparently this is what happens in many Bi- and Pb-containing ferroelectrics and multiferroics such as $BiFeO_3$, but it also helps to

improve the ferroelectric properties of $Pb[Zr_xTi_{(1-x)}]O_3$.

Ferroelectricity due to charge ordering

One more mechanism that can lead to ferroelectricity and to type-I multiferroicity can be charge ordering, often observed in transition metal compounds, especially those formally containing transition metal ions with different valence. If, after charge ordering, both sites and bonds turn out to be inequivalent, this can lead to ferroelectricity [Figure 2.10].A corresponding mechanism can work in systems like $Pr1/2Ca1/22MnO_3$ or in nickelates $RNiO_3$ with charge ordering. But more often we meet the situation in which there exist ions with different charge (often because they are different elements), but on top of that there occurs dimerization.

$TbMn_2O_5$ belongs to this class, as does the newly discovered multiferroic Ca_3CoMnO_6. Another similar possibility is when the bonds are in equivalent because of the structure of the material, the site-centered charge order appearing on top of that. This is the case in an organic ferroelectric $(TMTTF)_2X$, and also in the multiferroic $LuFe_2O_4$

Multiferroic perovskites

Probably the best-known ferroelectrics are the perovskites like $BaTiO_3$ or $Pb(ZrTi)O_3$ (PZT). There are many magnetic materials among perovskites [61], and also many ferroelectrics [62]. But comparing these extensive compilations, each containing more than 100 pages of tables, demonstrates that there seems to be mutual exclusion of magnetism and ferroelectricity in perovskites: there is practically no overlap of these tables. Why? Whereas for magnetism one needs partially filled d shells of a transition metal, practically all ferroelectric perovskites contain transition metal ions with an empty d shell, such as Ti^{4+}, Ta^{5+}, W^{6+}. Ferroelectricity in these systems is caused by the off-center shifts of the transition metal ion, which forms strong covalent bonds with one (or three) oxygens, using their empty d states. And somehow, the presence of real d electrons in d^n configurations of magnetic transition metals suppresses this process, preventing ferroelectricity in magnetic Perovskites. This so called" d^0 vs. d^n problem" was one of the first to be studied theoretically at the beginning of the recent revival of multiferroics [5,63],

and although there has been some progress, largely from ab initio calculations, still in my opinion there is no full solution of this problem[59]. The answer may well lie in the fact that this mutual exclusion is not a ―theorem," but rather a matter of numbers: in most cases a magnetic dn ion is stable in the center of its O_6 octahedra, but there may still be the cases where it is not. One possible way around this problem may be making" mixed" perovskites with d^0 and d^n ions, refer (Figure 2.10). Unfortunately the coupling of magnetic and ferroelectric subsystems in mixed perovskites is rather weak.

"Geometric" ferroelectricity

Lastly, we consider a case realized in, for example, $YMnO_3$ [64]. Ferroelectricity in $YMnO_3$ has nothing to do with the magnetic Mn^{3+}, but is caused by the tilting of the practically rigid MnO_5 block. This tilting occurs just to provide closer packing, and as a result the oxygen ions move closer to the rather small Y ions (Figure 2.10).

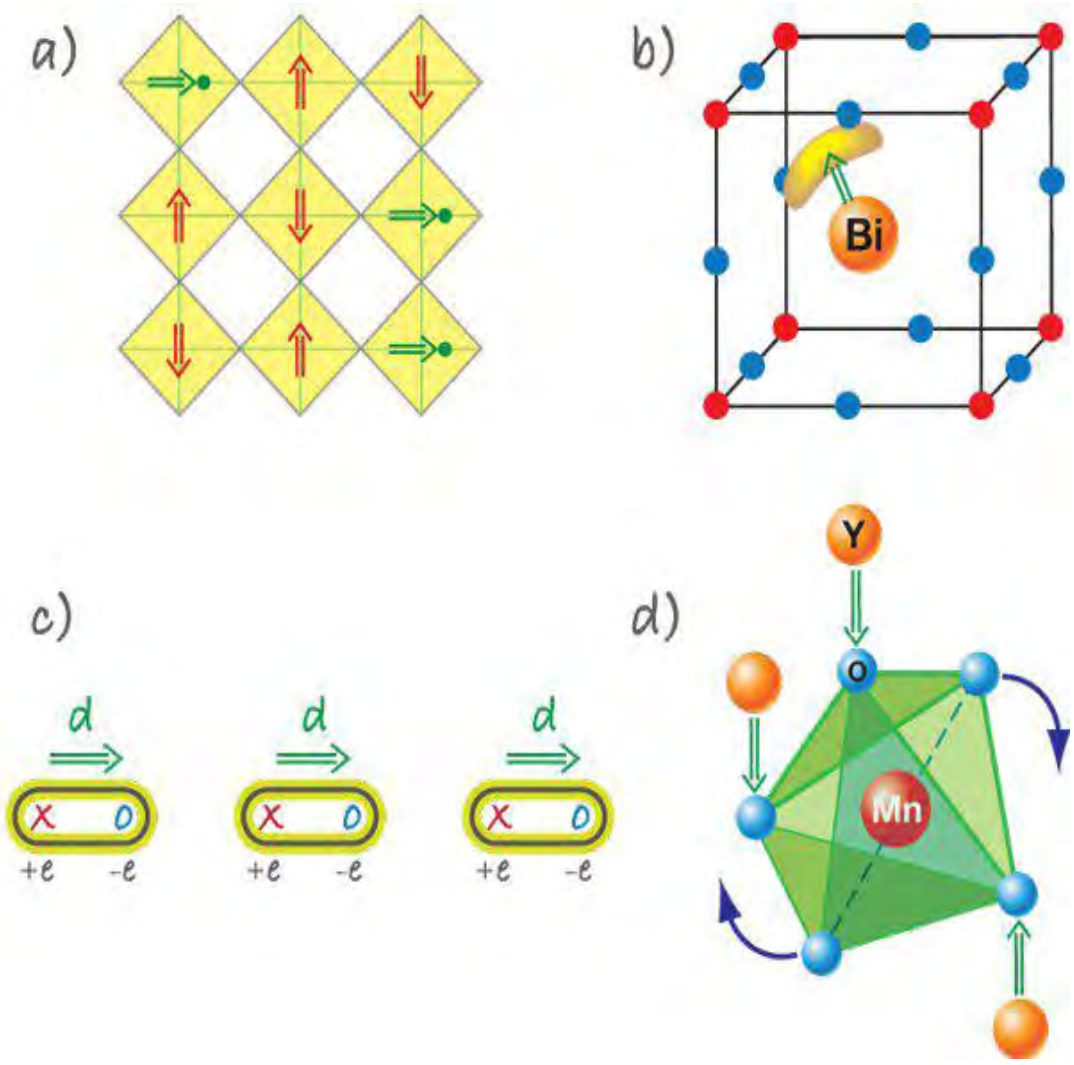

Figure 2.10: Different microscopic mechanisms found in type-I multiferroics. (a) In ―mixed" perovskites with ferroelectrically active d0 ions (green circles) and magnetic d^6 ions (red), shifts of d0 ions from the centers of O_6 octahedra (yellow plaquettes) lead to polarization (green arrows), coexisting with magnetic order (red arrows). (b) In materials like $BiFeO_3$ and $PbVO_3$, the ordering of lone pairs (yellow "lobes") of Bi^{3+} and Pb^{2+} ions (orange), contributes to the polarization (green arrow). (c) In charge ordered systems, the coexistence of inequivalent sites with different charges, and inequivalent (long and short) bonds, leads to ferroelectricity. (d) The ―geometric" mechanism of generation of polarization in $YMnO_3$ describes the tilting of a rigid MnO_5 block with a magnetic Mn remaining at the center. Because of the tilting, the Y-O bonds form dipoles (green arrows), and there appears two"up" dipoles per one ―down" dipole so that the system becomes ferroelectric (and multiferroic when Mn spins order at lower temperatures).

2.3.1.2 Type-II multiferroics: Magnetic multiferroics

The biggest excitement nowadays is caused by the discovery of a novel class of multiferroics in which ferroelectricity exists only in a magnetically ordered state and is caused by a particular type of magnetism. For example, in $TbMnO_3$ magnetic ordering appears at T_{N1} = 41 K, and at a lower temperature, T_{N2} = 28 K, the magnetic structure changes. It is only in the low temperature phase that a nonzero electric polarization appears. Similar behavior occurs in $TbMn_2O_5$. The first paper to study $TbMnO_3$ showed that a magnetic field can strongly influence the electric polarization: e.g., in $TbMnO_3$ the polarization rotates (or "flops") by 90 degrees when a critical magnetic field is applied along a certain direction [65]. In $TbMn_2O_5$[66] the influence of an external field is even stronger: the polarization changes sign with field, and a field alternating between +1.5 and -1.5 Tesla leads to corresponding oscillations in the polarization. Since the discovery of these materials, a number of other type-II multiferroics with strong magnetoelectric coupling have been discovered and studied. From the point of view of the mechanism of multiferroic behavior, one can divide type-II multiferroics into two groups: those in which ferroelectricity is caused by a particular type of magnetic spiral and those in which ferroelectricity appears even for collinear magnetic structures.

Spiral magnets

Spiral magnets are those where atomic spin rotate across the lattice in a defined plane, this breaks the symmetry and allows ferroelectricity. However, ferroelectricity only takes place in spiral magnets when the so-called cycloidal spin arrangement set, that is spins rotate in the plane of the propagation of the spiral. In this case, ferroelectricity arises in the plane of the cycloid and perpendicular to the propagation vector of the cycloid due to the so-called inverse Dzyaloshinsky-Moriya interaction ($P = A \sum rij \times (S_i \times S_j)$, being r_{ij} the vector connecting the S_i and S_j spins). Here, sizable spin-orbit interaction is needed (A), if A is large the magnetoelectric coupling is strong. The cycloid is sensible to the application of a magnetic field, which can produce rotation of cycloid plane by 90 (so-called flopping), inducing a change in the direction of o the ferroelectric polarization. $TbMnO_3$ is the archetype of this class of 3 multiferroic materials [67].

Collinear magnets

In these materials one-dimensional chains of up-up- down-down spins are formed due to the exchange striction. The distortion induced by up-up (down-down) or up-down (down-up) bonds is different, which provokes the formation of ordered electric dipoles. An example is Ca_3CoMnO_6 [68], or E-type rare earth manganites [69], f.i. $HoMnO_3$ [70].

2.3.2 Why is it difficult to find materials that are both ferroelectric and magnetic?

Most ferroelectrics are transition metal oxides, in which transition ions have empty *d* shells. These positively charged ions like to form _molœcules' with one (or several) of the neighbouring negative oxygen ions. This collective shift of cations and anions inside a periodic crystal induces bulk electric polarization. The mechanism of the covalent bonding (electronic pairing) in such molecules is the virtual hopping of electrons from the filled oxygen shell to the empty *d* shell of a transition metal ion. Magnetism, on the contrary, requires transition metal ions with partially filled *d* shells, as the spins of electrons occupying completely filled shells add to zero and do not participate in magnetic ordering. The exchange interaction between uncompensated spins of different ions, giving rise to long range magnetic ordering, also results from the virtual hopping of electrons between the ions. In this respect the two mechanisms are not so dissimilar, but the difference in filling of the *d* shells required for ferroelectricity and magnetism makes these two ordered states mutually exclusive.

Still, some compounds, such as $BiMnO_3$ or $BiFeO_3$ with magnetic Mn^{3+} and Fe^{3+} ions, are ferroelectric. Here, however, it is the Bi ion with two electrons on the 6*s* orbital (lone pair) that moves away from the centrosymmetric position in its oxygen surrounding. Because the ferroelectric and magnetic orders in these materials are associated with different ions, the coupling between them is weak. For example, $BiMnO_3$ shows a ferroelectric transition at $T_{FE} \approx$ 800 K and a ferromagnetic transition at $T_{FM} \approx 110$ K, below which the two orders coexist. $BiMnO_3$ is a unique material, in which both magnetization and electric polarization are reasonably large. This, however, does not make it a useful multiferroic. Its dielectric constant ε

shows only a minute anomaly at T_{FM} and is fairly insensitive to magnetic fields: even very close to T_{FM}, the change in ε produced by a 9-T field does not exceed 0.6%.

Still, some compounds, such as $BiMnO_3$ or $BiFeO_3$ with magnetic Mn^{3+} and Fe^{3+} ions, are ferroelectric. Here, however, it is the Bi ion with two electrons on the 6*s* orbital (lone pair) that moves away from the centrosymmetric position in its oxygen surrounding. Because the ferroelectric and magnetic orders in these materials are associated with different ions, the coupling between them is weak. For example, $BiMnO_3$ shows a ferroelectric transition at $T_{FE} \approx$ 800 K and a ferromagnetic transition at $T_{FM} \approx 110$ K, below which the two orders coexist12. $BiMnO_3$ is a unique material, in which both magnetization and electric polarization are reasonably large.

2.3.2.1 Requirements for magnetoelectric multiferroicity.

By definition, for a material to be a magnetoelectric multiferroic, it must be simultaneously ferromagnetic and ferroelectric. Therefore, its allowed physical, structural, and electronic properties are restricted to those that occur both in ferromagnetic and in ferroelectric materials. In this section, we analyze a range of properties and discuss how these properties limit our choice of potential materials. We discuss those that are the limiting factors in preventing the simultaneous existence of ferromagnetism and ferroelectricity.

Symmetry: A primary requirement for the existence of ferroelectricity is a structural distortion from the prototypical high-symmetry phase that removes the center of symmetry and allows an electric polarization. There are 31 point groups that allow a spontaneous electric polarization, P, and 31 that allow a spontaneous magnetic polarization, M [71].Thirteen point groups (1, 2, 2¢, m, m ¢, 3, 3m ¢, 4, 4m¢m¢, m¢m2¢, m¢m¢2¢, 6, and 6m¢m¢) are found in both sets, allowing both properties to exist in the same phase. Although this represents a considerable reduction from the total number of possible crystal structures (the total number of Shubnikov point groups is 122), it is not an insignificant number, and many candidate materials that are not in fact ferromagnetic and ferroelectric exist in one of the allowed symmetries. Therefore, it is unlikely

that symmetry considerations are responsible for the scarcity of ferromagnetic ferroelectric materials.

Electrical Properties: By definition, a ferroelectric material must be an insulator (otherwise, an applied electric field would inducing an electric current to flow, rather than causing an electrical polarization.) Ferromagnets, although not required to have specific electrical properties, are often metals. For example, the driving force for ferromagnetism in the elemental ferromagnets Fe, Co, and Ni and their alloys is the high density of states at the Fermi level, which also, of course, results in metallicity. Therefore, one could assume that the lack of the simultaneous occurrence of magnetic and ferroelectric ordering is simply the result of a dearth of magnetic insulators. However, if we extend our search to include ferrimagnets or weak ferromagnets (which have canted antiferromagnetic ordering, resulting in a weak magnetic moment in the direction of the canting), this argument no longer holds, because most ferrimagnets or weak ferromagnets are, in fact, insulators. In addition, there are also very few antiferromagnetic ferroelectrics, even though antiferromagnets are usually insulating materials. Therefore, it appears that we cannot blame the lack of magnetically ordered ferroelectrics simply on a shortage of magnetically ordered insulators.

Chemistry: "d^0-ness": The common perovskite oxide ferroelectric materials have a formal charge corresponding to the d^0 electron configuration on the B cation. Clearly, if there are no d electrons creating localized magnetic moments, then there can be no magnetic ordering of any type, either ferro-, ferri-, or antiferromagnetic. It appears however that, in most cases, as soon as the d shell on the small cation is partially occupied, the tendency for it to make a distortion that removes the center of symmetry is eliminated.This could be the result of a number of effects, including size, the tendency to undergo a different, more dominant distortion, electronic properties, magnetic properties, or some combination of the above. We now consider the likely influence of each of these factors.

1) **Size of the Small Cation:** Are transition metal ions with occupied d shells simply too large to move away from the large space at the center of the oxygen octahedron? In this section, we compare the ionic radii of typical d0 cations in perovskite ferroelectrics with

those of typical dn cations in nonferroelectric perovskite oxides to see if this argument is correct. The Shannon ionic radii [72] of some common d^0 small cations found in ferroelectric perovskite oxides are: $Ti^{4+,}$ 74.5 pm; Nb^{5+}, 78 pm; and Zr^{4+}, 86 pm. Some representative dn cations that are found as the small cations in nonferroelectric perovskite oxides include Mn^{3+} (d^4), Ti^{3+} (d^1), and V^{4+} (d^1) with radii of 78.5, 81, and 72 pm, respectively. Therefore, typical B-site cations with d electron occupation do not have systematically larger radii than typical d^0 B-site cations. We conclude that the size of the B cation is not the deciding factor in the existence or otherwise of ferroelectricity.

2) **Structural Distortions:** Ferroelectric materials must undergo a phase transition to a low-temperature phase that does not have a center of symmetry. This is most often achieved in conventional perovskite ferroelectrics by an off-center displacement of the small (B) cation from the center of the oxygen octahedron. However, for cations with certain d-orbital occupancies, the tendency to undergo a Jahn-Teller distortion is strong and will likely be the dominant structural effect. The Jahn-Teller distorted structure might have a lower driving force for offcenter displacement than the otherwise undistorted structure.

Examples of this effect are seen in lanthanum manganite, $LaMnO_3$, in which the Mn^{3+} ion has a d^4 configuration, and yttrium titanate, $YTiO_3$, in which the Ti^{3+} ion is d^1. Both materials have a d-type Jahn-Teller distortion, in which the elongated axes of the oxygen octahedra are oriented parallel to each other along the crystallographic c axis [73] Orbital ordering is observed to occur simultaneously with the Jahn-Teller ordering [73].$LaMnO_3$ is insulating and an A-type antiferromagnet, in which planes of ferromagnetically aligned Mn^{3+} ions are aligned antiparallel to each other. $YTiO_3$ is a strongly correlated ferromagnetic Mott-Hubbard insulator. Neither material is ferroelectric.

Note the relevance of the formal charge on the B cation here. In $BaTiO_3$, the actual occupation of the 3d electrons is closer to d^1 than to d^0 because of donation of charge density from the oxygen ligands [74]. A d^1 cation should undergo a Jahn-Teller distortion. No Jahn-Teller distortion is observed in $BaTiO_3$ however, which is consistent with the d^0 formal charge.

3) **Magnetism Versus d-Orbital Occupancy**: It is clear that the existence of d electrons on the B-site cation reduces the tendency of perovskite structure oxides to display ferroelectricity. However, it is not clear whether it is merely the presence of d electron density or the influence of the magnetic spin polarization that is the dominant factor in creating this effect. Using firstprinciples density functional theory calculations, it is possible to answer this question by artificially removing the spin polarization in materials that are experimentally found to be magnetic and determining whether they then become ferroelectric. Comparisons for some representative systems and show that removal of the magnetic polarization does not significantly affect the calculated phonon frequencies, suggesting that d-orbital occupancy, rather than d-electron magnetism, is dominant in overriding the tendency to undergo ferroelectric distortion.

2.3.2.2 Conclusion.

We do not know for sure why there are so few magnetic ferroelectrics. We do, however, have some clues: multiferroism involves a number of subtle competing factors, with d-electron occupancy on the transition metal being a critical variable.

2.4 $BiFeO_3$ multiferroics

Bismuth ferrite (BFO) is one of the most interesting members of multiferroic family which shows both ferroelectric and ferromagnetic properties in a single phase at room temperature. It is one of the few multiferroics that has Curie and Neel temperatures far above room temperature. It shows magnetoelectric coupling at room temperature and such coupling is strongly enhanced by proper dopings.

2.4.1 History of $BiFeO_3$

The basic idea that crystals could be simultaneously ferromagnetic and ferroelectric probably originated with Pierre Curie in the 19th century [75]. After switching was discovered in ferroelectric Rochelle Salt by Valasek in 1920 [76] there was a rash of supposed discoveries of

magnetoelectric properties by Perrier [77, 78], but unfortunately in materials such as Ni in which they are now understood to be impossible. A history of this period of solid-state physics is given in O‘ Dell‘s text [79].

True magnetoelectricity –defined as a linear term in the free energy was first understood theoretically by Dzyaloshinskii [80] with special predictions being made for Cr_2O_3 and discovered experimentally in that material by Astrov [81]. However this material is paraelectric and antiferromagnetic, making microelectronics applications impractical.

The more interesting case of ferromagnetic ferroelectrics waited for some years until the work of Schmid on boracites [82]. The boracites are also impractical materials for device applications: they have low symmetry with large unit cells and grow in needle shapes; more importantly, they exhibit magnetoelectricity only at extremely low temperatures. Meanwhile Smolenskii‘s group in Leningrad pioneered [83] the study of bismuth ferrite, $BiFeO_3$, but they found that they could not grow single crystals and that ceramic specimens were too highly conducting (probably caused by oxygen vacancies and mixed Fe valences) to be used in applications [84]. They tried to address the conductivity problem by doping other ions into both the A and B sites of the lattice.

Reviews of the general study of magnetoelectricity appeared by Schmid in 1994 [85] and more recently by Fiebig [86] and by Eerenstein et al. [87]. The current interest in bismuth ferrite was stimulated primarily by a 2003 paper from Ramesh‘s group [88], which showed that it had unexpectedly large remnant polarization. At any rate, the 2003 Science paper has proved enormously stimulating, and has inspired both new fundamental physics and exciting device applications. Increasing efforts have now been devoted to the research focusing on the preparation and characterization of $BiFeO_3$ in forms of film, bulk and nanostructure.

2.4.2 Science of $BiFeO_3$

In parallel with the specific investigation of bismuth ferrite and related compounds has been a more general approach to the idea of multiferroics. NicolaHill (now Spaldin) has asked [5] why there are so few materials that are magnetic and ferroelectric; implicitly limiting her discussion

to transition-metal oxides, especially perovskites, she observed that the ferroelectrics (e.g., titanates) have B-site ions with d^8 electrons,[89] whereas the magnets require d^j electrons with j different from zero.

However, oxide perovskites do not all have the same mechanism of ferroelectricity: the center Ti ion plays the key role in $BaTiO_3$ but the lone-pair Pb ion is dominant in $PbTiO_3$.[89] Indeed, this seems to be the case in $BiFeO_3$, where the polarization is mostly caused by the lone pair (s2 orbital) of Bi^{3+}, so that the polarization comes mostly from the A site while the magnetization comes from the B site (Fe^{3+}); this same idea has led Spaldin and co-workers to propose a host of other perovskites with possible A-site ferroelectricity and B-site magnetism, such as $Bi(Cr,Fe)O_3$ and $BiMnO_3$.

2.4.2.1 Structure of $BiFeO_3$

The room-temperature phase of $BiFeO_3$ is classed as rhombohedral (point group R3c).[59] The perovskite-type unit cell has a lattice parameter, a_{rh}, of 3.965A° and a rhombohedral angle, α_{rh}, of 89.3–89° at room temperature [90,91] with ferroelectric polarization along $[111]_{pseudocubic}$ [92].

A very important structural parameter is the rotation angle of the oxygen octahedra. This angle would be 0° for a cubic perovskite with perfectly matched ionic sizes. A measure of how well the ions fit into a perovskite unit cell is the ratio $(r_{Bi} + r_O)/l$, where r is the ionic radius of the respective ion and l is the length of the octahedral edge. This is completely analogous to the commonly used Goldschmid tolerance factor, [91] which is defined as $t = (r_{Bi} + r_O)/(r_{Fe} + r_{O)}$. For $BiFeO_3$ we obtain t=0.88 using the ionic radii of Shannon, [93] with Bi^{+3} in eightfold coordination (the value for 12-fold coordination is not reported) and Fe^{+3} in sixfold coordination and high spin. When this ratio is smaller than one, the oxygen octahedra must buckle in order to fit into a cell that is too small. For $BiFeO_3$, ω is ca. 11–14° around the polar [111] axis [91, 93]. The displacement of the A-site bismuth cation (shown in figure 2.11) along the [111] axis brings about a non-centrosymmetric polarization resulting in the ferroelectric property.

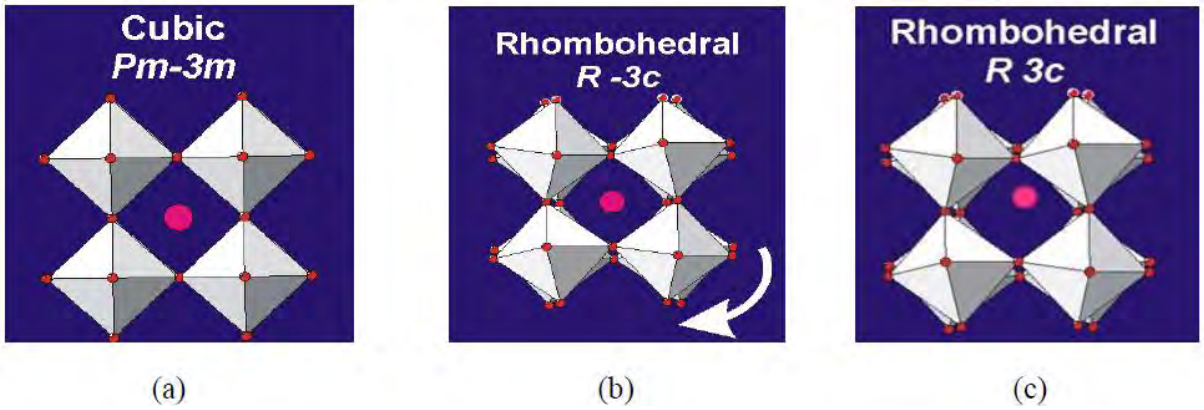

Figure 2.11: Schematic illustration of a structural transition process (a) ideal cubic structure Pm-3m without tilting (a0a0a0) ; (b) R-3c structure tilted along three axes with the same angle (a-a-a-) ; (c) Displacement of Bi ion towards [111] direction based on R-3c.

The lattice parameter and crystal structure of $BiFeO_3$ are dependent on the temperature. It was well documented that, except for the long Bi-Fe bond distance, the lattice parameter a, c, the volume of unit cell, the short bond distance of Bi-Fe as well as the bond angles gradually increase with increase in temperature. As a consequence of these variations, magnetism and polarization are reported to be gradually reduced, and structural phase transitions are also induced from the rhombohedrally distorted R_3c perovskite structure to an orthorhombic Pnma structure and eventually to a cubic structure.

2.4.2.2 Phase diagram of $BiFeO_3$

The phase diagram of Fe_2O_3 and Bi_2O_3 is presented below in figure 2.12, unequal amount of Fe_2O_3 and Bi_2O_3 is seen to bring about impurity phases $Bi_{25}FeO_{39}$ (bismuth-rich) and Bi_2FeO_9 (bismuth-deficient). $BiFeO_3$ is usually prepared from equal parts of Bi_2O_3 and Fe_2O_3, and under high temperatures it can decompose back into these starting materials, as shown in Equation 2.1.

$$2BiFeO_3 \longrightarrow Fe_2O_3 + Bi_2O_3 \quad (2.1)$$

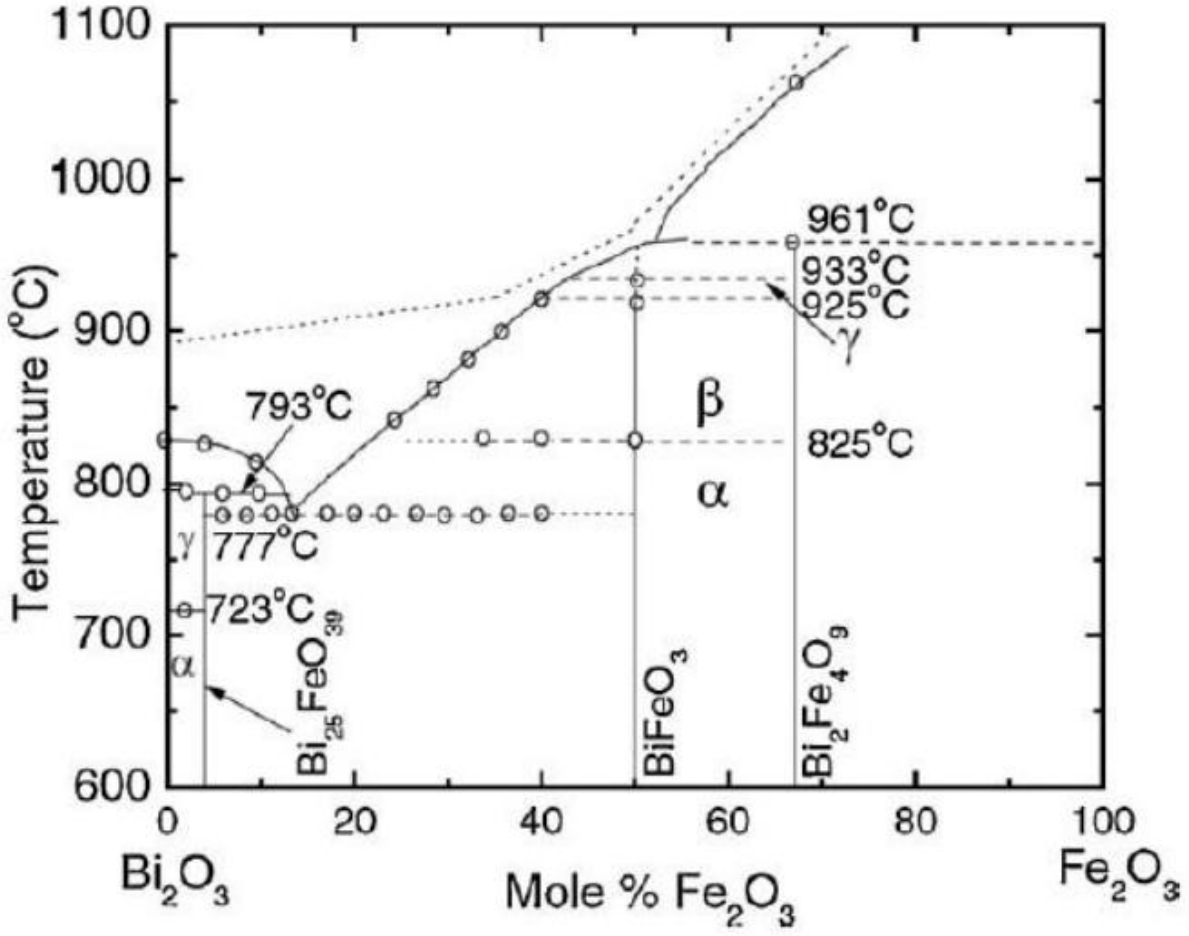

Figure 2.12: Phase Diagram of Fe_2O_3 and Bi_2O_3.

At approximately 825°C there is a first-order transition to a high-temperature β phase that is accompanied by a sudden volume contraction [94,95]. The transition is also accompanied by a peak in the dielectric constant [95,96]; this has been taken as an indication of a ferroelectric–paraelectric transition, although dielectric peaks can also occur in ferroelectric–ferroelectric transitions, such as the orthorhombic–rhombohedral transition in the archetypal perovskite ferroelectric $BaTiO_3$ (which is also first order). Nevertheless, although there is disagreement about the exact symmetry of the β phase above 825°C, most reports agree that it is centrosymmetric [98–102], so it is probably a safe bet that the α–β transition at T_C = 825°C is indeed the ferroelectric–paraelectric transition.

Palai et al. [94] propose that the symmetry of the β phase is orthorhombic, although their data does not allow establishing the exact space group with certainty. Some authors have argued that the b phase may be tetragonal or pseudotetragonal [94, 97, 98], but that is impossible, since the domain structure rules out a tetragonal symmetry and the perovskite a,b,c lattice constants are each quite different [94,99]. It was also proposed that this phase may instead be monoclinic;[98,99] the measured monoclinic angle was nevertheless initially quoted as 90° within experimental error,[98] so that the β phase was in effect ‗metrically orthorhombic'' (i.e., the angles may be 90°, but internal ion positions in each unit cell do not satisfy orthorhombic constraints). More recently, however, Haumont et al. have quoted a monoclinic angle of 90.01° [99].

2.4.3 Electrical properties of $BiFeO_3$

The ferroelectric state arises from a large displacement of the Bi ions relative to the FeO_6 octahedra in $BiFeO_3$ as shown in figure 2.13. The ferroelectric polarization lies along the pseudocubic <111> leading to the formation of eight possible polarization variants, corresponding to four structural variants1 [104].

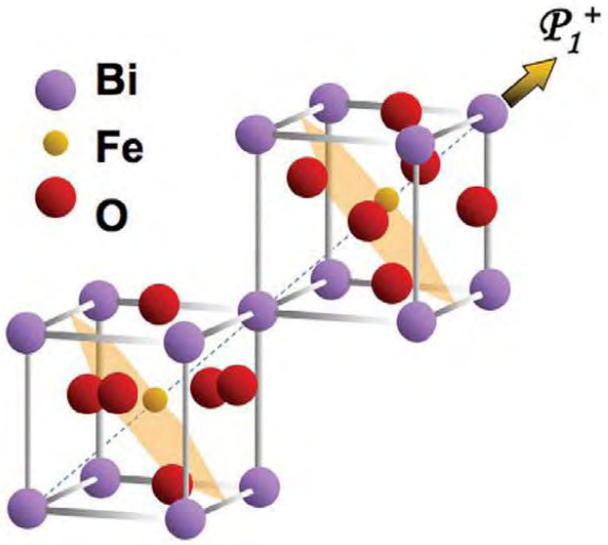

Figure 2.13: Schematic of crystal structure of BFO and ferroelectric polarization (arrow) .

Electrical characterization on bulk $BiFeO_3$ has been very difficult due to the low resistivity of samples. The controversy about whether it is ferroelectric or antiferroelectric was finally settled based on the hysteresis loop measured by Teague et al. [103]. They performed the experiment in liquid nitrogen, which lowered the charge carrier density and mobility, and in turn lowered the leakage current. The measured spontaneous polarization was $3.5\mu C/cm^2$ along the <100> direction, which represents $6.1\mu C/cm^2$ in the <111>direction. This value is much smaller than what would be expected for a ferroelectric material with such high Curie temperature and large distortion. The leakage problem, likely due to defects and non-stoichiometry, has been hampering more comprehensive studies about the bulk $BiFeO_3$ and has limited applications of this material. To overcome this problem, recent work has focused on reducing leakage current using proper dopants.

2.4.3.1 Dielectric constant of $BiFeO_3$

The radio frequency dielectric constant of $BiFeO_3$ at room temperature is $\varepsilon_r = 30$. [105-108] It peaks at the rhombohedral–orthorhombic transition (825–840^oC), possibly – though not necessarily – due to a ferroelectric–paraelectric transition. This dielectric constant is small compared with those of typical perovskite ferroelectrics such as $BaTiO_3$, (Ba, Sr)TiO_3 and Pb(Zr,Ti)O_3 (PZT). The mean refractive index, n, of $BiFeO_3$ is [109] ca. 2.62, so the optical frequency dielectric constant can be estimated as $\varepsilon_r = n2 = 6.86$. This is only an average value, however; dielectric constant at optical frequencies is very anisotropic.

Although 30 can be regarded as the intrinsic dielectric constant of this compound at radiofrequencies, the impedance measurements in parallel-plate capacitors often yield higher values: between 50 and 300 depending on sample morphology, orientation, and frequency range. This is because at the frequencies typically accessible by impedance analyzers (100 Hz to 1 MHz), domain-wall motion and space-charge contributions can be important and add to the measured permittivity. While the intrinsic value $\varepsilon_r = 30$ may seem small for a ferroelectric, this value is not unreasonable. For one thing, the ferroelectric Curie temperature of $BiFeO_3$ is very high, meaning that at room temperature the ferroelectric polarization is already saturated and,

thus, small electric fields will barely affect it (the dielectric constant is essentially a measure of polarizability).

Finally, and this is just a hypothesis, it may be that perovskite ferroelectrics in which the polarization comes from the A site (e.g., $PbTiO_3$ and $BiFeO_3$) have intrinsically lower dielectric constants than those where polarization comes from the B site (e.g., $BaTiO_3$). Experimentally this certainly seems to be the case, but at present we know of no satisfactory explanation for this fact, if indeed it is more than just a coincidence.

2.4.4 Magnetic properties of $BiFeO_3$

The local short range magnetic ordering of BFO is G-type antiferromanget: each Fe^{3+} spin is surround by six antiparallel spins on the nearest Fe neighbours (figure 2.14). The antiferromagnetic spin ordering is not homogeneous but is manifested as an incommensurated cycloid structure with a wavelength of ~ 64 nm along <110>, as can be seen in figure 2.15 [110]. The spin rotation plane can also be determined because the magnetic scattering amplitude depends on the component of magnetic moments perpendicular to the scattering vector [112]. The magnetic Néel temperature is about 643 K and the cycloid could be distorted at low temperatures [111].

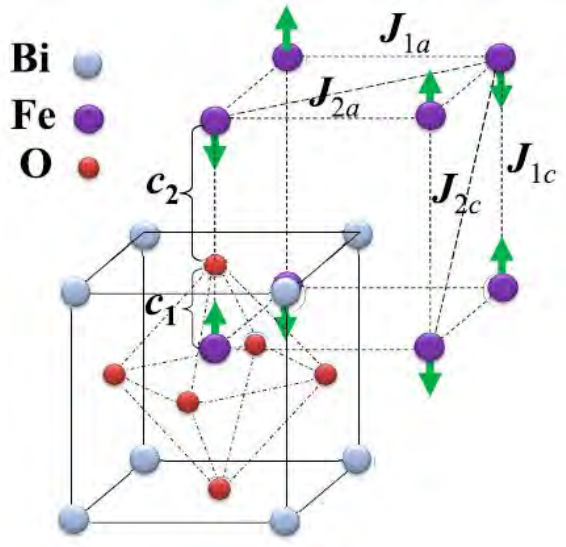

Figure 2.14: (Colour on-line) Schematic of tetragonal-like $BiFeO_3$ (BFO) with G-type antiferromagnetic ordering.

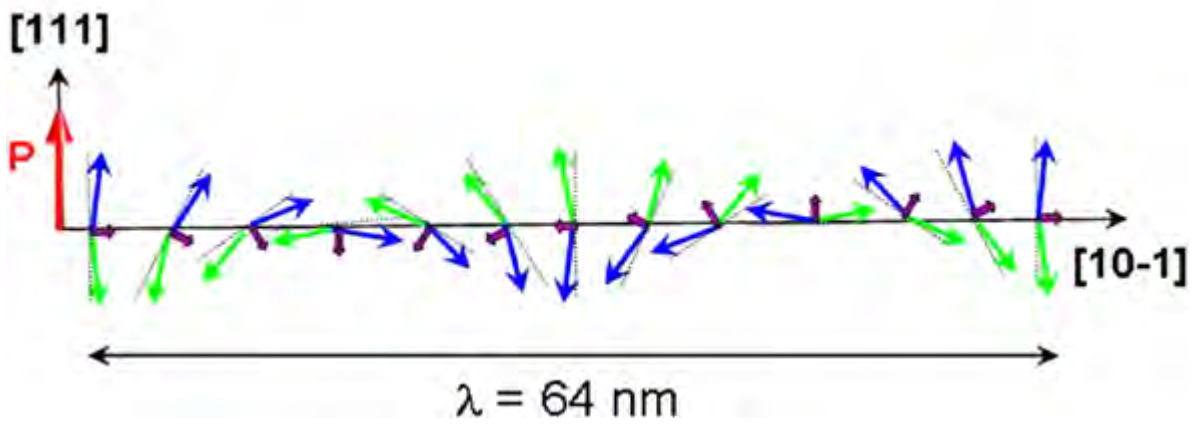

Figure 2.15: Schematics of the 64 nm antiferromagnetic circular cycloid. The canted antiferromagnetic spins (blue and green arrows) give rise to a net magnetic moment (purple arrows) that is specially averaged out to zero due to the cycloidal rotation. The spins are contained within the plane defined by the polarization vector [113].

Sc, Mn, Nb, Zr, Co and Ti ions substitute of Fe ions would increase the magnetization by changing the Fe valence state due to charge compensation and varying the Fe-O-Fe bond angle to increase the spin [114-118]. For Bi-site substitution, Yb, La, Gd, Nd, Pb, Ca, Sr ions may also impact the magnetization of the BFO stem from the spatial homogenization of spin arrangement. The disturbed spin cycloid structure when La ions positions in Bi-site, the formation of partial Fe2+ due to the Bi ions volatilization or oxygen vacancies, varied canting angle of Fe-O-Fe bond due the distortion of FeO_6 octahedron caused by introducing La ions. The increased tensile strain changes the balance between the antiferromagnetic and ferromagnetic interactions [119-122]. As for the impact for dopants on the magnetic phase transition, there are very few report studies.

2.4.5 Applications of $BiFeO_3$

2.4.5.1 Ferroelectric and Piezoelectric Devices

Being a room-temperature multiferroic, $BiFeO_3$ is an obvious candidate for applications. Interestingly, however, the first application that may reach the market might not use the multiferroic properties of $BiFeO_3$ at all. The remnant polarization of $BiFeO_3$ is very large, 100 μCcm^{-2} along the polar [111] direction. To put this into context, this is the biggest switchable polarization of any perovskite ferroelectric, and is roughly twice as big as the polarization of the most widely used material in ferroelectric memories, PZT. Moreover, unlike PZT, $BiFeO_3$ is a lead-free material, a bonus regarding health and safety. It is therefore not surprising that manufacturers of ferroelectric memories such as Fujitsu are considering $BiFeO_3$ as the potential active material in their next generation of ferroelectric memory devices.[123] For such an application to ever come into fruition, however, important obstacles must be removed, such as:

i) the higher conductivity (and thus also dielectric losses) of $BiFeO_3$ relative to PZT,
ii) its tendency to fatigue [124], and
iii) the fact that it appears to thermally decompose at voltages quite close to the coercive voltage [125].

A second potential application unrelated to magnetoelectric properties is piezoelectricity. The piezoelectric coefficient of pure $BiFeO_3$ is actually quite small. However, its rhombohedral ground state means that mixing it with a tetragonal ferroelectric such as $PbTiO_3$ leads to a morphotropic phase boundary (MPB) at a composition of 30% mol $PbTiO_3$[126].

This is important because MPBs are commonly thought to be the key behind the large piezoelectric coefficients of PZT and relaxors, [127] so the MPB of $BiFeO_3$–PT might lead to equally large piezoelectric constants. A newer MPB with enhanced piezoelectric coefficients has been reported [128] for a solid solution of rhombohedral $BiFeO_3$ with orthorhombic $SmFeO_3$; it is likely that other solid solutions between BiFeO3 and any of the other orthoferrites should also

display similar MPBs. In this context, it is surprising that the widely studied solid solution between $BiFeO_3$ and $LaFeO_3$ does not appear to have yet been piezoelectrically characterized; perhaps this is due to its high conductivity.

2.4.5.2 Spintronics

The real drivers behind most of the applied research on $BiFeO_3$ are magnetoelectric and spintronic applications [129]. Chief among these would be memories that can be written using a voltage and read using a magnetic field. Using a voltage for writing has three advantages:

i) this can be implemented in a solid-state circuit without mobile parts,
ii) it has a low-energy requirement, and
iii) the voltage requirements automatically scale down with thickness.

Reading the memory magnetically, on the other hand, has the advantage that it is a non-destructive readout process, unlike direct ferroelectric reading, which requires switching the polarization in order to read it. For such memories to actually work, the magnetic state therefore must be a) electrically switchable and b) magnetically readable.

The first condition is met by $BiFeO_3$, because the easy plane of its antiferromagnetic domains is correlated with the polar direction, and rotating the ferroelectric polarization results in a rotation of the sub lattice magnetization [130-132], i.e., the magnetic state of the sample can be changed by a voltage. On the other hand, the second condition is not directly met, because antiferromagnetic (or, at best, weakly canted antiferromagnetic) domains cannot be easily read.
An elegant solution to the problem of reading antiferromagnetic states consists in using the mechanism known as exchange bias. Crudely, exchange bias is the magnetic interaction between the spins at the uppermost layer of an antiferromagnet and a thin ferromagnetic layer attached to it. The exchange bias modifies the hysteresis loops of the ferromagnetic layer, either offsetting or widening them [133]. What is relevant here is that voltage-induced changes to the underlying antiferromagnetic domains will result in changes to the ferromagnetic hysteresis of the upper

layer, which can then be read by conventional mechanisms. The implementation of this concept for Cr_2O_3 (which is magnetoelectric but not ferroelectric) was first done by Borisov et al. [134]. and the first investigation with an actual multiferroic ($YMnO_3$) was done by Laukhin et al.[135] The race to implement this idea using $BiFeO_3$ (which has the advantage over YMnO3 that it works at room temperature) has been on for a while, and has been punctuated by several important milestones, such as the observation of exchange bias in thin ferromagnetic layers grown on $BiFeO_3$ [136,137], the correlation between exchange bias and ferroelectric domains [138], the observation that the antiferromagnetic domains can be switched by a voltage [132], and, most recently, the final proof of- concept that the exchange-biased ferromagnetic layer can indeed be switched by a voltage [139].

A second line of work uses $BiFeO_3$ as a barrier layer in spintronics. Sandwiching BiFeO3 between two ferromagnetic metals results in tunneling magnetoresistance [129,138]. For this, the only requirement is that the $BiFeO_3$ layer be reasonably insulating down to tunneling thicknesses. However, an extra ingredient provided by $BiFeO_3$ is the fact that it also remains a robust and switchable ferroelectric down to a thickness of 2 nm [140], and thus it could in principle be used as an electrically switchable tunnel junction, whereby the ferroelectric state controls the magnetic state of the thin ferromagnetic electrodes, thus modifying the tunneling magnetoresistance. A similar concept using a ferromagnetic multiferroic (La–BMO) was indeed demonstrated by Gajek et al. [141], who showed that the tunneling resistivity could be controlled both by electric and magnetic fields, giving rise to a four-state memory device. The voltage-dependent barrier characteristics of $BiFeO_3$ have not yet been established.

The above developments show that, at least in principle, it is now possible to develop an MERAM (Magnetoelectric Random Access Memory) based on $BiFeO_3$. A schematic of such a device has been proposed by Bibes and Barthelemy [142], and is reproduced in figure 2.16.

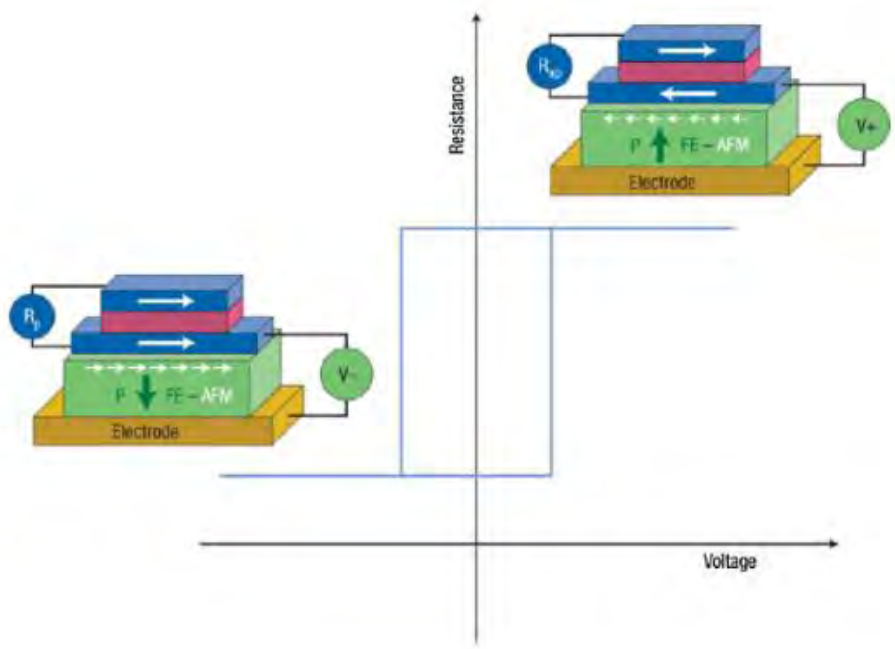

Figure 2.16: MERAM based on exchange-bias coupling between a multiferroic that is ferroelectric and antiferromagnetic (FE-AFM, green layer),and a thin ferromagnetic electrode (blue). A tunneling barrier layer between the two top ferromagnetic layers provides the two resistive states. Interestingly, BiFeO3 could act not only as the magnetoelectric active layer, but also as the tunneling barrier.

2.4.6 Processing of bismuth ferrite based ceramics

In case of ceramic bodies, properties of the final parts largely depend on the processing route. In the present days bismuth ferrite powders are being processed through many routes. Of them, most modern sol-gel precipitation route, chemical precipitation, hydrothermal and combustion reaction are prominent to obtain ultra-pure powders. Choices of route depend on the applications. But till now the conventional route is the most popular method from the industrial point of view. The conventional solid state synthesis route, also known as the ceramic method, refers to a procedure of heating two or more non-volatile solid state materials that can react with one another forming a new compound.

Typically, the high temperature treatment (500°C-2000°C) is required during the process, which provides the energy condition that enables the ions to leave their original sites and diffuse to different sites. The solid state reaction is quite slow but the reaction can speed up considerably if the temperature is increased. However, due to the decomposition or melting of materials, extremely high temperature is not favored. In principal, the optimal temperature is defined by a rule of thumb that two-thirds of the melting temperature of the compound always gives best reaction time

2.4.6.1 BALL MILLING

Before ball milling the raw materials like Bi_2O_3 and Fe_2O_3 powders are weighed according to the stoichiometry. The weighed powders are thoroughly mixed in a ball mill or in an attrition mill. Milling is carried out to fulfil twofold purposes. One is to reduce the particle size and another is to mix the raw materials homogenously. Both finer particle and homogeneity of raw powders eases the diffusion controlled solid state reactions.

The schematic representation of a ball mill is illustrated in figure: 2.17. In the present days, powders are only mixed properly in a laboratory type pot mill. Size reduction of the powders are not now the primary objective of ball milling as the nano sized powders are now available for laboratory type research, rather the objective of ball milling is to homogenize the mixture. The balls should be of the same material as powders so that wear of balls does not contaminate the powder mix. For example, in the past days hardened steel balls were used in a porcelain pot. Bt iron has a very detrimental effect on the dielectric properties of barium titanate based materials. In the present days high density polyethylene (HDPE) pots are used as the container and Y_2O_3 stabilized ZrO_2 balls are used to mill the powders.

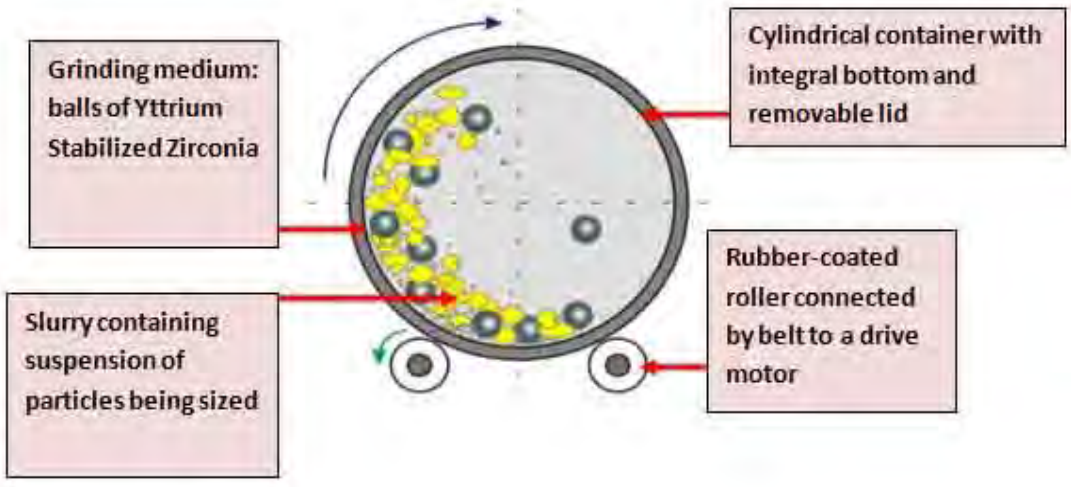

Figure 2.17: Schematic representation of ball milling.

In the wet milling process, milling medium is another important consideration for two reasons. It must not react with the balls, the container or the powder. Secondly, it must avoid decrease of colloidal stability.. After milling the suspension is dried to evaporate the milling medium.

2.4.6.2 Shaping and drying

The milled powder ready for further processing is commonly referred as ‗green' body. The green bodies should have a certain minimum density before they can be sintered. Common practice is to achieve 60% of the theoretical density during shaping and pre-sintered state.

The desired shape and a minimum green density can be provided by various techniques including powder compaction, slip-casting, extrusion, doctor blading, dipping, etc. We should go for hot pressing although it is expensive method. But the process is becoming popular for better quality ceramic material used in high end application. The choice of the method depends on the type of powder used, particle size distribution, state of agglomeration, desired shape, and thickness of the part. Hydraulic or mechanical presses are used to press powder into desired shape at the pressure of ~100 to 300 MPa. Owing to the nature of this process, only simple and

symmetric shape can be prepared. No sintering aid or liquid is added to the powder for solid phase sintering route. Hence, strength of the green powder compact is achieved through addition of a suitable binder such as PVA, glycol phthalate, etc.

After shaping, the green bodies are heated very slowly to between 400-800^{o}C in order to remove any binder present. Initial heating rate is slow to allow the gases to come out slowly without forming cracks and blisters in the ceramic part. After the binder burnout is over, the samples are taken to a higher temperature for sintering.

2.4.6.3 Sintering

The densification of a particulate ceramic compact is technically referred to as sintering. Sintering is essentially the removal of the pores between the starting particles (accompanied by shrinkage of the component), combined with growth together and strong bonding between adjacent particles.

The following criteria must be met before sintering can occur:

1. A mechanism for material transport must be present.
2. A source of energy to activate and sustain this material transport must be present.

The primary mechanisms for transport are diffusion and viscous flow. Heat is the primary source of energy, in conjunction with energy gradients due to particle-particle contact and surface tension.

All properties of ceramic depends on the sintered body which is the direct result of the sintering parameter such as sintering temperature, hold time, atmosphere, thermal profile, etc. There are many sintering methods used but this discussion would be limited to solid phase method. Heat causes the powder particles to develop intergranular bonds by surface diffusion and other physical driving force. The typical green density of ceramic body at the

start is about 60% of theoretical density. Strength starts to develop gradually as more and more particles bond.

At about ~ 80% to 85% density the pores are still open and the ceramic has a typical –chalky" appearance. The dielectric constant is usually low and the T_c is not pronounced strongly. The pores of a ceramic are generally closed above ~90% of theoretical density. Additional heat work causes greater densification as trapped gasses diffuse out along grain boundaries. At densities below 90% of theorectical density the presence of open pores would cause the dielectric loss and undoubtedly inferior dielectric properties.

Setting of sintering temperature is not that straight forward. Low temperature sintering results in ceramic of poor density. On the other hand, too high temperature and long hold time may cause open structure with low density. Also, at high temperatures grain growth is accelerated resulting in low dielectric properties. The sintering temperature and time should be optimum for proper densification to occur without abnormal grain growth. This is usually done by trial and error method depending on various process parameters

CHAPTER 3
EXPERIMENTAL

3.1 Introduction

For advanced research, it is very important to use high purity raw materials. At the same time, it is vital to ensure that during sample preparation no impurity gets incorporated into the ceramic powders. Moreover, accurate weight calculation and measurement are also important to guarantee single phase formation. After sample preparation, sample characterization and property measurement is carried out and finally a relationship between structure and property is established. During all experiments starting from sample preparation to property measurement, all parameters should be maintained for getting good consistent results.

3.2 Raw materials and their characterization

Key materials:

a) Bismuth Oxide (Bi_2O_3) nano powder
Size: 100 nm
Manufacturer: INFRAMAT (USA)
Purity: 99.99%

b) Iron oxide (Fe_2O_3) powder
Size: <2μm
Manufacturer: INFRAMAT (USA)
Purity: 99.99%

c) Lanthanum Oxide (La_2O_3) powder
Size: <2μm
Manufacturer: INFRAMAT (USA)
Purity: 99.99%

d) Tantalum oxide (Ta_2O_5) powder
Size: < 2μm
Manufacturer: INFRAMAT (USA)
Purity: 99.99%

e) Binder: Polymeric
81.0% C, 13.5% H, 2.9% O, 2.6% N

Table 3.1: Information of raw materials

Elements/Oxides	Atomic Number	Atomic Weight	Molecular weight	Density g/cm^3
Bismuth(Bi)	81	208.98	-	9.78
Iron(Fe)	26	55.85		7.86
Lanthanum (La)	57	138.91		6.15
Tantalum (Ta)	73	180.95		16.4
Bismuth Oxide (Bi_2O_3)	-	-	465.96	8.90
Iron oxide (Fe_2O_3)			159.70	5.24
Lanthanum Oxide (La_2O_3)			325.81	6.51
Tantalum Oxide (Ta_2O_5)			441.90	8.20

3.3 Sample Preparation

At first, constituent powders were mixed at proper amount depending on the doping level. Next. the mixture was ball milled at 120 rpm in acetone**.** After that, binder was added into the dried powder mixture. Finally, the mixture was pressed into pellets using a pressing unit.

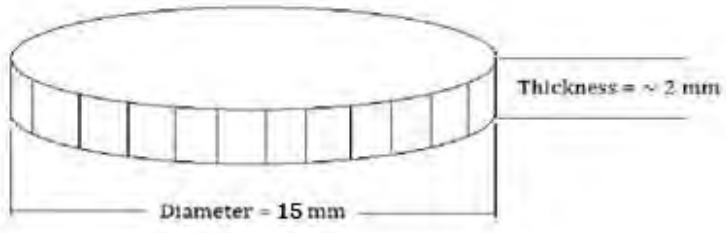

Figure 3.1: Disk shape sample.

3.3.1 Weight measurement

The basic raw materials used in this thesis are Bi_2O_3, Fe_2O_3, La_2O_3 and Ta_2O_5 powders. These powders were taken at proper amount depending on the percentage of the doped element. Four compositions were prepared: a) $Bi_{0.8}La_{0.2}FeO_3$ b) $Bi_{0.8}La_{0.2}Fe_{0.99}Ta_{0.1}O_3$ c) $Bi_{0.8}La_{0.2}Fe_{0.97}Ta_{0.3}O_3$ and d) $Bi_{0.8}La_{0.2}Fe_{0.95}Ta_{0.5}O_3$. Depending upon the percentage of the doped element the amount of raw materials for mixing was varied.

Table 3.2: Raw powder requirements for formulation of samples

Samples	Powder	Weight of powder in batch (g)	Total weight of batch (g)
$Bi_{0.8}La_{0.2}FeO_3$	Bi_2O_3	12.48	20
	Fe_2O_3	5.34	
	La_2O_3	2.18	
$Bi_{0.8}La_{0.2}Fe0.99Ta_{0.1}O_3$	Bi_2O_3	12.42	20
	Fe_2O_3	5.27	
	La_2O_3	2.17	
	Ta_2O_5	0.15	
$Bi_{0.8}La_{0.2}Fe_{0.97}Ta_{0.3}O_3$	Bi_2O_3	12.32	20
	Fe_2O_3	5.12	
	La_2O_3	2.15	
	Ta_2O_5	0.44	
$Bi_{0.8}La_{0.2}Fe_{0.95}Ta_{0.5}O_3$	Bi_2O_3	12.22	20
	Fe_2O_3	4.97	
	La_2O_3	2.14	
	Ta_2O_5	0.72	

3.3.2 Milling

The main purpose of milling was mixing and homogenization. At first, the powder mixtures were milled manually using a mortar and pestle. Next the hand milled powders were ball milled using laboratory type grinding bowl made of Silicon Nitride (Si_3N_2). Balls made of Si_3N_2 having dia of 10 mm (shown in figure-3.2) were used together with acetone (purity>99%) as milling media. The grinding balls and the materials in the grinding bowl are acted upon by the centrifugal forces due to the rotation of the grinding bowl about its own axis and due to the rotating supporting disk. The grinding bowl and the supporting disc rotate in opposite directions, so that the centrifugal forces alternately act in the same and opposite directions. Ball milling machine (Fritsch, Pulverisette 6) used for this purpose is also shown in figure-3.2.

Before adding the powder in the milling pot, the balls and the pot were cleaned ultrasonically to remove slightest of dust which may show up as impurity in the final structure with resultant harmful properties. The balls usually stay at the bottom of the pot having the added powders on top of them. Then, after adding sufficient amount of acetone the mouth of pot was closed tightly and shaken to mix the ingredients. Finally the powders were milled at 120 rpm to get a homogenize mixture**.**

Figure 3.2: Ball milling machine and two different size milling media.

After milling the extracted powders were dried; for quick drying powders were kept at 100°C for at least 2 to 3 hours. It is very important to dry the powders completely otherwise they cannot be pressed properly to get the desired shape.

Figure 3.3: Drier used for drying sample.

3.3.4 Compaction

Around 1 gm of powder was pressed into pellets using pressure of 40 KN and the pellets were held under the pressure for 1 minute using a pressing unit (Herzog, Model No. HTP 40, Japan). After ejecting the pellets from the dies the pellets were dried in an oven and then lightly ground with grit #800 SiC paper to a smooth surface, removing surface irregularities. Green densities of the samples were measured before the pellets were sintered. Green samples were not made thick to avoid density variation. The compaction process is shown in figure 3.4.

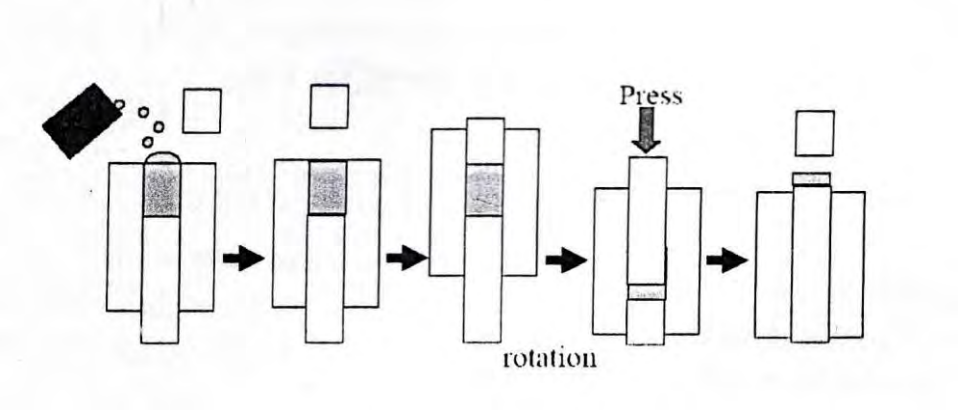

Figure 3.4: Schematic representation of compaction process.

Figure 3.5: Pressing unit.

3.3.5 Sintering

Muffle Furnace (Nabertherm Gmblt Bahnhofstr, 20, Lilienthal / Bremen Germany) was used to sinter the disk shaped samples in air atmosphere.

Figure 3.6: Furnaces used for sintering ceramics sample.

The basic sintering cycles used in the experiments is shown in figure 3.7. The maximum sintering temperature, sintering rate and cooling rate were varied to find the optimum between percent theoretical density and grain size so that the density of the sample increases significantly.

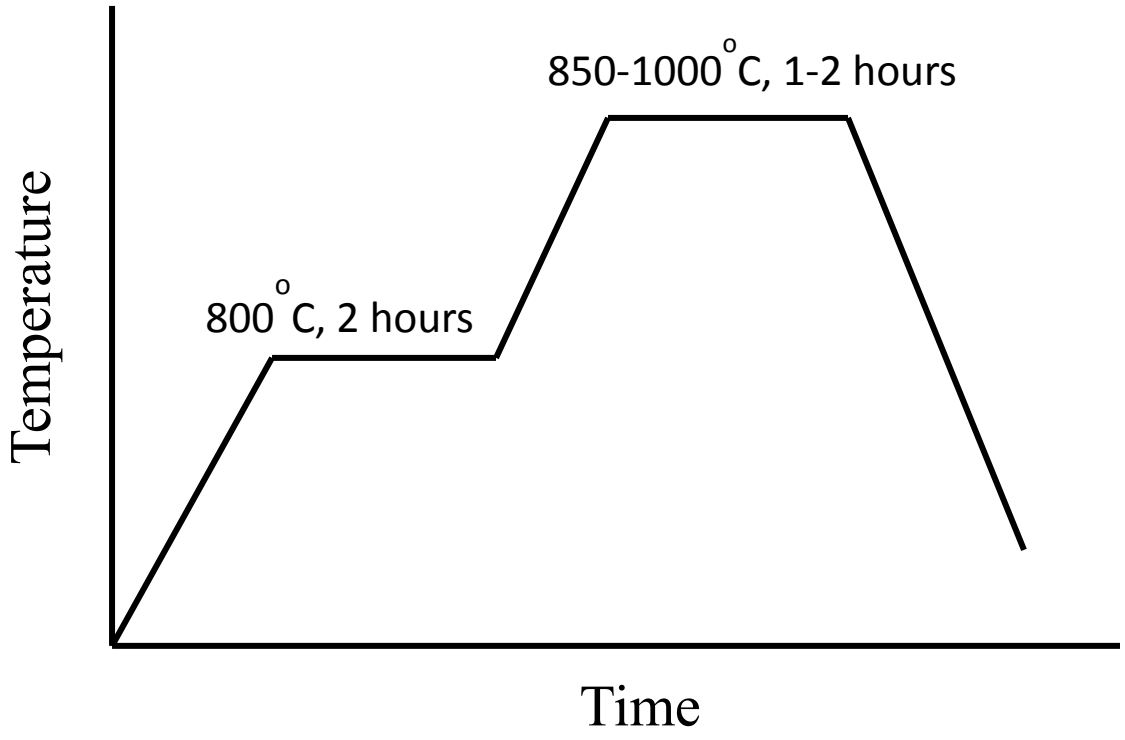

Figure 3.7: Sintering cycle.

The sintering temperature, sintering rate, and the soaking time were modified progressively as the experiment proceeds on trial and error basis. Different parameters applied are shown in the table below:

Table 3.3: Table showing experimental parameters applied

Experiment No.	Heating Rate °C/min	Binder Removal Temperature (°C)	Dwell Time (Hour)	Sintering Rate (°C/min)	Maximum Sintering Temperature (°C)	Holding Time (min)	Cooling Rate (°C/min)	End Temp. (°C)
1	**3**	**800**	**2**	**3**	**850**	**2**	**5**	**40**
2	**3**	**800**	**2**	**3**	**875**	**2**	**5**	**40**
3	**3**	**800**	**2**	**3**	**900**	**2**	**5**	**40**
4	**3**	**800**	**2**	**3**	**925**	**1**	**5**	**40**
5	**3**	**800**	**2**	**3**	**925**	**2**	**5**	**40**
6	**3**	**800**	**2**	**3**	**950**	**1**	**5**	**40**
7	**3**	**800**	**2**	**3**	**950**	**2**	**5**	**40**

8	**3**	**800**	**2**	**3**	**975**	**1**	**5**	**40**
9	**3**	**800**	**2**	**3**	**975**	**2**	**5**	**40**
10	**3**	**800**	**2**	**3**	**1000**	**1**	**5**	**40**
11	**3**	**800**	**2**	**3**	**1000**	**2**	**5**	**40**

The dwell time at the primary stages was set to remove the binder and for calcination. It is important to keep the heating rate low up to this point otherwise during binder burning samples may crack. The heating rate may be changed at each stage depending upon the composition and the sample‘s tendency to warp during sintering.

3.3.6 Post sintering operations

Post sintering operations are necessary to measure different material properties.

To measure dielectric properties, samples were grinded, polished and particular geometric shape was given such as rectangle, square or triangle to measure dielectric constant. 120 grit paper of SiC was used for rough polishing.

For field emission scanning electron microscopy (FESEM) samples were cleaned in acetone and dried in oven for 30 minutes. As the ceramic samples were non-conducting, they were coated with platinum dust by ion sputtering method in order to make them conducting which was essential for FESEM observations.

3.4 Property measurement

3.4.1 Percent theoretical density measurement

After completion of sintering dimensions of disk shape samples were measured with digital micrometer as well as slide callipers and samples were weighed by electronic balance. Percent theoretical density (%TD) achieved was calculated by comparing the actual and theoretical density. Theoretical densities are listed below for he tested compositions.

Table 3.4: Theoretical densities of different composition

Material	Theoretical Density g/cm^3

$Bi_{0.8}La_{0.2}FeO_3$	7.96
$Bi_{0.8}La_{0.2}Fe_{0.99}Ta_{0.01}O_3$	7.99
$Bi_{0.8}La_{0.2}Fe_{0.97}Ta_{0.03}O_3$	8.07
$Bi_{0.8}La_{0.2}Fe_{0.95}Ta_{0.05}O_3$	8.13

3.4.2 Microstructure study

To observe ceramics sample in FESEM, sample was made conductive, coated with platinum by ion sputtering method. Then sample was mounted on a holder and inserted in FESEM.

Figure 3.8: Field Emission Scanning Electron Microscope (FESEM).

The micrographs obtained from FESEM analysis was used for microstructural study which include grain size measurement, porosity observation etc.

3.4.3 Phase study:

X-ray diffraction analysis was conducted using the XRD (Bruker D8 Advance) facility available at BCSIR, Dhaka in order to determine the phases present in the samples.

Figure 3.9: XRD Machine.

X-rays are a type of electromagnetic radiation. The wavelength of x-rays is approximately 1 Å which has the same size equivalent to that of an atom. X-ray diffraction (XRD) is a non-destructive analytical technique mainly used for the phase identification and structural characterization of crystalline materials. r X-ray diffraction combined with Rietveld analysis, provides detailed information regarding unit cell dimensions, bond-lengths, bond-angles and the site ordering of crystallites.

The relationship between the wavelengths of the X-rays λ, the incidence angle q, and spacing between two crystal lattice planes (hkl) d, is shown in the Bragg's Law expressed as:

$$2d_{hkl} \sin q = l$$

After characterization by X-ray diffraction, a number of peaks are seen in the diffraction patterns. These patterns are identified by comparing their positions and relative intensities with the known structures in the database. Sometimes extra peaks might appear due to the impurity or structural transformation after thermal treatment. In fact, the intensities, widths and positions of peaks in the patterns reflect information about structure, quantity, texture etc. of crystallites.

Rietveld Refinement

Rietveld Refinement is a method used to determine detailed information of crystalline materials. In order to get authentic information about crystalline materials, the least square value of the difference between theoretical and experimental peak intensities are supposed to be minimized based on releasing and refining appropriate parameters.

Rieveld Refinement directly matches the intensities of all the peaks throughout the test range with the intensities of peaks from the model structures, and it is less sensitive to both model and experimental errors.

3.4.4 Dielectric property measurement

An impedance analyzer [WAYNE KERR 6500B series] was used to measure the dielectric property of samples. All the measurements were subjected to AC current only.

First of all samples were prepared properly to measure dielectric properties correctly. Samples were kept clean and dry. They were polished with 120 grit paper in order to produce crack free solid sample. Samples were given geometrical shape commonly rectangle in order to measure the area. Sample thickness was kept quite uniform which was essential for correct measurement. Then after taking dimensions, silver paint was applied on both sides of the sample keeping the edges clean. Next the samples were kept in the holder of the impedance analyzer to measure the properties.

Both room temperature and high temperature frequency dependency were measured. Dielectric constant was measured from the capacitance value obtained from the analyzer according to equation as below –

$$k = C_p \, d/(A\varepsilon_0)$$

Where k' is the dielectric constant, C_p is the capacitance value measured by the impedance analyzer, d is the thickness of the sample, ε_0 is the permittivity of vacuum, A is the area of the sample in contact with the conducting layer.

A set up of tube furnace type oven accompanied with custom sample holder was used to heat the sample during high temperature property measurement

Figure 3.10: Impedance Analyzer.

3.4.5 Transition temperature study

Thermal analysis was conducted using Differential Thermal Analyzer (Brand: Seiko Instruments, Model: EXSTAR6000) available at BCSIR, Dhaka to study the ferroelectric transition point.

Figure 3.11: Differential Thermal Analyzer.

The technique is based on the facts that as a substance is heated, it undergoes reactions and phase changes that involve absorption or emission of heat. In DTA the temperature of the test material is measured relative to that of an adjacent inert material. A thermocouple imbedded in the test piece and another in the inert material are connected so that any differential temperatures generated during the heating cycle are graphically recorded as a series of peaks on a moving chart. The amount of heat involved and temperature at which these changes take place are characteristic of individual elements or compounds.

According to literature at ferroelectric transition point $BiFeO_3$ undergoes a phase change. So, DTA was conducted in the temperature range of 200-1000^oC to find out this phase transition point.

3.4.6 Magnetic property measurement

The frequency dependent magnetic permeability spectra were investigated using precision impedance analyzer [WAYNE KERR 6500B series].

The permeability measurements on toroid-shaped samples were carried out at room temperature in the frequency range 100 KHz–15MHz. The real part (μ_i') and the imaginary part (μ_i'') of the complex permeability was calculated using the following relations:

$\mu_i' = Ls/Lo$,

where, Ls is the self-inductance of the sample core and
Lo ($=\mu_o N^2 h/(2pi) \ln r_o/r_i$ is derived geometrically) is the inductance of the winding coil without the sample core.
N is the number of turns of the coil (N=5), h is the thickness, r_o is the outer radius and r_i is the inner radius of the toroidal specimen.

and, $\mu_i'' = \mu_i' \tan\delta$

CHAPTER 4
RESULTS AND DISCUSSION

4.1 Introduction

The main target of this thesis project was to develop a novel multiferroic material exhibiting both ferroelectric and ferromagnetic properties. For this purpose the starting material used was Bi_2O_3, Fe_2O_3, La_2O_3 and TaO_5. According to Hill [5], the net magnetization in BFO originates from Fe atoms and the net polarization in BFO mainly originates from Bi atoms. Several doping strategies have been adopted for suppressing the leakage currents of BFO ceramics among which recently, co-substitutions of Bi^{3+} ions by La^{3+} and Fe^{3+} ions partially by high valence ions like Nb^{5+}, Ta^{5+} or Ti^{4+} has been proved to be effective for increasing the resistivity and, hence, improving the overall ferroelectric properties of BFO . Addition of La reduces significantly the volatilization of bismuth oxide and hence improves oxygen ion stability in the lattice due to the similar radii values of Bi^{3+} (1.030) and La^{3+} (1.032), and therefore La doping at the Bi site enhances the ferromagnetic property of BFO. On the other hand, partial substitution of Fe^{3+} by higher valence ions like Ta^{5+} can decrease the charge defects and increase the electrical resistivity of BFO. So, it is interesting to investigate the effect of codoping of La and Ta in order to combine the advantages of La doping and Ta doping. So far, there have been no reports on the codoping of La and Ta in BFO.

The initial aim of the experiment was to determine the optimum sintering zone for the doped bismuth ferrite that was revealed to be above 850^0C from literature. Determining the optimum sintering zone was a challenge of this research since no previous work has been reported on the sintering of tantalum doped $BiFeO_3$. So a trial and error method was employed to determine the correct sintering temperature. Sintering cycles were conducted in the range of 850 to 1000^oC for 1-2 hrs. To develop an understanding of the effect of Ta on sintering we studied the effect of Ta on $BaTiO_3$ where Ta acted as a grain growth inhibitor [160,161]. Thus, a similar effect was expected when Ta was added to $BiFeO_3$.

At sintering temperatures in the range of 850-900^0C for a holding time of 2 hours no significant densification was obtained and the % theoretical density (%TD) obtained was unsatisfactory for all compositions. At 925^0C for a holding time of 1-2 hours the $Bi_{0.8}La_{0.2}FeO_3$ samples attained a % TD above 80%. However, the %TD deteriorated significantly, below 60%, with increasing additions of Ta. Addition of Ta severely inhibited the densification process and resulted in porous samples of reduced compactness. Sintering at 925^0C for 1-2 hours was inadequate to offer sufficient energy for proper coalescence hence resulting in poor densification. These results clearly indicated the necessity for higher temperature of sintering in order to obtain proper densification, especially for the $Bi_{0.8}La_{0.2}Fe_{1-x}Ta_xO_3$ (x = 0.01, 0.03 and 0.05) ceramics where the solute drag or pinning effect of Ta inhibits the densification process. Finally, by further increasing the sintering temperature the best combination of % TD, grain size and optimum multiferroic properties was found in samples sintered at 1000^0C for 2 hours holding time.

The XRD analysis of the $Bi_{0.8}La_{0.2}Fe_{1-x}Ta_xO_3$ (x = 0.0, 0.01, 0.03 and 0.05) ceramics sintered at 1000^oC for 2 hours confirmed the formation of single phase distorted R3c structure.

The %TD and grain size of $Bi_{0.8}La_{0.2}Fe_{1-x}Ta_xO_3$ (x = 0.0, 0.01, 0.03 and 0.05) sintered in the range of 850-1000^oC for holding times 1 and 2 hours are tabulated in Table 4.1. The results (Table 4.1) reveal that with an increase in sintering temperature and holding time at a particular sintering temperature the % TD increases significantly for all compositions. Moreover, the highest % TD of 97.9% is achieved for $Bi_{0.8}La_{0.2}FeO_3$ ceramics at an optimum sintering temperature of 1000^oC for 2 hours.

Microstructural analysis of $Bi_{0.8}La_{0.2}Fe_{1-x}Ta_xO_3$ (x = 0.0, 0.01, 0.03 and 0.05) samples confirm the grain growth suppression action of Ta. Moreover, it is also confirmed that for a particular sintering temperature the grain size decreases with increasing Ta addition. At 1000^oC for 2 hours, grain size decreases from 10.6 μm in $Bi_{0.8}La_{0.2}FeO_3$ to 0.92 μm in $Bi_{0.8}La_{0.2}Fe0_{.95}Ta0_{.05}O_3$. However, even though high densification of $Bi_{0.8}La_{0.2}FeO_3$ was achieved when sintered at 1000^oC for 2 hours, the excessive grain growth has detrimental effects on its ferroelectric properties due to decrease in grain boundary length. Addition of Ta reduced the grain size to 0.92-.98 μm, thus increasing the grain boundary length and resistance to leakage current and as a result bringing about the best combination of ferroelectric and ferromagnetic properties.

Table 4.1: Percent theoretical density (%TD) and average grain size of $Bi_{0.8}La_{0.2}Fe_{1-x}TaxO_3$ (x = 0.0, 0.01, 0.03 and 0.05) ceramics at sintering temperatures from 850 to 1000^oC.

Sl No.	Sintering Temperature (^oC)	Holding Time (hours)	Composition	Percent Theoretical Density (%TD)	<Grain Size> μm
1	850	2	$Bi_{0.8}La_{0.2}FeO_3$	70.1	0.80
			$Bi_{0.8}La_{0.2}Fe_{0.99}Ta_{0.01}O_3$	49.8	<0.2
			$Bi_{0.8}La_{0.2}Fe_{0.97}Ta_{0.03}O_3$	49.2	<0.2
			$Bi_{0.8}La_{0.2}Fe_{0.95}Ta_{0.05}O_3$	48.4	<0.2
2	875	2	$Bi_{0.8}La_{0.2}FeO_3$	76.2	2.20
			$Bi_{0.8}La_{0.2}Fe_{0.99}Ta_{0.01}O_3$	52.6	<0.2
			$Bi_{0.8}La_{0.2}Fe_{0.97}Ta_{0.03}O_3$	52.1	<0.2
			$Bi_{0.8}La_{0.2}Fe_{0.95}Ta_{0.05}O_3$	51.7	<0.2
3	900	2	$Bi_{0.8}La_{0.2}FeO_3$	79.6	3.00
			$Bi_{0.8}La_{0.2}Fe_{0.99}Ta_{0.01}O_3$	54.1	<0.3
			$Bi_{0.8}La_{0.2}Fe_{0.97}Ta_{0.03}O_3$	53.8	<0.2
			$Bi_{0.8}La_{0.2}Fe_{0.95}Ta_{0.05}O_3$	53.2	<0.2
4	925	1	$Bi_{0.8}La_{0.2}FeO_3$	85.2	3.80
			$Bi_{0.8}La_{0.2}Fe_{0.99}Ta_{0.01}O_3$	57.3	0.38
			$Bi_{0.8}La_{0.2}Fe_{0.97}Ta_{0.03}O_3$	53.1	0.30
			$Bi_{0.8}La_{0.2}Fe_{0.95}Ta_{0.05}O_3$	52.6	0.27
5	925	2	$Bi_{0.8}La_{0.2}FeO_3$	85.8	4.20
			$Bi_{0.8}La_{0.2}Fe_{0.99}Ta_{0.01}O_3$	65.7	0.40

			$Bi_{0.8}La_{0.2}Fe_{0.97}Ta_{0.03}O_3$	59.6	0.33
			$Bi_{0.8}La_{0.2}Fe_{0.95}Ta_{0.05}O_3$	53.4	0.29
6	950	1	$Bi_{0.8}La_{0.2}FeO_3$	91.2	4.40
			$Bi_{0.8}La_{0.2}Fe_{0.99}Ta_{0.01}O_3$	74.6	0.44
			$Bi_{0.8}La_{0.2}Fe_{0.97}Ta_{0.03}O_3$	74.1	0.43
			$Bi_{0.8}La_{0.2}Fe_{0.95}Ta_{0.05}O_3$	72.9	0.41
7	950	2	$Bi_{0.8}La_{0.2}FeO_3$	91.9	5.60
			$Bi_{0.8}La_{0.2}Fe_{0.99}Ta_{0.01}O_3$	77.2	0.48
			$Bi_{0.8}La_{0.2}Fe_{0.97}Ta_{0.03}O_3$	76.4	0.47
			$Bi_{0.8}La_{0.2}Fe_{0.95}Ta_{0.05}O_3$	75.1	0.45
8	975	1	$Bi_{0.8}La_{0.2}FeO_3$	94.4	7.50
			$Bi_{0.8}La_{0.2}Fe_{0.99}Ta_{0.01}O_3$	87.9	0.76
			$Bi_{0.8}La_{0.2}Fe_{0.97}Ta_{0.03}O_3$	85.2	0.74
			$Bi_{0.8}La_{0.2}Fe_{0.95}Ta_{0.05}O_3$	82.8	0.73
9	975	2	$Bi_{0.8}La_{0.2}FeO_3$	95.2	7.80
			$Bi_{0.8}La_{0.2}Fe_{0.99}Ta_{0.01}O_3$	93.1	0.84
			$Bi_{0.8}La_{0.2}Fe_{0.97}Ta_{0.03}O_3$	92.8	0.79
			$Bi_{0.8}La_{0.2}Fe_{0.95}Ta_{0.05}O_3$	92.4	0.76
10	1000	1	$Bi_{0.8}La_{0.2}FeO_3$	97.6	10.4
			$Bi_{0.8}La_{0.2}Fe_{0.99}Ta_{0.01}O_3$	96.1	0.91
			$Bi_{0.8}La_{0.2}Fe_{0.97}Ta_{0.03}O_3$	95.5	0.85
			$Bi_{0.8}La_{0.2}Fe_{0.95}Ta_{0.05}O_3$	95.2	0.83
11	1000	2	$Bi_{0.8}La_{0.2}FeO_3$	97.9	10.6
			$Bi_{0.8}La_{0.2}Fe_{0.99}Ta_{0.01}O_3$	96.5	0.98
			$Bi_{0.8}La_{0.2}Fe_{0.97}Ta_{0.03}O_3$	95.9	0.94
			$Bi_{0.8}La_{0.2}Fe_{0.95}Ta_{0.05}O_3$	95.6	0.92

In contrast to pure BFO, La and Ta codoped BFO shows superior values of dielectric constant. The best values of dielectric constant (> 2000) at room temperature were attained for the Ta doped samples at grain sizes in the range of 0.92-.98 μm. At higher temperatures a considerable increase in the dielectric constant of $Bi_{0.8}La_{0.2}FeO_3$ samples occurred due to space charge polarization. However, in Ta-substituted BFO the stability of dielectric constant with temperature is considerably improved.

DTA analysis revealed that the peak for ferroelectric transition (T_C) shifted towards higher temperatures for the Ta-substituted ceramics and reached 870^oC for x=0.05. Thus codoped BFO exhibited ferroelectric characteristics over a wider temperature range than pure BFO.

Opposed to pure BFO, that according to literature [154] has no magnetic permeability due to its G-type antiferromagnetic ordering, La and Ta doped BFO ceramics revealed the presence of magnetic permeability. This is because doping changes cycloid spin structure of BFO to a canted spin structure which destructs the spin cycloid, releases locked magnetization and enhances the

magnetoelectric interaction hence resulting in significantly improved magnetic properties. $Bi_{0.8}La_{0.2}FeO_3$ ceramics exhibited the best magnetic permeability and addition of Ta reduced the magnetic permeability to some extent due to reduction of grain size but in return improved the dielectric properties. The optimum balance between dielectric properties and magnetic permeability was obtained for grain size between of 0.92-.98 μm for samples sintered at the 1000^{o}C for 2 hours.

4.2 Dependence of % theoretical density and <grain size> on sintering temperature and Tantalum content

The variation of % theoretical density with sintering temperature for 1 and 2 hours of holding time for $Bi_{0.8}La_{0.2}Fe_{1-x}Ta_xO_3$ (x = 0.0, 0.01, 0.03 and 0.05) ceramics are shown in figure 4.1 and 4.2 respectively. From figure 4.1 and 4.2 it is obvious that the %TD of $Bi_{0.8}La_{0.2}FeO_3$ ceramics are least affected by temperature in comparison to the ceramics with added Ta. This can be explained by the absence of Ta in these samples. However, the samples that have a composition of $Bi_{0.8}La_{0.2}Fe_{1-x}Ta_xO_3$ (x = 0.01, 0.03 and 0.05) exhibit a sharp increase in %TD during the transition of sintering temperature from 925 to 975^{o}C, after which the %TD increases only slightly up to a sintering temperature of 1000^{o}C.This effect is more prominent when the holding time is increased from 1 to 2 hours as shown in figure 4.2. This implies that at sintering temperatures above 975^{o}C the pinning effect of Ta becomes less significant. Moreover, this pinning effect becomes even less significant when the holding time is increased. All samples sintered at 1000^{o}C for 2 hours have a % TD above 95%.

Figure 4.3 and 4.4 show the variation of %TD with Ta addition for $Bi_{0.8}La_{0.2}Fe_{1-x}Ta_xO_3$ (x = 0.0, 0.01, 0.03 and 0.05) ceramics at holding times of 1 and 2 hours respectively. Both figures confirm that with increasing additions of Ta the %TD decreases at all sintering temperatures and for all compositions. Ta suppresses the grain growth during sintering by pinning of grain boundaries thus resulting in poorer densification and hence lower %TD.

Figure 4.5 and 4.6 show the variation of grain size of $Bi_{0.8}La_{0.2}Fe_{1-x}Ta_xO_3$ (x = 0.0, 0.01, 0.03 and 0.05) ceramics with sintering temperature for holding time of 1 and 2 hours respectively. From both figures it is clear that with an increase in sintering temperature the grain size increases

due to the increased rate of diffusion at higher temperatures. However, as expected this effect is most prominent in the $Bi_{0.8}La_{0.2}FeO_3$ samples where grain increases from 4.2 µm at 925°C to 10.6 µm at 1000°C for a holding time of 2 hours at both temperatures. As stated earlier this is due to the absence of Ta in $Bi_{0.8}La_{0.2}FeO_3$ samples, which suppresses grain growth as a result of its pinning effect. In samples containing Ta the grain size increases only slightly with sintering temperature and this increase is much less prominent than in the case of $Bi_{0.8}La_{0.2}FeO_3$ ceramics. For the $Bi_{0.8}La_{0.2}Fe_{0.99}Ta_{0.01}O_3$ ceramics the grain increases from 0.4µm at 925°C to 0.98 µm at 1000°C for a holding time of 2 hours.

Finally the variation of grain size of $Bi_{0.8}La_{0.2}Fe_{1-x}Ta_xO_3$ (x = 0.0, 0.01, 0.03 and 0.05) ceramics with Ta addition for holding time of 1 and 2 hours are shown in figures 4.7 and 4.8 respectively. As expected, both figures confirm that the grain size of the $Bi_{0.8}La_{0.2}Fe_{1-x}Ta_xO_3$ (x = 0.0, 0.01, 0.03 and 0.05) ceramics decrease with an increase in the Ta addition as a consequence of its pinning effect. Increasing the holding time from 1 to 2 hours at 1000°C results in an increase in the grain size of $Bi_{0.8}La_{0.2}FeO_3$ from 10.4 to 10.6 µm and of $Bi_{0.8}La_{0.2}Fe_{0.95}Ta_{0.05}O_3$ from 0.83 to 0.92 µm. This shows that along with sintering temperature, with an increase in holding time the pinning effect of Ta becomes less prominent.

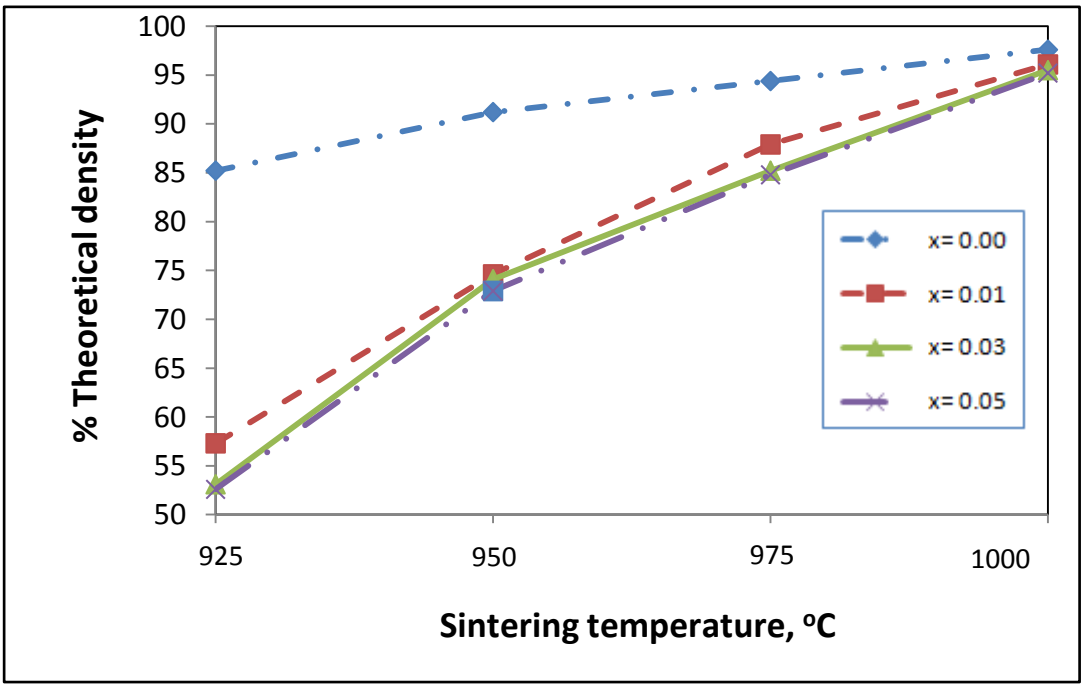

Figure 4.1: Variation of % theoretical density with sintering temperature for 1 hour holding time for $Bi_{0.8}La_{0.2}Fe_{1-x}Ta_xO_3$ (x = 0.0, 0.01, 0.03 and 0.05) ceramics.

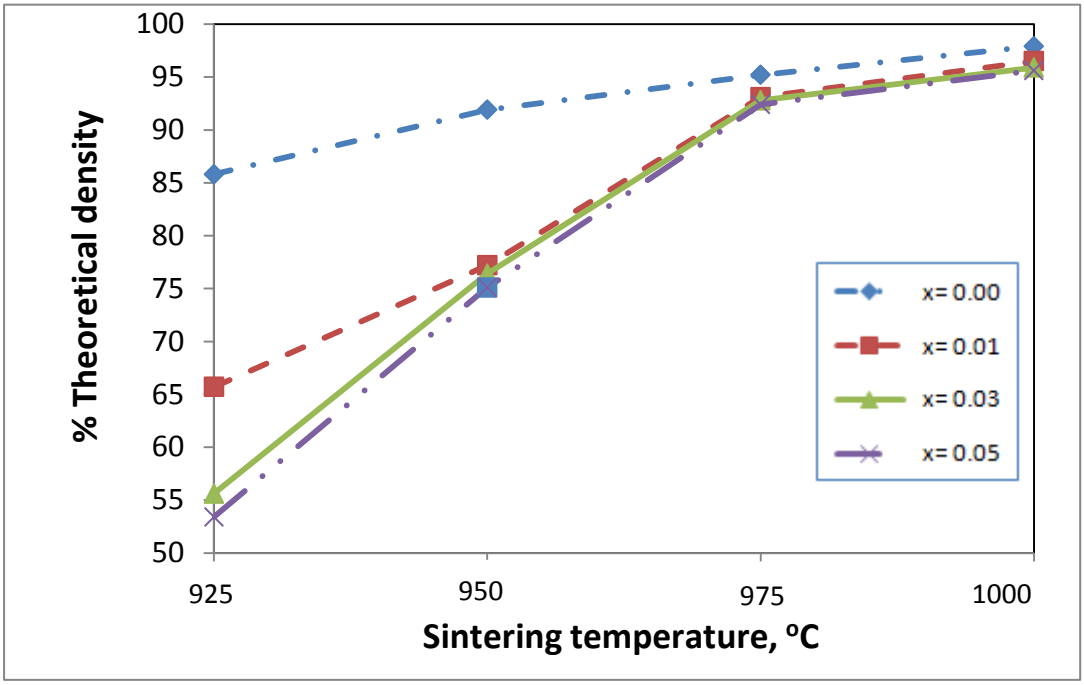

Figure 4.2: Variation of % theoretical density with sintering temperature for 2 hours holding time for $Bi_{0.8}La_{0.2}Fe_{1-x}Ta_xO_3$ (x = 0.0, 0.01, 0.03 and 0.05) ceramics.

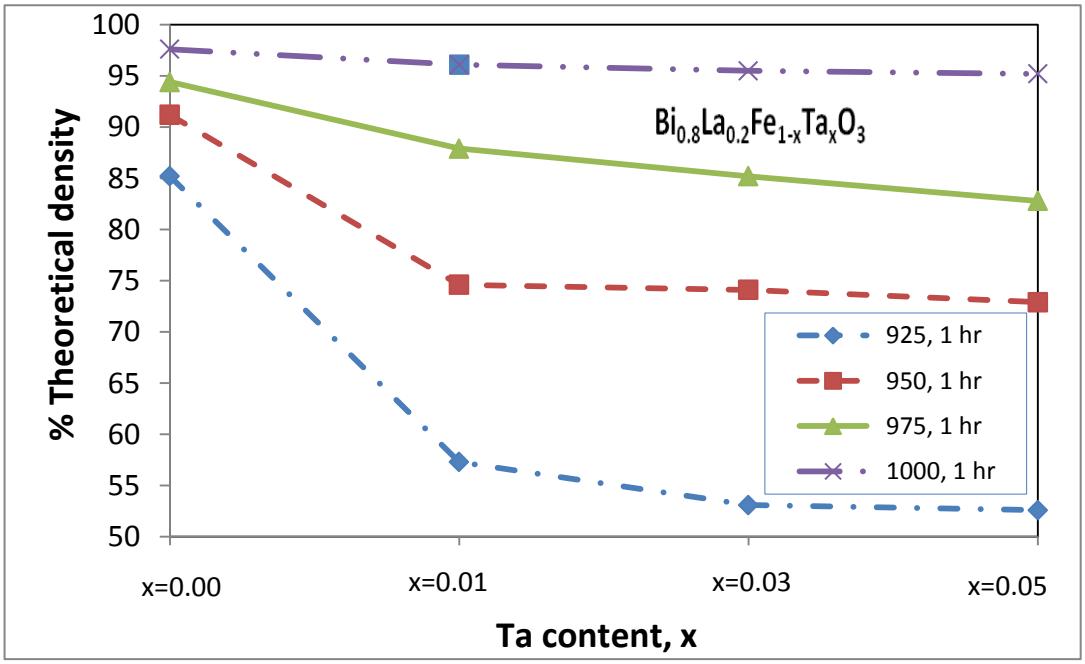

Figure 4.3: Variation of %TD with Ta addition (x) $Bi_{0.8}La_{0.2}Fe_{1-x}Ta_xO_3$ (x = 0.0, 0.01, 0.03 and 0.05) ceramics (holding time 1 hr).

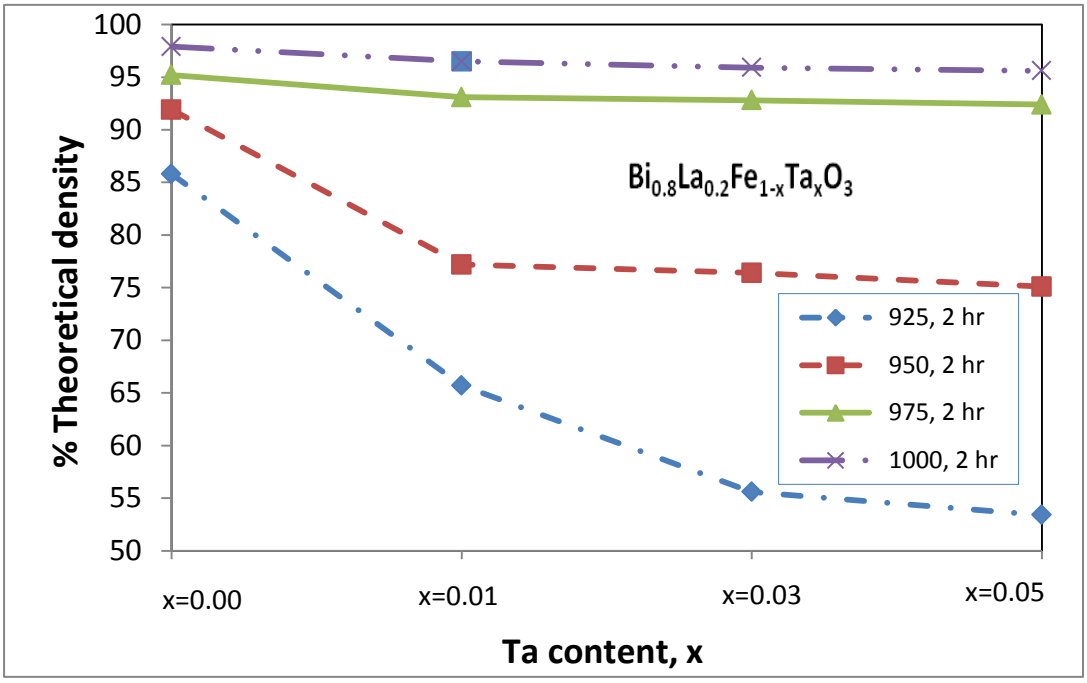

Figure 4.4: Variation of %TD with Ta addition (x) $Bi_{0.8}La_{0.2}Fe_{1-x}Ta_xO_3$ (x = 0.0, 0.01, 0.03 and 0.05) ceramics (holding time 2 hr).

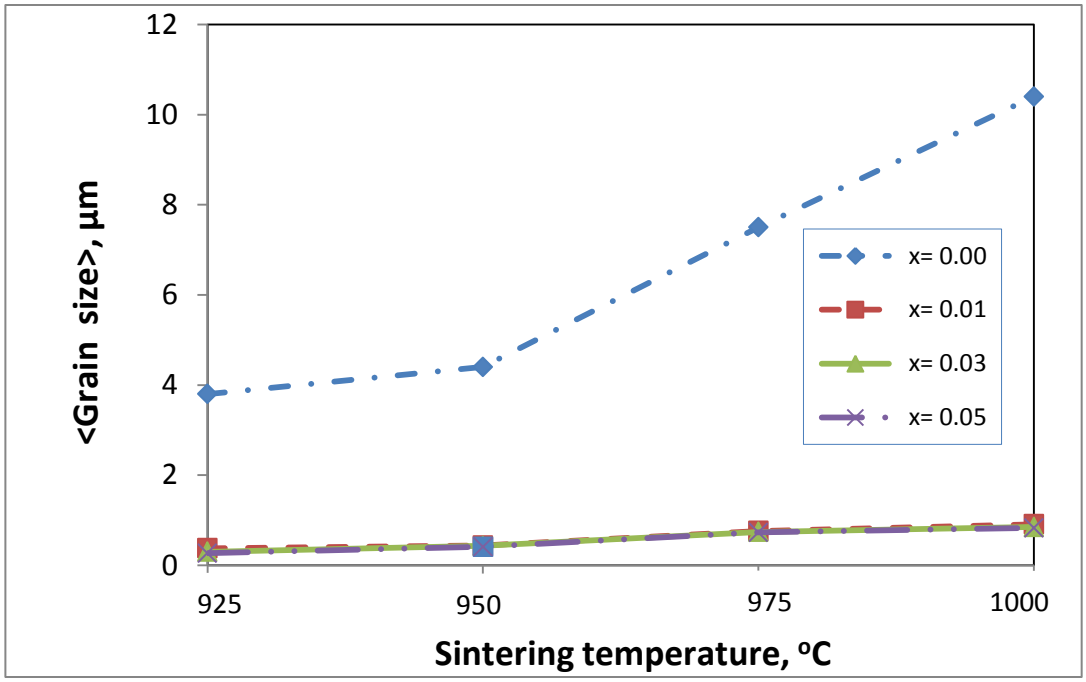

Figure 4.5: Variation of <grain size> for $Bi_{0.8}La_{0.2}Fe_{1-x}Ta_xO_3$ (x = 0.0, 0.01, 0.03 and 0.05) ceramics with sintering temperature (holding time 1 hr)

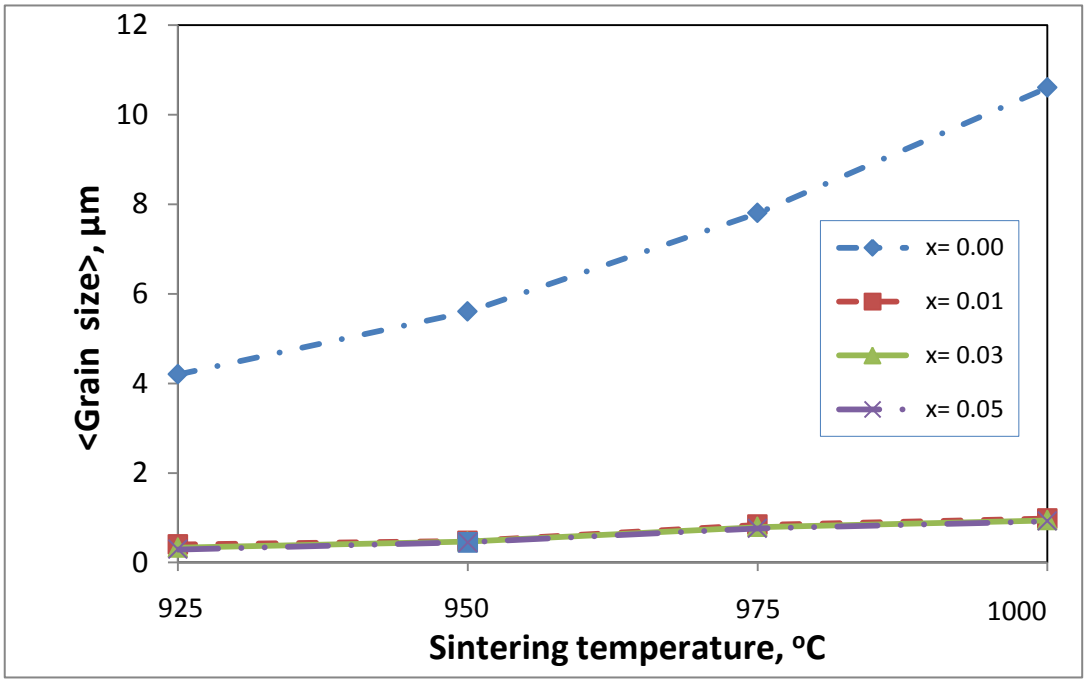

Figure 4.6: Variation of <grain size> for $Bi_{0.8}La_{0.2}Fe_{1-x}Ta_xO_3$ (x = 0.0, 0.01, 0.03 and 0.05) ceramics with sintering temperature (holding time 2 hr)

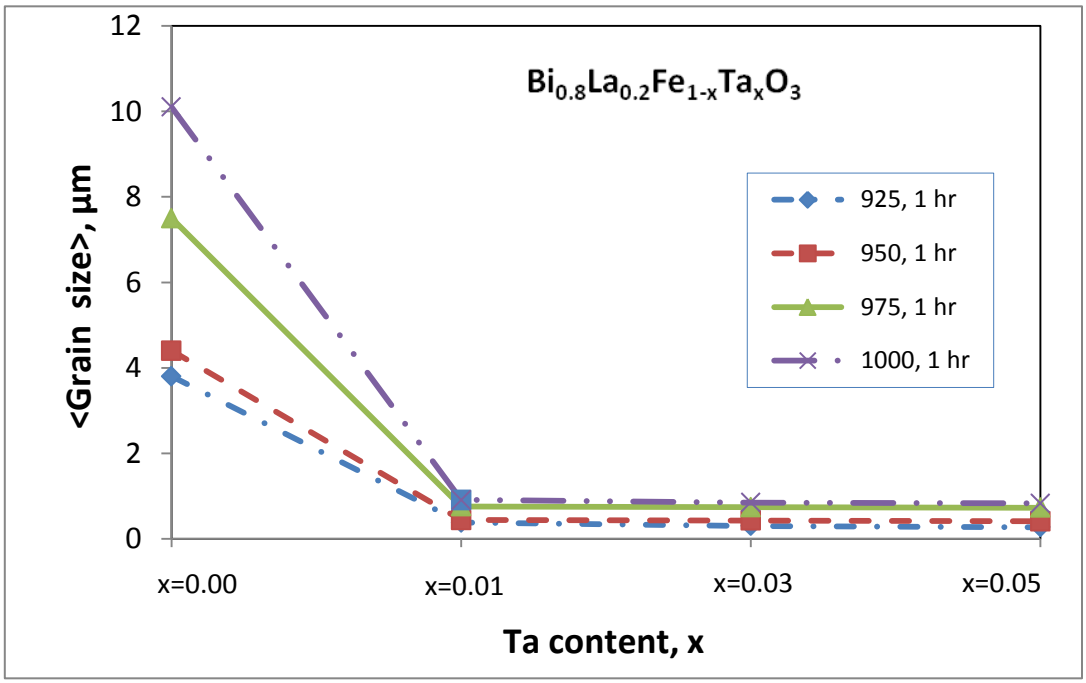

Figure 4.7: Variation of <grain size> of $Bi_{0.8}La_{0.2}Fe_{1-x}Ta_xO_3$ (x = 0.0, 0.01, 0.03 and 0.05) ceramics with Ta addition (x) (holding time 1 hr).

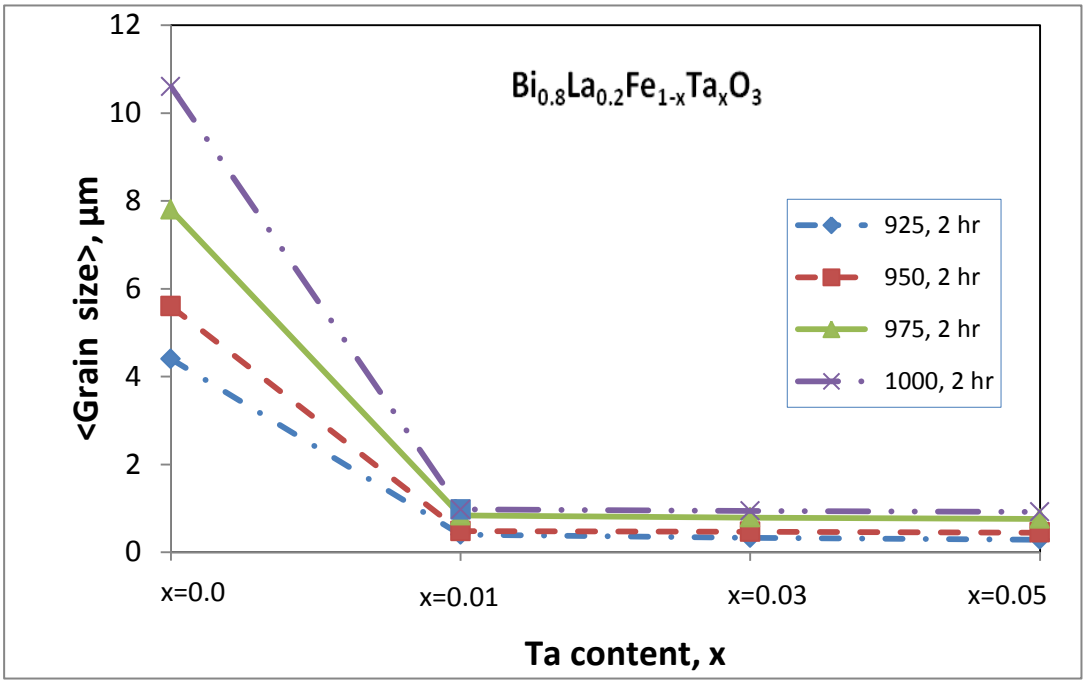

Figure 4.8: Variation of <grain size> of $Bi_{0.8}La_{0.2}Fe_{1-x}Ta_xO_3$ (x = 0.0, 0.01, 0.03 and 0.05) ceramics with Ta addition (x) (holding time 2 hr).

4.3 Microstructure development:

According to literature A-site substitution of $BiFeO_3$ with lanthanum significantly increases its magnetic properties at room temperature. Single-phase $Bi_{0.8}La_{0.2}FeO_3$ ceramic, which has ferroelectric order below a high Curie temperature T_C~830 °C and ferromagnetic order below a high Néel temperature T_N~370 °C, is one of the most widely studied multiferroic materials. But $Bi_{0.8}La_{0.2}FeO_3$ becomes unsuitable for applications owing to its high leakage current, which reduces the dielectric property of the material. The excessive grain growth at high %TD results in shorter grain boundary length, less resistance to electron flow and thus high leakage current. This leakage current can be reduced by controlling the microstructure using proper dopants at B-site. In this thesis B-site was doped with Ta using three compositions, i.e $Bi_{0.8}La_{0.2}Fe_{1-x}Ta_xO_3$ (x=0.01, 0.03 and 0.05). The effect of these compositions on the microstructure was studied in this research as fine-grained (~1μm) structure and high density of the doped $BiFeO_3$ are the prerequisite to obtain good properties.

It still remains a significant challenge to prepare single phase $Bi_{0.8}La_{0.2}FeO_3$ ceramics with sufficiently low leakage current densities. The challenge can further be described by the reaction mechanisms shown in Eqs. 4.1– 4.5. Equations 4.1– 4.5 indicate that if Bi_2O_3, Fe_2O_3, and La_2O_3 powders do not react with each other during the sintering process due to some specific reasons such as the volatilization of Bi_2O_3, insufficient mixing of powders, or inadequate sintering conditions, it will be difficult to form single-phase $Bi_{0.8}La_{0.2}FeO_3$ ceramics [143,144]. The reaction mechanisms are as follows:

$Bi_2O_3 + Fe_2O_3 = (1 - x)\ BiFeO_3 + x/2\ (Bi_2O_3 + Fe_2O_3)$ [no reaction], (4.1)

$(1 - x)Bi_2O_3 + x\ La_2O_3 + Fe_2O_3 = 2(1 - x)\ BiFeO_3 + x\ (La_2O_3 + Fe_2O_3)$ [no reaction], (4.2)

$Bi_2O_3 + Fe_2O_3 = (4/25)\ Bi_{12}\ (Bi_{1/2}Fe_{1/2})\ O_{19} + (24/25)\ Fe_2O_3$ [no reaction], (4.3)

$Bi_2O_3 + Fe_2O_3 = (1/18)\ Bi_{36}Fe_2O_{57} + (17/18)\ Fe_2O_3$ [no reaction], (4.4)

$Bi_2O_3 + Fe_2O_3 = (1/2)\ Bi_2Fe_4O_9 + (1/2)\ Bi_2O_3$ [volatilization or no reaction]. (4.5)

Same conditions apply to $Bi_{0.8}La_{0.2}Fe_{1-x}Ta_xO_3$ (x=0.01, 0.03 and 0.05) ceramics. However, XRD analysis of $Bi_{0.8}La_{0.2}FeO_3$ pellets calcined at 800°C for 2 hours followed by sintering at 850°C

for 2 hours proved the formation of single phase. The XRD analysis of these pellets indicated that the initial raw materials: Bi_2O_3, Fe_2O_3, and La_2O_3 powders reacted completely with each other during the sintering process. Moreover, the XRD analysis of $Bi_{0.8}La_{0.2}Fe_{1-x}Ta_xO_3$ (x=0.01, 0.03 and 0.05) samples prepared under same condition also proved the formation of single phase.

Our next step was to attain an optimum balance between % theoretical density and grain size to improve the multiferroic properties of the samples. Following data reported in literature, the ceramics were calcined at 800°C for 2 hours and then sintered at 25°C intervals in the temperature range of 850-900°C and the microstructure was studied. The % TD attained for all compositions was unsatisfactory after sintering in this temperature range. Although the grains of $Bi_{0.8}La_{0.2}FeO_3$ samples increased from 0.8 µm to about 3 µm between 850-900°C, the densification was still insufficient with %TD below 80% as can be seen in the following figures:

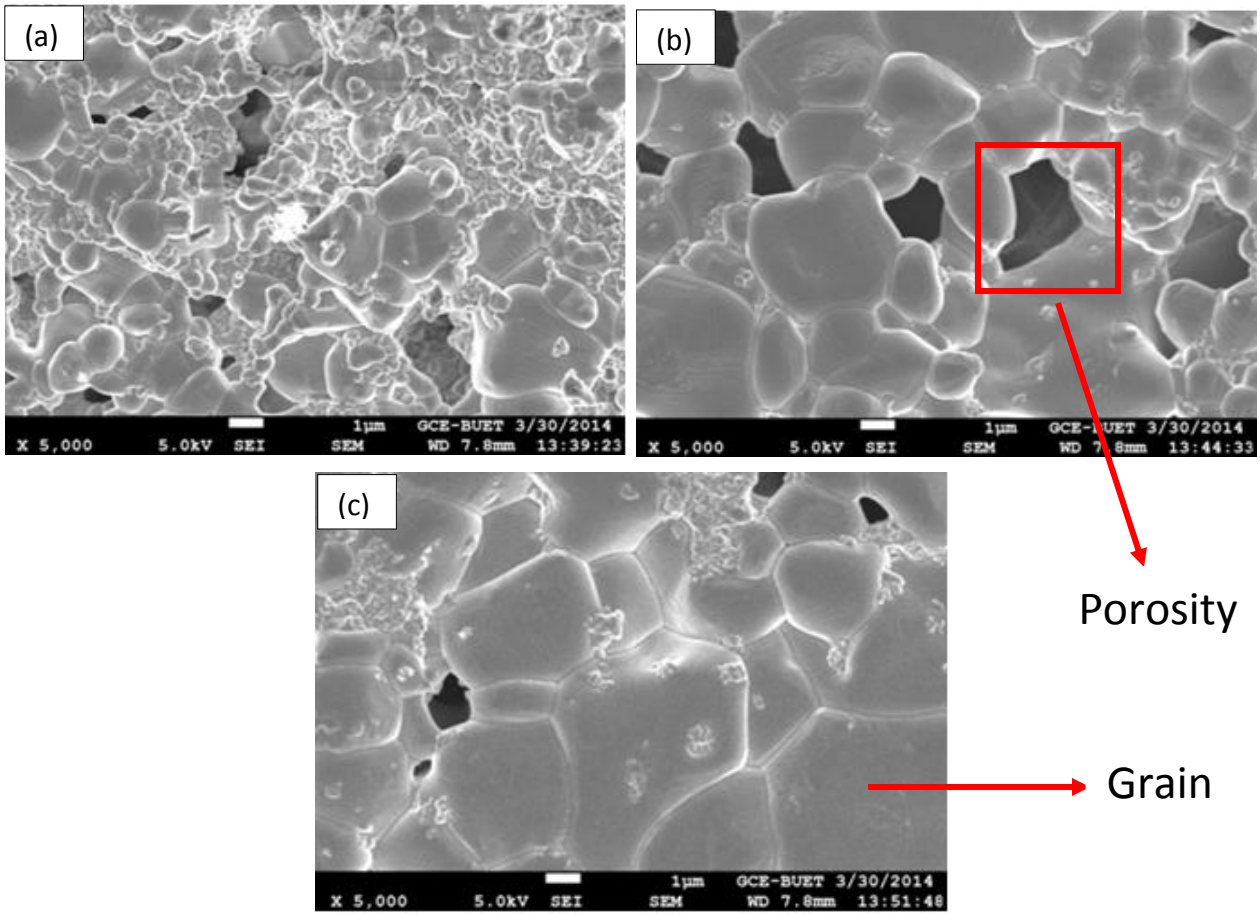

Figure 4.9: FESEM micrograph of $Bi_{0.8}La_{0.2}FeTaO_3$ samples sintered at 850, 875 and 900°C for 2 hours showing variation of <grain size> with temperature.

(a) At 850°C, <Grain size> = 0.8 µm; % TD = 70.1 (b) At 875°C, <Grain size> = 2.2 µm; % TD = 76.2
(c) At 900°C, <Grain size> = 3.0 µm; % TD = 79.6

Figures 4.9 (a) , (b) and (c) show the gradual elimination of porosity by increase in sintering temperature and a corresponding increase in grain size at higher temperatures. At 900^{o}C although the porosity has significantly decreased than ceramics sintered at lower temperatures the %TD attained is still insufficient.

The %TD of $Bi_{0.8}La_{0.2}Fe_{1-x}Ta_xO_3$ (x=0.01, 0.03 and 0.05) ceramics sintered in this temperature range was even worse and it deteriorated with increasing Ta percentage. The grain size of the samples was too small with no indication of proper grain growth. This clearly indicated that the provided temperature and holding time was not sufficient to achieve the desired densification for these samples. Evidently, the microstructure of these samples contained lots of visible pores, as shown in figures below:

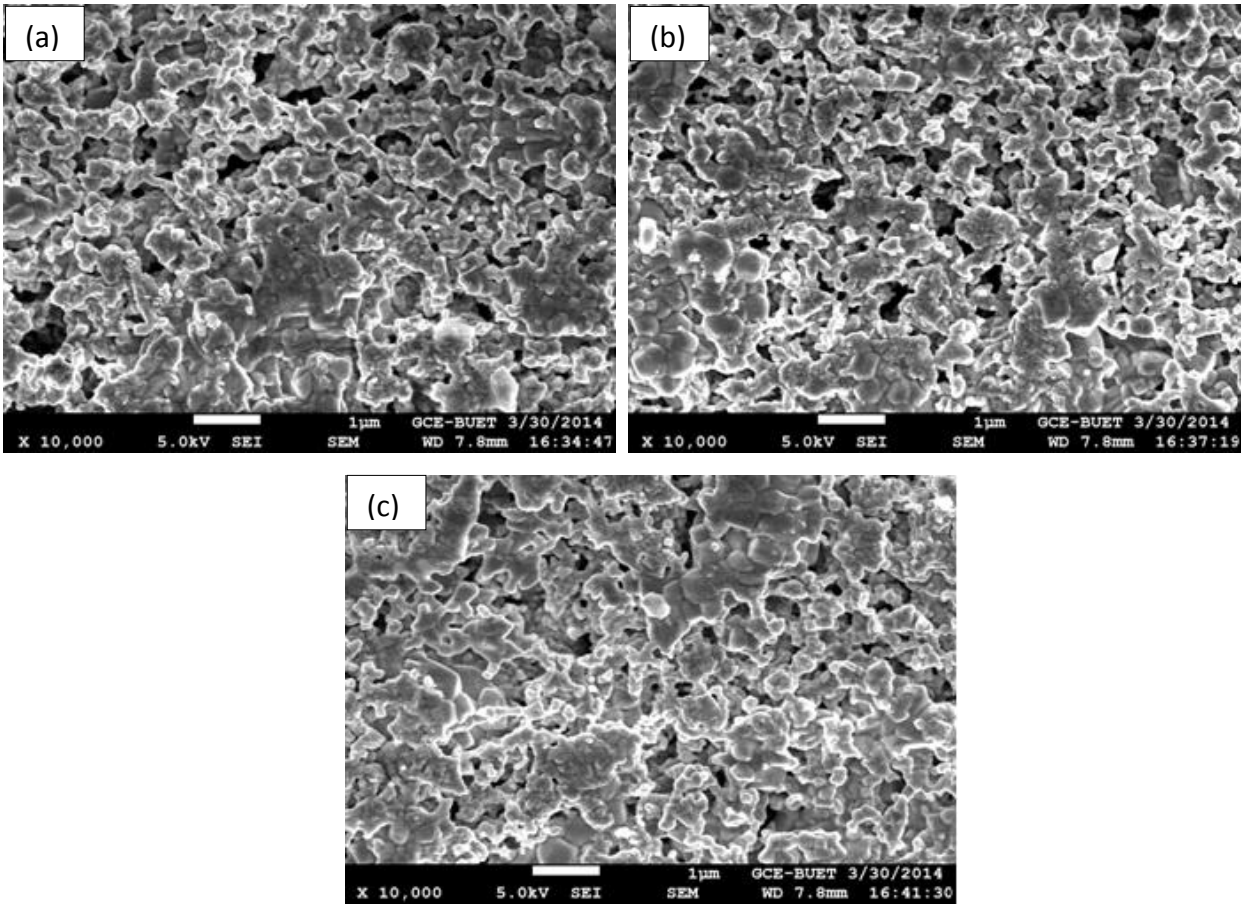

Figure 4.10: FESEM micrograph of $Bi_{0.8}La_{0.2}Fe_{1-x}Ta_xO_3$ samples sintered at 850^{o}C for 2 hours showing variation of <grain size>with Ta content.

(a) x = 0.01; <Grain size> = < 0.2 µm; % TD = 49.8 (b) x = 0.03; <Grain size> = < 0.2 µm; % TD = 49.2
(c) x = 0.05; <Grain size> = < 0.2 µm; % TD = 48.4

Figures 4.10 (a), (b) and (c) show $Bi_{0.8}La_{0.2}Fe_{1-x}Ta_xO_3$ (x=0.01, 0.03 and 0.05) ceramics sintered at 850^oC for 2 hours. From these figures it is evident that this sintering temperature is inadequate for pore removal and attainment of satisfactory %TD. The %TD is below 50% for all compositions at this sintering temperature.

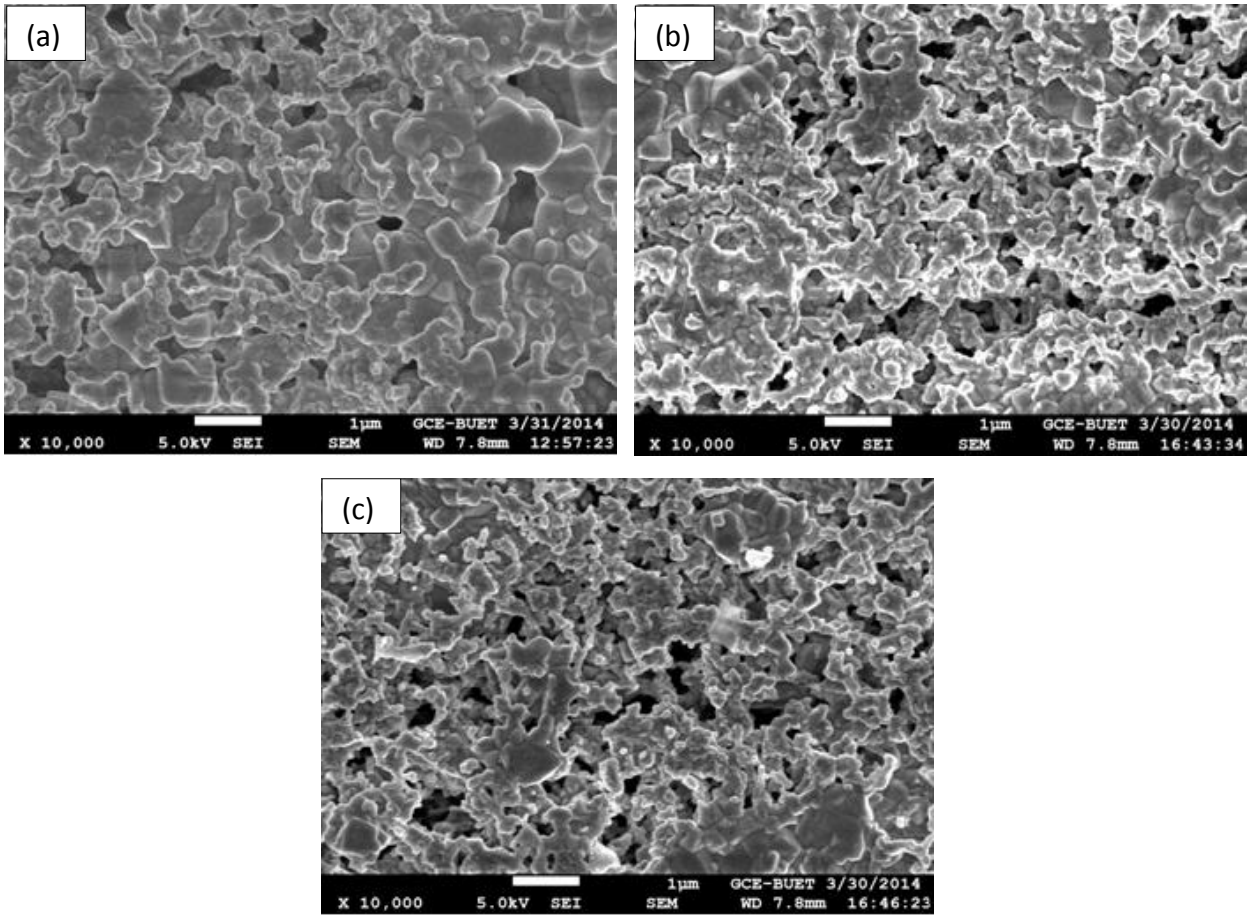

Figure 4.11: FESEM micrograph of $Bi_{0.8}La_{0.2}Fe_{1-x}Ta_xO_3$samples sintered at 875$^oC$ for 2 hours showing variation of <grain size> with Ta content.

(a) x = 0.01; <Grain size> = < 0.2 µm; % TD = 52.6 (b) x = 0.03; <Grain size> = < 0.2 µm; % TD = 52.1
(c) x = 0.05; <Grain size> = < 0.2 µm; % TD = 51.7

Figures 4.11 (a), (b) and (c) show $Bi_{0.8}La_{0.2}Fe_{1-x}Ta_xO_3$ samples sintered at 875^oC for 2 hours. Comparing with Figure 4.10 it is obvious that the porosity level has decreased with increase in temperature. Moreover, comparing figure 4.11 (a), (b) and (c) it is obvious that with increase in Ta content the densification becomes poorer and the porosity level increases gradually from x=0.01 to x=0.05. The %TD achieved at this temperature is still very poor (around 50%) and the grain size is below 0.2 µm.

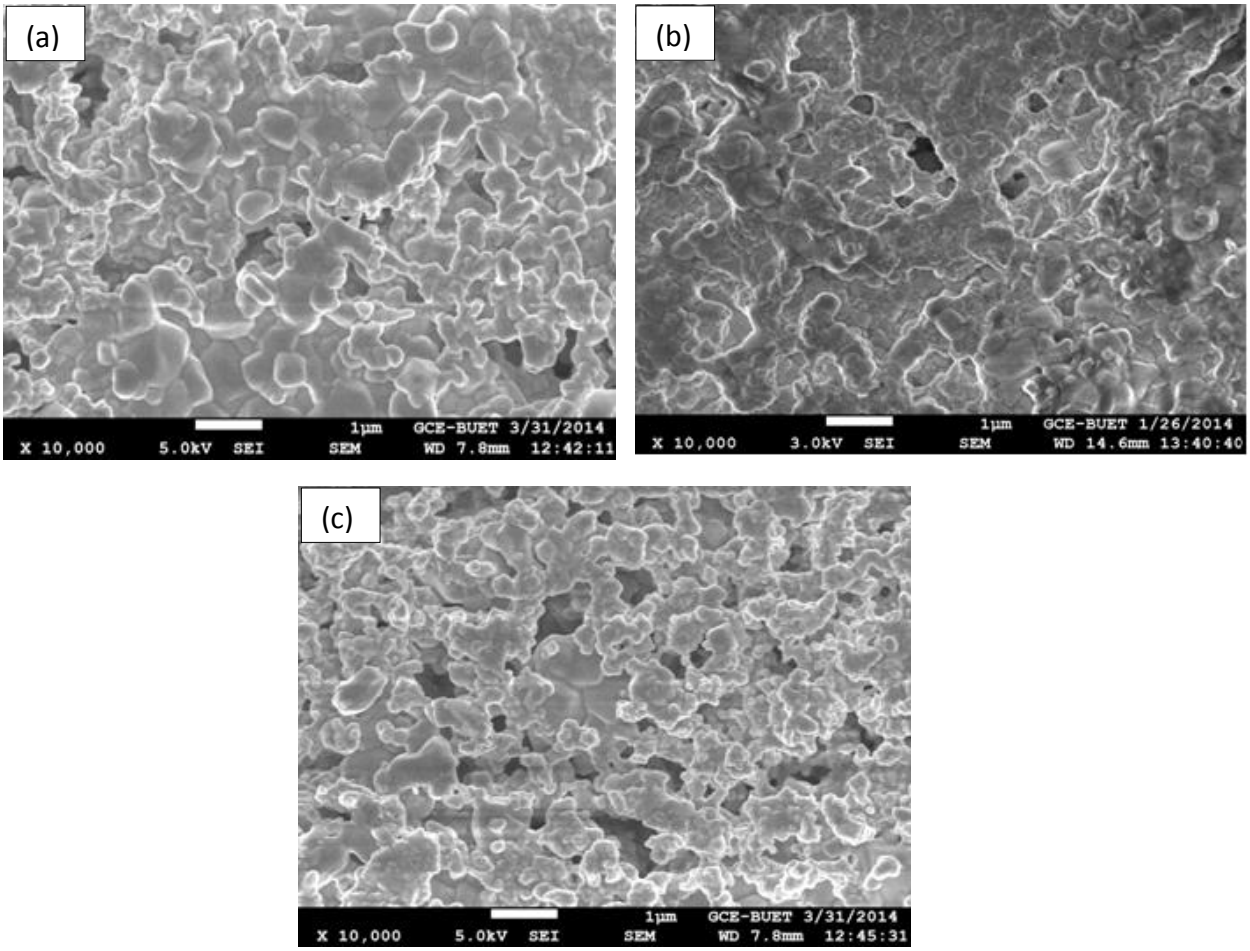

Figure 4.12: FESEM micrograph of $Bi_{0.8}La_{0.2}Fe_{1-x}Ta_xO_3$ samples sintered at 900°C for 2 hours showing variation of <grain size> with Ta content.

(a) x= 0.01; <Grain size> = < 0.3 µm; % TD = 54.1 (b) x = 0.03; <Grain size> = < 0.2 µm; % TD = 53.8
(c) x = 0.05; <Grain size> = < 0.2 µm; % TD = 53.2

Figures 4.12 (a), (b) and (c) show $Bi_{0.8}La_{0.2}Fe_{1-x}Ta_xO_3$ samples sintered at 900°C for 2 hours. Comparing figure 4.12 with figures 4.11 and 4.10 it is clear that the extent of densification has improved and the grain size has slightly increased. Again, the porosity level has decreased with increase in temperature. As stated earlier, comparing figure 4.12 (a), (b) and (c) shows that with increase in Ta content the densification becomes poorer and the visible porosity level increases gradually figure 4.12 (a) to (c). The %TD achieved at this temperature is still very poor, below 60%.

As no work has been reported on Ta doped $BiFeO_3$ till now, so identifying the proper sintering zone for $Bi_{0.8}La_{0.2}Fe_{1-x}Ta_xO_3$ (x = 0.01, 0.03 and 0.05) samples was a challenging task in this thesis. But the effects of Ta doping on the microstructure has been studies earlier by previous researchers. According to literature donor dopants deteriorate the grain growth rate and inhibit densification of ceramic materials. In this case, Ta^{5+} substituting the Fe^{3+} ions act as a donor dopant.

It is well known that in $BiFeO_3$ perovskites, the oxygen vacancies (Vo^{2+}) could be formed in the process of sintering due to the escape of oxygen from the lattice [145]. Vo^{2+} comes mainly from Bi volatility and the transition from Fe^{3+} to Fe^{2+} which can be described by equations (4.6) and (4.7): [146]

$$2Fe^{3+} + O^{2-} \rightarrow 2Fe^{2+} + Vo^{2+} + 0.5O_2 \quad (4.6)$$

$$2Bi^{3+} + 3O^{2-} \rightarrow 2V_{Bi}^{3-} + 3Vo^{2+} + Bi_2O_3 \quad (4.7)$$

The addition of Ta^{5+} at Fe-site required charge compensation which can be achieved by filling of oxygen vacancies. The decrease in grain growth of $Bi_{0.8}La_{0.2}Fe_{1-x}Ta_xO_3$ (x=0.01, 0.03 and 0.05) ceramics can be interpreted by the suppression of oxygen vacancy concentration, which in return results in slower oxygen ion motion and consequently lower grain growth rate and less densification.

In order to provide sufficient energy for proper densification and grain growth the samples were then sintered above 900^oC. Keeping other parameters constant, the samples were sintered at 925°C, 950°C, 975°C and 1000°C for a holding time of 1 and 2 hours. Higher holding times at the assigned temperatures were avoided to control excessive grain growth of the $Bi_{0.8}La_{0.2}FeO_3$ ceramics.

Figure 4.13 and 4.14 show the microstructure of the $Bi_{0.8}La_{0.2}Fe_{1-x}Ta_xO_3$ ceramics sintered at 925°C for both 1 and 2 hours, respectively.

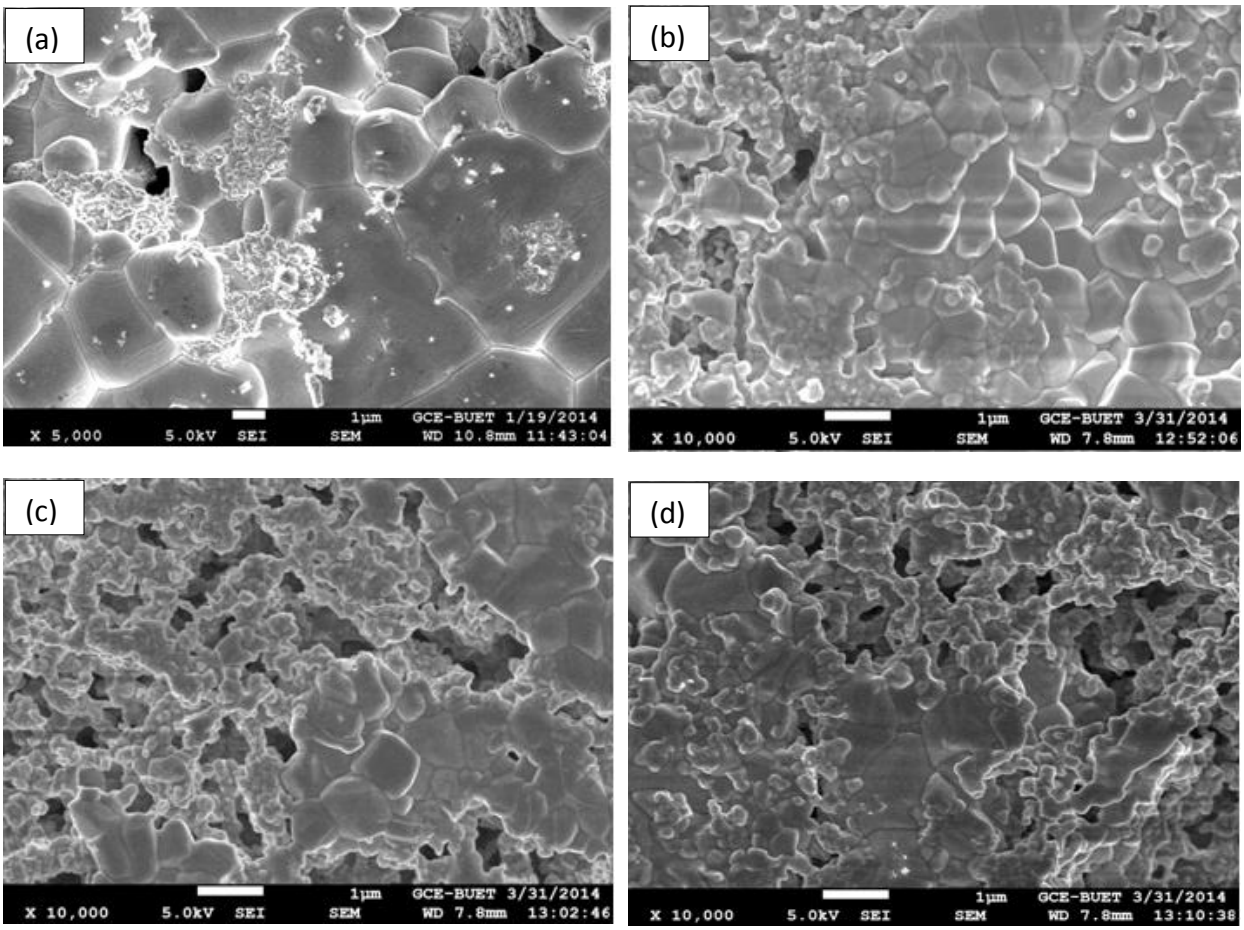

Figure 4.13: FESEM micrograph of $Bi_{0.8}La_{0.2}Fe_{1-x}Ta_xO_3$ samples sintered at 925°C for 1 hour showing variation of <grain size> with Ta content.

(a) x = 0.0; <Grain size> = 3.8µm; % TD = 85.2 (b) x = 0.01; <Grain size> = 0.38 µm; % TD = 57.3
(c) x = 0.03; <Grain size> = 0.3 µm; % TD = 53.1 (d) x=.05; <Grain size> = 0.27 µm; % TD = 52.6

FESEM micrograph of Figure 4.13 (a), shows that for $Bi_{0.8}La_{0.2}FeO_3$ ceramics sintering was moderate for 1 hour holding time at 925°C and resulted in % TD above 85%. But, addition of Ta dramatically decreased the extent of densification and resulted in porous structures for $Bi_{0.8}La_{0.2}Fe_{1-x}Ta_xO_3$ (x=0.01, 0.03 and 0.05) ceramics. The % TD achieved in these ceramics fell below 60% and the grain size attained at this temperature was 3.8µm for $Bi_{0.8}La_{0.2}FeO_3$ and decreased to 0.27 µm for $Bi_{0.8}La_{0.2}Fe_{0.95}Ta_{0.05}O_3$ ceramics.

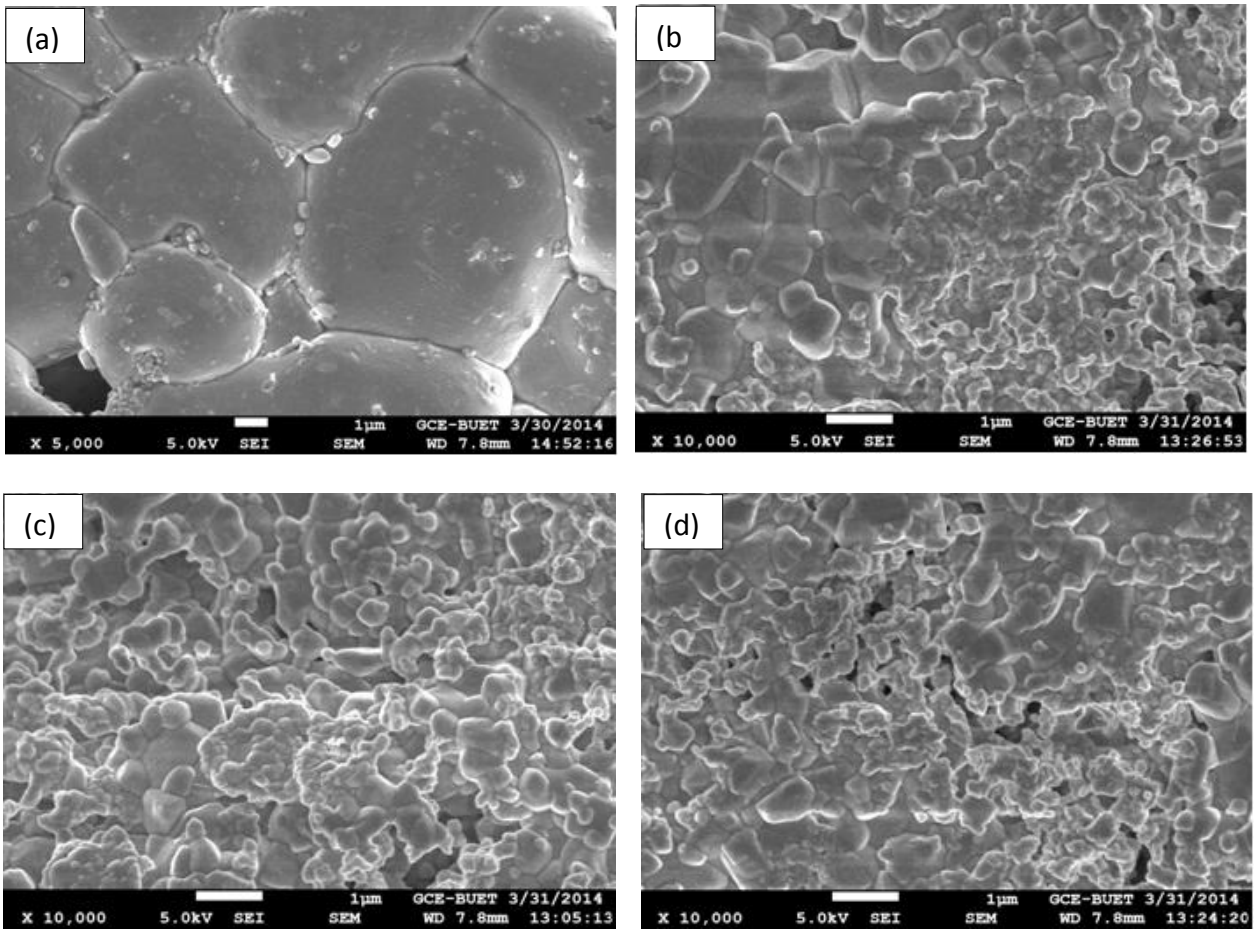

Figure 4.14: FESEM micrograph of $Bi_{0.8}La_{0.2}Fe_{1-x}Ta_xO_3$samples sintered at 925$^oC$ for 2 hours showing variation of <grain size> with Ta content.

(a) x = 0.0; <Grain size> = 4.2 µm; % TD = 85.8 (b) x = 0.1; <Grain size> = 0.4 µm; % TD = 65.7
(c) x = 0.03; <Grain size> = 0.33µm; % TD = 59.6 (d) x = 0.05; <Grain size> = 0.29µm; % TD = 53.4

Figure 4.14 reveals that after 2 hours of holding at 925^oC, although the porosity deceased considerably compared to the ceramics sintered up to 900^oC but this was accompanied with rapid increase in grain size of the $Bi_{0.8}La_{0.2}FeO_3$ samples to 4.2 µm with increasing temperature as shown in Figure 4.14 (a). Furthermore increasing the holding time from 1 to 2 hours resulted in better densification of the ceramics. However, the sintering was still insufficient for $Bi_{0.8}La_{0.2}Fe_{1-x}Ta_xO_3$ (x=0.01, 0.03 and 0.05) ceramics as shown in figures 4.14 (b), (c) and (d) and %TD deteriorated with increasing additions of Tantalum.

The microstructure of the $Bi_{0.8}La_{0.2}Fe_{1-x}Ta_xO_3$ ceramics sintered at 950°C for both 1 and 2 hours are shown in figures 4.15 and 4.16 respectively.

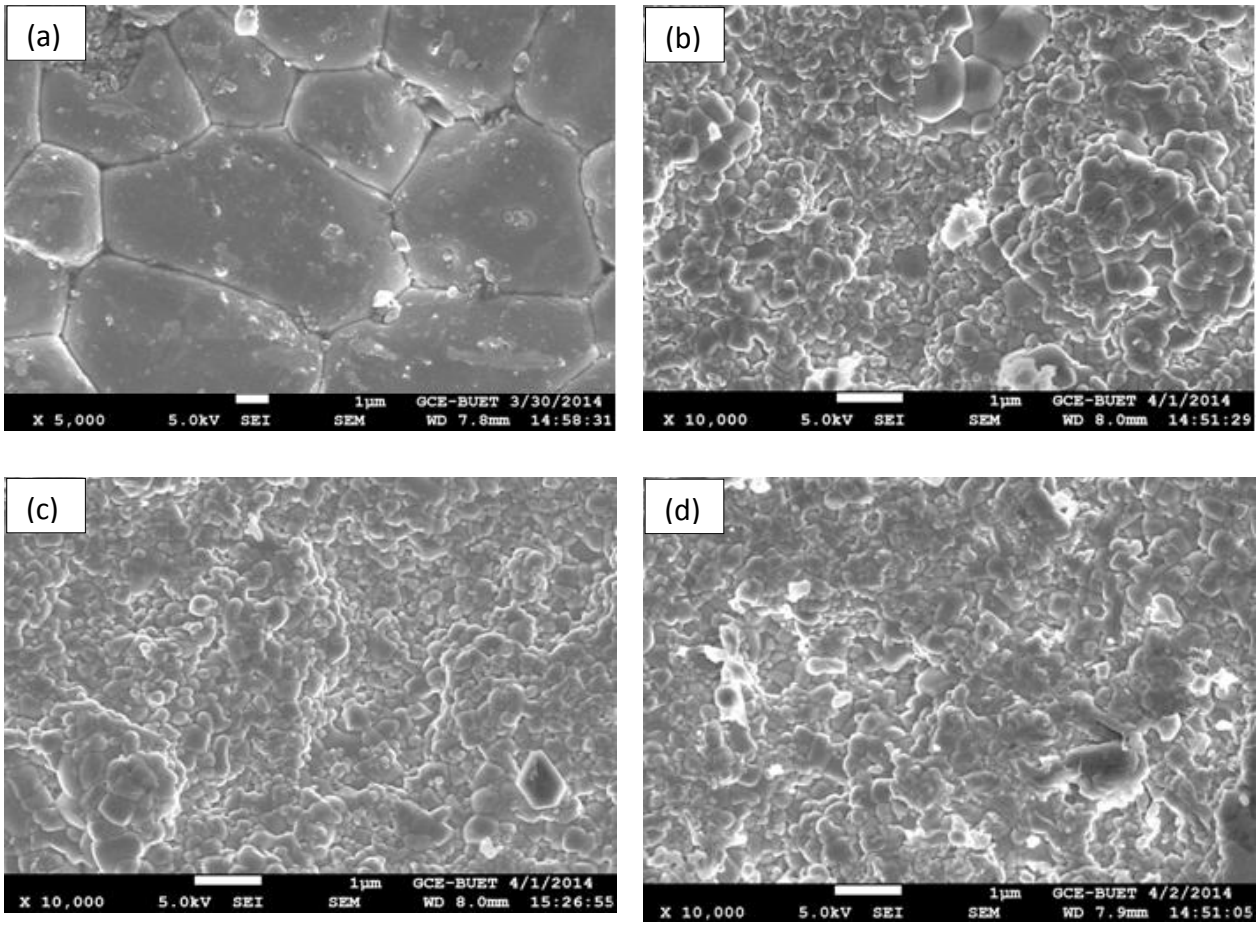

Figure 4.15: FESEM micrograph of $Bi_{0.8}La_{0.2}Fe_{1-x}Ta_xO_3$ samples sintered at 950°C for 1 hour showing variation of <grain size> with Ta content.

(a) x = 0.0; <Grain size> = 4.4 µm; % TD = 91.2 (b) x = 0.1; <Grain size> = 0.44 µm; % TD = 74.6
(c) x = 0.03; <Grain size> = 0.43µm; % TD = 74.1 (d) x = 0.05; <Grain size> = 0.41µm; % TD = 72.9

Comparing figures 4.15 (a) with that of figure 4.13 and 4.14 (a) it is apparent that the porosity of the $Bi_{0.8}La_{0.2}FeO_3$ ceramics has been completely eliminated. Hence, the % TD obtained for $Bi_{0.8}La_{0.2}FeO_3$ is above 90%. Nevertheless, the grain size of the $Bi_{0.8}La_{0.2}FeO_3$ ceramics continued to grow rapidly. Moreover, micrographs above show that addition of Ta inhibited the densification process and resulted in samples of reduced compactness. From the figures 4.15 (a), (b), (c) and (d) it is clearly evident that sintering up to 950°C was inadequate to offer sufficient energy for proper coalescence hence resulting in inadequate densification for the Ta doped

samples. Increasing the holding time from 1 to 2 hours at 950°C results slightly in improved %TD and larger grain size for $Bi_{0.8}La_{0.2}FeO_3$ but the %TD of $Bi_{0.8}La_{0.2}Fe_{1-x}Ta_xO_3$ (x=0.01, 0.03 and 0.05) ceramics is still below 80%.

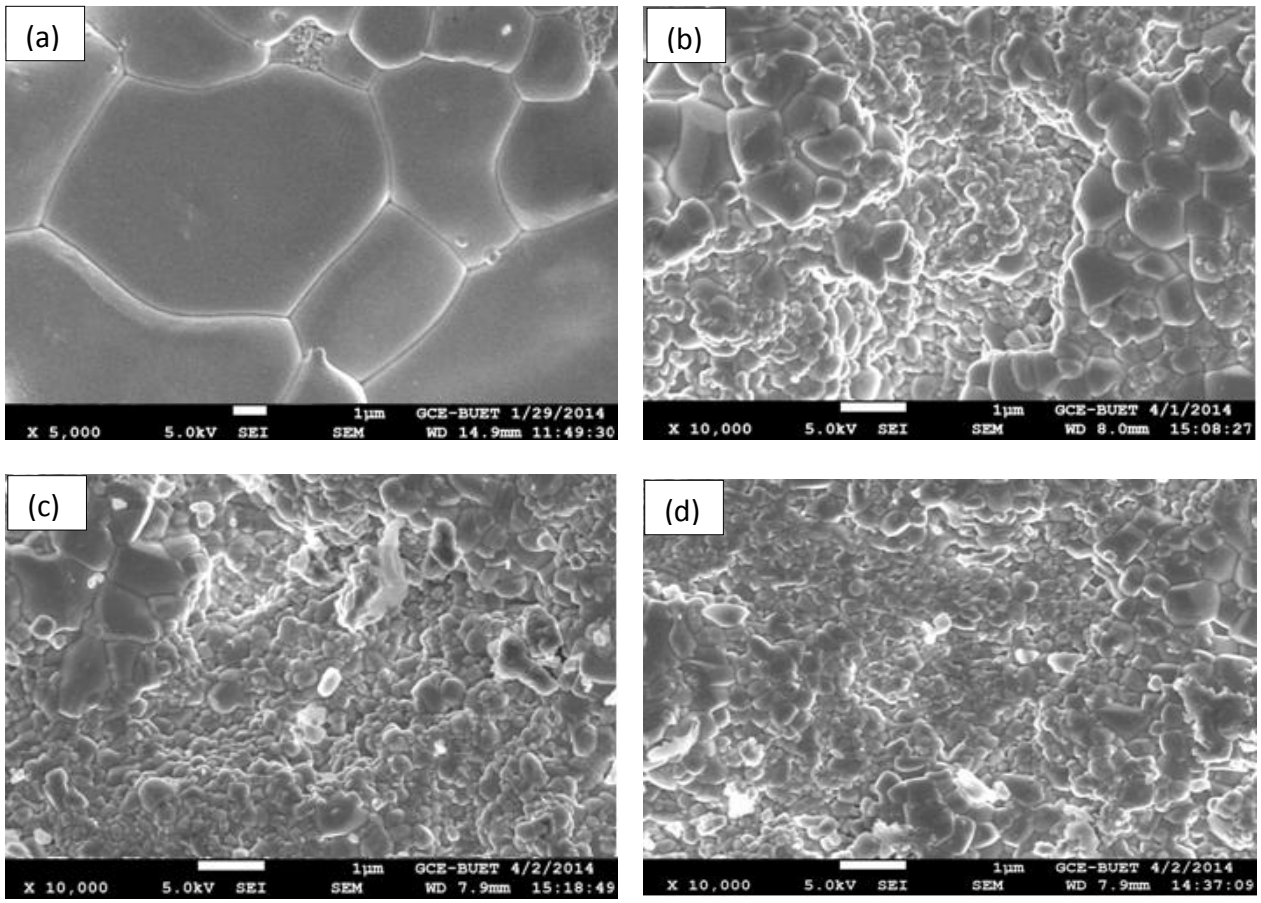

Figure 4.16: FESEM micrograph of $Bi_{0.8}La_{0.2}Fe_{1-x}Ta_xO_3$samples sintered at 950°C for 2 hours showing variation of <grain size> with Ta content.

(a) x = 0.0; <Grain size> = 5.6 µm; % TD = 91.9 (b) x = 0.01; <Grain size> = 0.48 µm; % TD = 77.2
(c) x = 0.03; <Grain size> = 0.465 µm; % TD = 76.4 (d) x = 0.05; <Grain size> = 0.45 µm; % TD = 75.1

These results clearly indicates the necessity for even higher temperature of sintering in order to obtain better densification, especially for $Bi_{0.8}La_{0.2}Fe_{1-x}Ta_xO_3$ where the solute drag or pinning effect of Ta inhibits the densification process [147]. So, this time the sintering temperature was increased to 975°C keeping other parameters constant.

Sintering temperature of 975^{o}C proved to be adequate for all compositions providing good %TD. However, the grain size in Ta added BFO was still below 0.8 µm so further increase in grain size was required for the $Bi_{0.8}La_{0.2}Fe_{1-x}Ta_xO_3$ (x =0.01, 0.03 and 0.05) samples for better ferroelectric properties as average grain size of about 0.8 µm - 1 µm is normally required to obtain good values of permittivity in ceramics.

The FESEM micrograph of all the samples sintered at 975^{o}C for holding times of 1 and 2 hours are shown in figures 4.17 and 4.18 respectively.

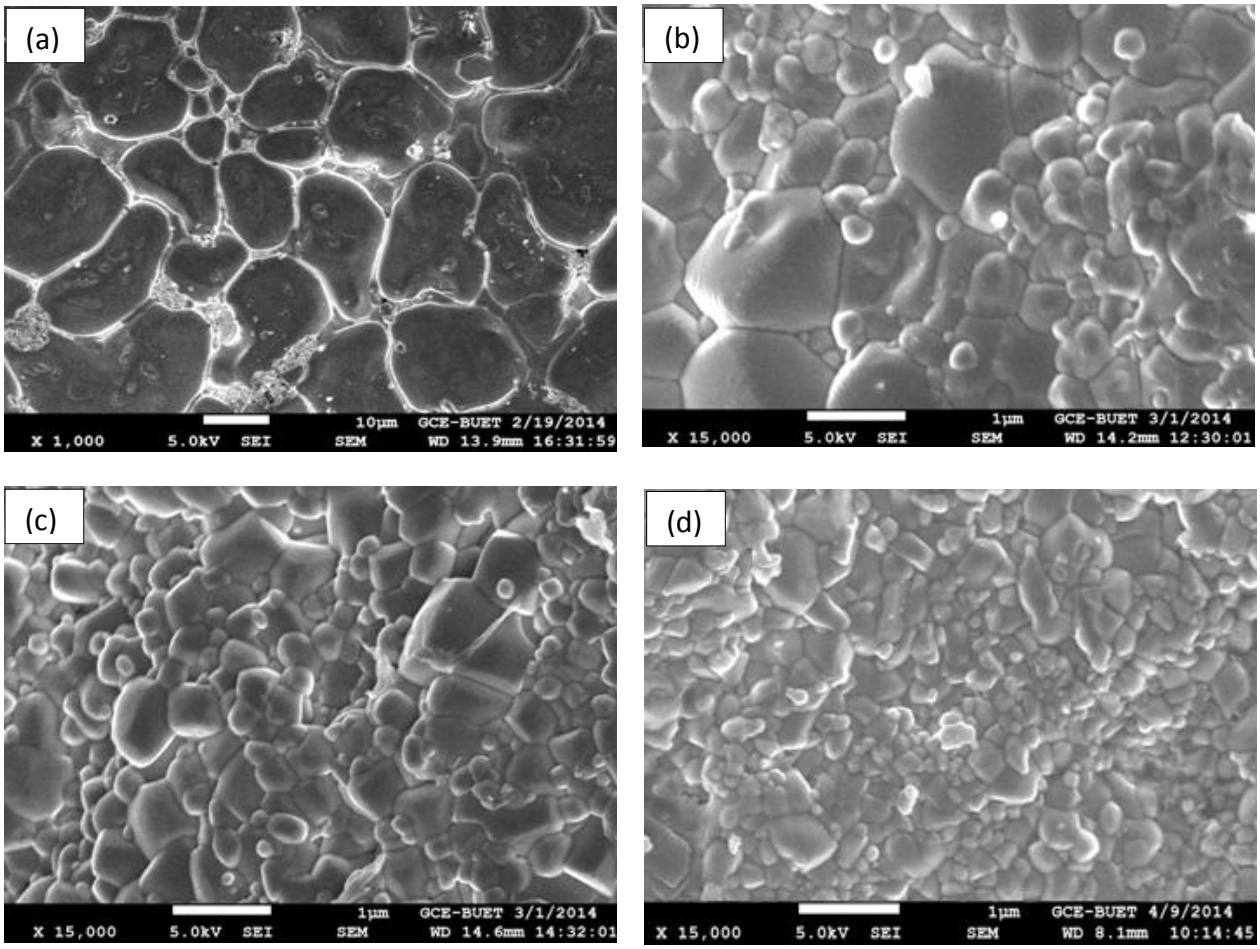

Figure 4.17: FESEM micrograph of $Bi_{0.8}La_{0.2}Fe_{1-x}Ta_xO_3$samples sintered at 975^{o}C for 1 hour showing variation of <grain size> with Ta content.

(a) x = 0.0; <Grain size> = 7.5 µm; % TD = 94.4 (b) x = 0.01; <Grain size> = 0.76 µm; % TD = 87.9
(c) x = 0.03; <Grain size> = 0.74 µm; % TD = 85.2 (d) x = 0.05; <Grain size> = 0.73 µm; % TD = 82.8

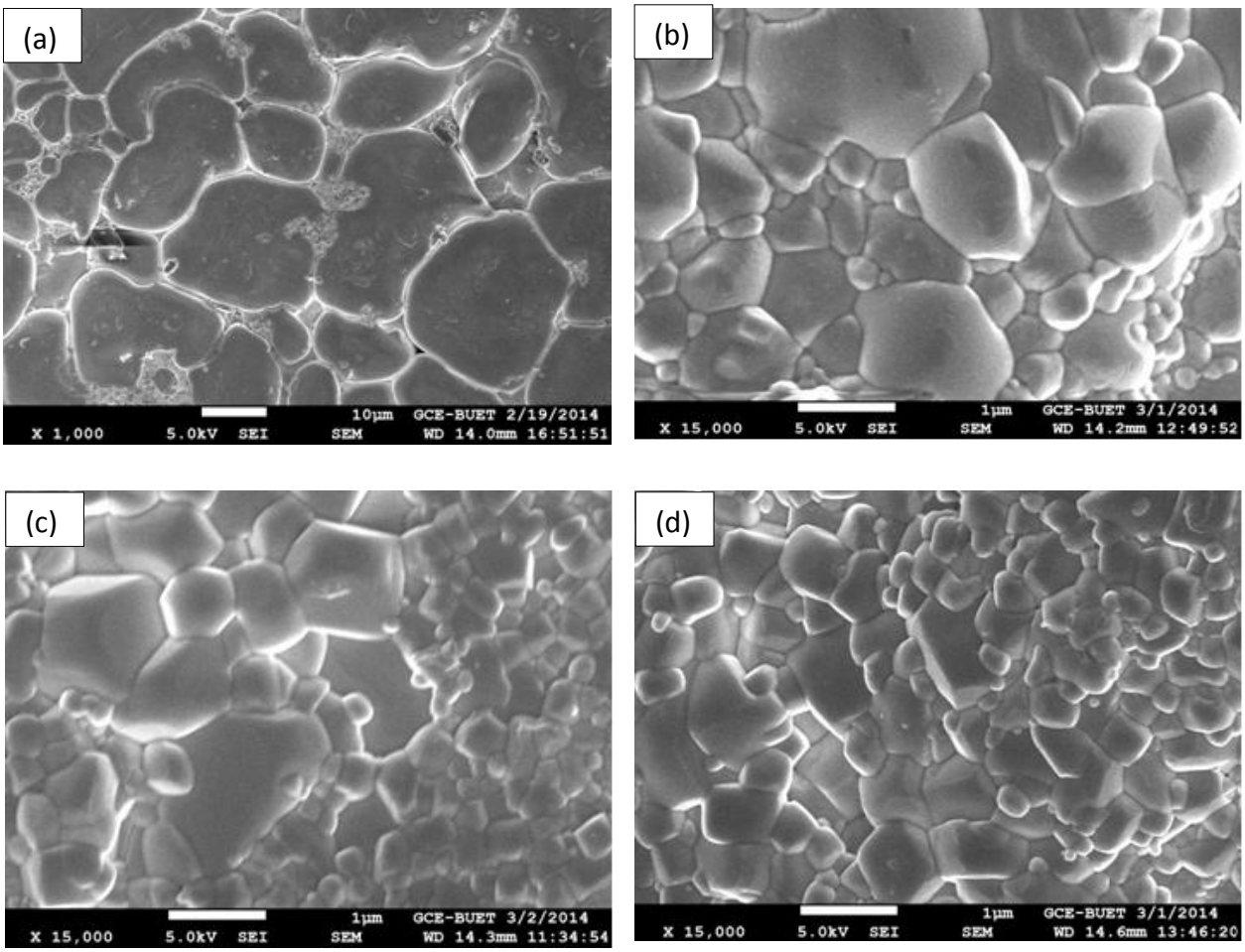

Figure 4.18: FESEM micrograph of $Bi_{0.8}La_{0.2}Fe_{1-x}Ta_xO_3$ samples sintered at 975^oC for 2 hours showing variation of <grain size> with Ta content.

(a) x = 0.0; <Grain size> = 7.8 µm; % TD = 95.2 (b) x = 0.01; <Grain size> = 0.84 µm; % TD = 93.1
(c) x = 0.03; <Grain size> = 0.79 µm; % TD = 92.8 (d) x= .05; <Grain size> = 0.76 µm; % TD = 92.4

In order to further improve the %TD and also the ferroelectric properties by attaining the desired grain size, the samples were next sintered at 1000^oC for 1 and 2 hours. Good combination of %TD (>95%) and grain size (0.92-.98 µm) was attained for all $Bi_{0.8}La_{0.2}Fe_{1-x}Ta_xO_3$ (x = 0.0, 0.01, 0.03 and 0.05) samples sintered at this temperature for 2 hours. However, for $Bi_{0.8}La_{0.2}FeO_3$ samples, the excellent %TD attained at sintering temperatures of 975^oC and 1000^oC for both 1and 2 hours holding time was accompanied by excessive grain growth which may have detrimental effects on the ferroelectric properties due to shortening of the grain boundary length that decreases resistance to leakage current.

The FESEM micrograph of all the samples sintered at 1000^{o}C for holding times of 1 and 2 hours are shown in figures 4.19 and 4.20 respectively.

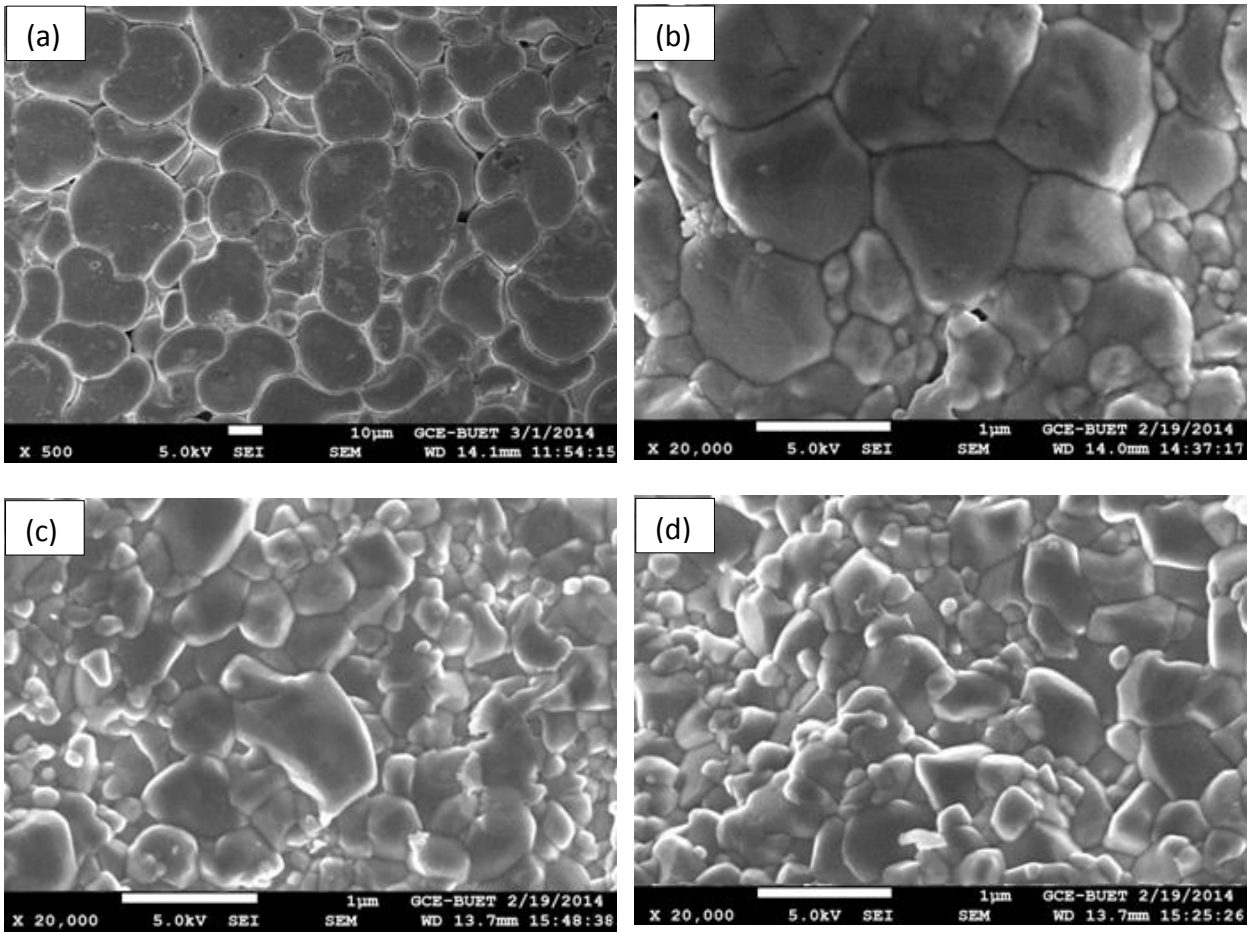

Figure 4.19: FESEM micrograph of $Bi_{0.8}La_{0.2}Fe_{1-x}Ta_xO_3$samples sintered at 1000^{o}C for 1 hour showing variation of <grain size> with Ta content.

(a) x = 0.0; <Grain size> = 10.4 µm; % TD = 97.6 (b) x = 0.01; <Grain size> = 0.91 µm; % TD = 96.1
(c) x= 0.03; <Grain size> = 0.85 µm; % TD = 95.5 (d) x=.05; <Grain size> = 0.83 µm; % TD = 95.2

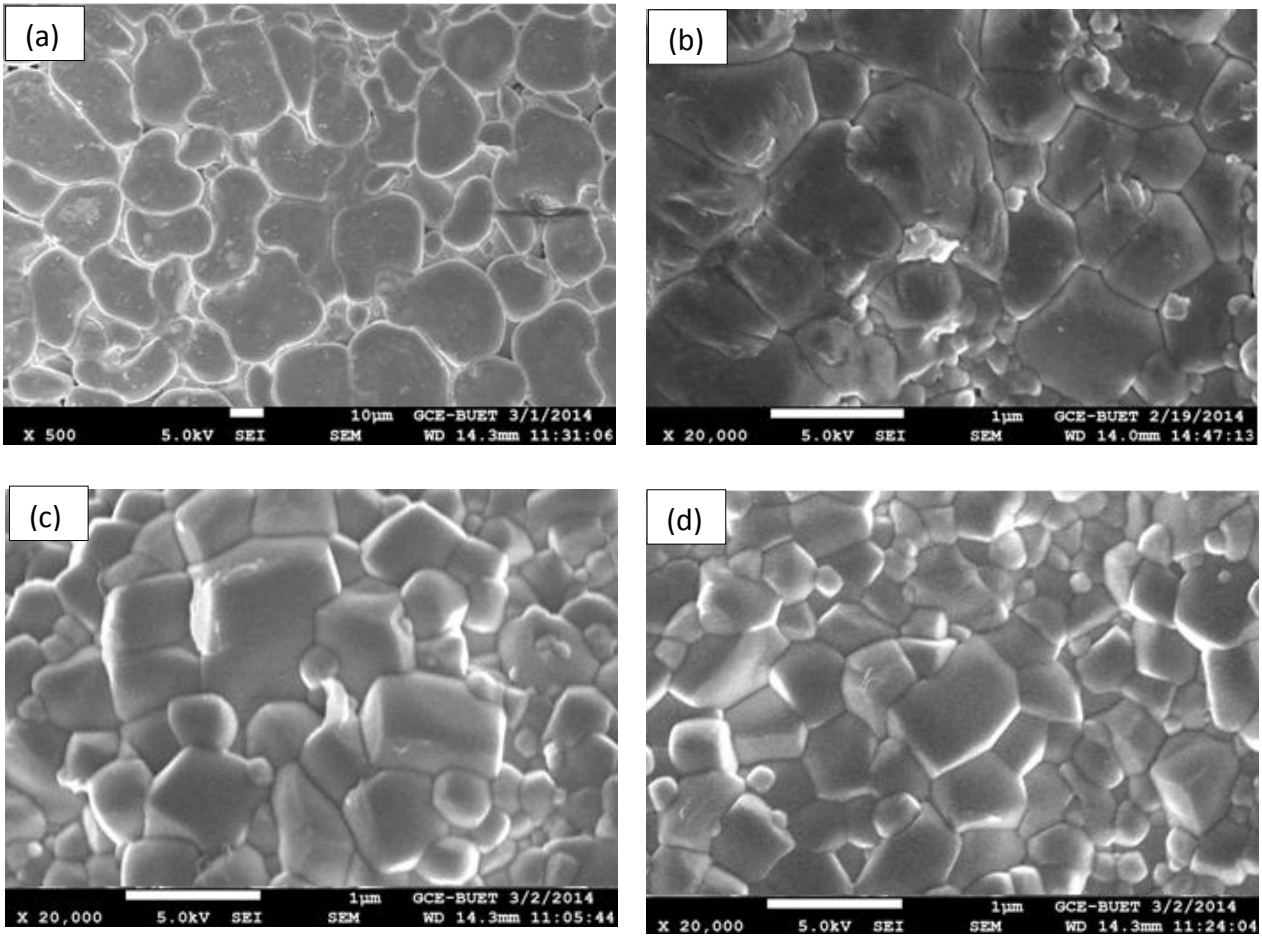

Figure 4.20: FESEM micrograph of $Bi_{0.8}La_{0.2}Fe_{1-x}Ta_xO_3$samples sintered at 1000$^oC$ for 2 hours showing variation of <grain size> with Ta content.

(a) x = 0.0; <Grain size> = 10.6 µm; % TD = 97.9 (b) x = 0.01; <Grain size> = 0.98 µm; % TD = 96.5
(c) x = 0.03; <Grain size> = 0.94 µm; % TD = 95.9 (d) x = 0.05; <Grain size> = 0.92 µm; % TD = 95.6

The results shown till now reveal that, the effect of holding time on sintering is linear but the effect of sintering temperature is exponential on grain size. In figure 4.20, the FESEM images of the $Bi_{0.8}La_{0.2}Fe_{1-x}Ta_xO_3$ (x = 0.0, 0.01, 0.03 and 0.05) samples sintered at 1000^oC confirm the grain growth suppression action of Ta. Moreover, it is obvious that for a particular sintering temperature such as 1000^oC the grain size decreased with increasing Ta addition from 10 µm in $Bi_{0.8}La_{0.2}FeO_3$ to 0.8 µm in $Bi_{0.8}La_{0.2}Fe0_{.95}Ta0_{.05}O_3$. Density measurement also indicates that with increase in grain size the density of the samples increases which is in accordance to previous researchers [148]. However, even though high densification of $Bi_{0.8}La_{0.2}FeO_3$ was achieved when sintered at 1000^oC for 2 hours, the excessive grain growth may have detrimental

effects on its multiferroic properties. The best combination of %TD and grain size was attained for $Bi_{0.8}La_{0.2}Fe_{1-x}Ta_xO_3$ samples when sintered at 1000°C for 2 hours.

4.4 XRD analysis:

Figure 1 shows the XRD patterns at room temperature of $Bi_{0.8}La_{0.2}Fe_{1-x}Ta_xO_3$ samples (x= 0.00, 0.01, 0.03, 0.05) sintered at 1000°C for 2 hours indicating that distorted rhombohedral R3c structure was formed without any second phase. The figure shows no significant difference in the position of the planes from that of original rhombohedral R3c structure planes (designated by dark green lines at the bottom) of pure $BiFeO_3$. However, the slight splitting of the peak at 2θ= 46° may indicate a possible phase transformation from rhombohedral to tetragonal.

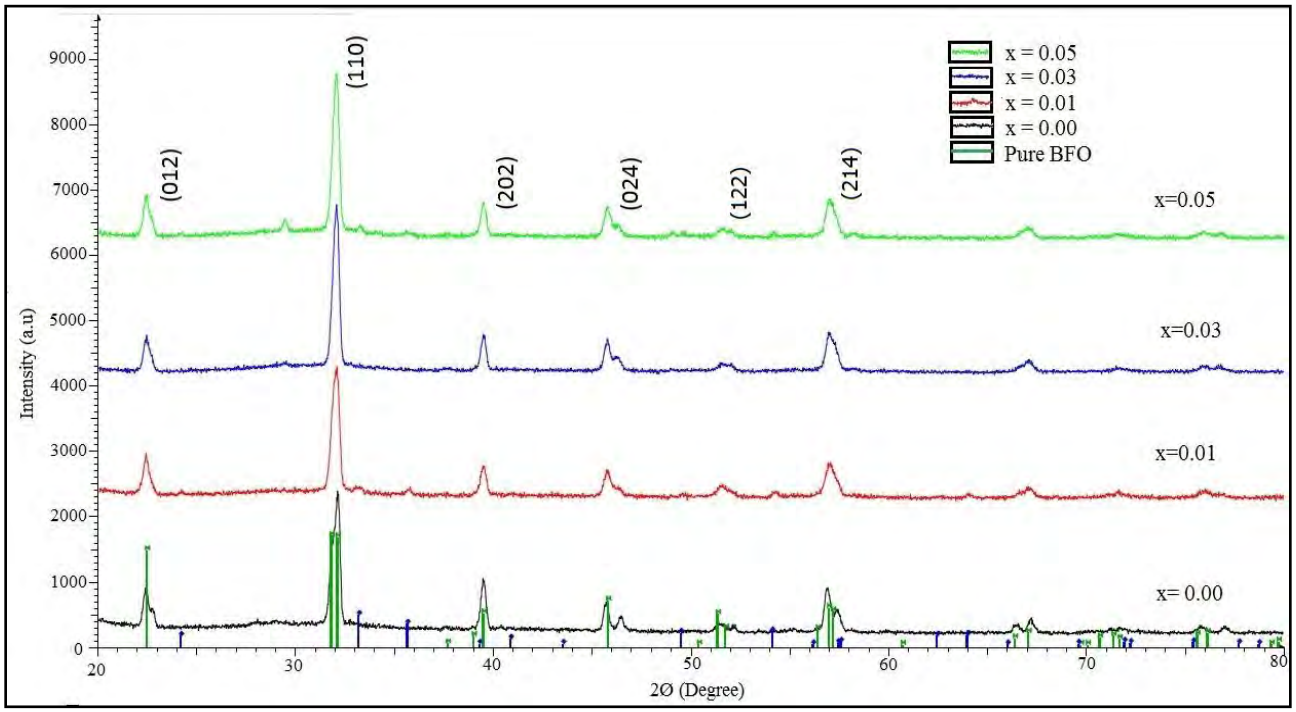

Figure 4.21: XRD patterns at room temperature of $Bi_{0.8}La_{0.2}Fe_{1-x}Ta_xO_3$ samples (x= 0.00, 0.01, 0.03, and 0.05) sintered at 1000°C for 2 hours

It is known that the RT phase of pure BFO is a rhombohedrally distorted perovskite structure described by space group R3c. Rhombohedral cell is very close to the cubic one (angle α in the rhombohedral cell is about 89.4°). In this structure, cations are displaced from their centrosymmetric position along the pseudocubic [1 1 1] C axes [153]. The unit cell can also be

described in a hexagonal frame of reference with hexagonal c-axis parallel to the diagonals of the perovskite cube. Therefore, the miller indices (hkl) of diffraction peaks in figure 4.21 are referred to as hexagonal axes rather than rhombohedral axes.

In order to obtain the detailed crystal structure parameters of $Bi_{0.8}La_{0.2}Fe_{1-x}Ta_xO_3$ ceramics, Rietveld refinements were used to analyze the XRD data of the samples. To model a crystal structure with the Rietveld refinement, we must fit a large number of experimental parameters in addition to the crystallographic parameters. The Rietveld refinement of the XRD patterns for of $Bi_{0.8}La_{0.2}Fe_{1-x}Ta_xO_3$ ceramics was performed using same space group, i.e. R3c and the structural model allowed us to reproduce all the observed peaks. The initial Rietveld refinement was carried out by zero point shift, the unit cell and background parameters. After a good match, the peak positions were achieved, the peak profile parameters including the peak symmetry were refined. Rietveld refinement confirmed the formation of a single phase in all samples. The detailed parameters obtained from Rietveld refinements are listed in Table 4.2.

Table 4.2: Structural parameters of refined of $Bi_{0.8}La_{0.2}Fe_{1-x}Ta_xO_3$ samples (x= 0.00, 0.01, 0.03, 0.05) samples

Composition	Lattice parameters (Å)	Volume/unit cell (Å^3)	R-factors
x= 0.00	c= 13.8660	V= 373.39	R_{wp} = 12.430
	a= 5.56621		R_f = 8.890
			R_{Bragg} = 7.440
x= 0.01	c= 13.7924	V= 370.53	R_{wp} = 11.230
	a= 5.56961		R_f = 8.229
			R_{Bragg} = 7.980
x= 0.03	c= 13.6996	V= 368.28	R_{wp} = 10.760
	a= 5.57551		R_f = 7.840
			R_{Bragg} = 8.552
x= 0.05	c= 13.6756	V= 368.83	R_{wp} = 9.830
	a= 5.57644		R_f = 7.390
			R_{Bragg} = 11.955

4.5 Dielectric property measurement

Fine grained and dense samples exhibit good dielectric properties. However, too fine a grain size has an adverse effect on dielectric property. From literature it is evident that usually microstructures having ~1μm average grain size provide good dielectric properties. However, attainment of an optimum between grain size and %TD is the prerequisite for excellent dielectric properties.

In this thesis, the %TD attained was not satisfactory up to 950^{o}C for all compositions. The %TD values started to improve significantly after increasing the sintering temperature to 975^{o}C. Hence, moderately good values of dielectric constant were obtained for samples sintered at this temperature. The values increased rapidly for samples sintered at 1000^{o}C due to achievement of optimum %TD and grain size. The key conditions which provided high values of dielectric constant are listed below:

Table 4.3: List of key conditions providing high dielectric constant

Sl No.	Sintering Temperature (^{o}C)	Holding Time (hours)	Composition	Percent Theoretical Density (%TD)	Grain Size μm	Dielectric Constant k
1	975	1	$Bi_{0.8}La_{0.2}FeO_3$	94.4	7.50	240
			$Bi_{0.8}La_{0.2}Fe_{0.99}Ta_{0.01}O_3$	87.9	0.76	560
			$Bi_{0.8}La_{0.2}Fe_{0.97}Ta_{0.03}O_3$	85.2	0.74	575
			$Bi_{0.8}La_{0.2}Fe_{0.95}Ta_{0.05}O_3$	84.8	0.73	580
2	975	2	$Bi_{0.8}La_{0.2}FeO_3$	95.2	7.80	210
			$Bi_{0.8}La_{0.2}Fe_{0.99}Ta_{0.01}O_3$	93.1	0.84	1140
			$Bi_{0.8}La_{0.2}Fe_{0.97}Ta_{0.03}O_3$	92.8	0.79	1260
			$Bi_{0.8}La_{0.2}Fe_{0.95}Ta_{0.05}O_3$	92.4	0.76	1290
3	1000	1	$Bi_{0.8}La_{0.2}FeO_3$	97.6	10.4	180
			$Bi_{0.8}La_{0.2}Fe_{0.99}Ta_{0.01}O_3$	96.1	0.91	1710
			$Bi_{0.8}La_{0.2}Fe_{0.97}Ta_{0.03}O_3$	95.5	0.85	1800
			$Bi_{0.8}La_{0.2}Fe_{0.95}Ta_{0.05}O_3$	95.2	0.83	1820
4	1000	2	$Bi_{0.8}La_{0.2}FeO_3$	97.9	10.6	160
			$Bi_{0.8}La_{0.2}Fe_{0.99}Ta_{0.01}O_3$	96.5	0.98	2100
			$Bi_{0.8}La_{0.2}Fe_{0.97}Ta_{0.03}O_3$	95.9	0.94	2210
			$Bi_{0.8}La_{0.2}Fe_{0.95}Ta_{0.05}O_3$	95.6	0.92	2290

The results of the table are represented in graphical form in the next page:

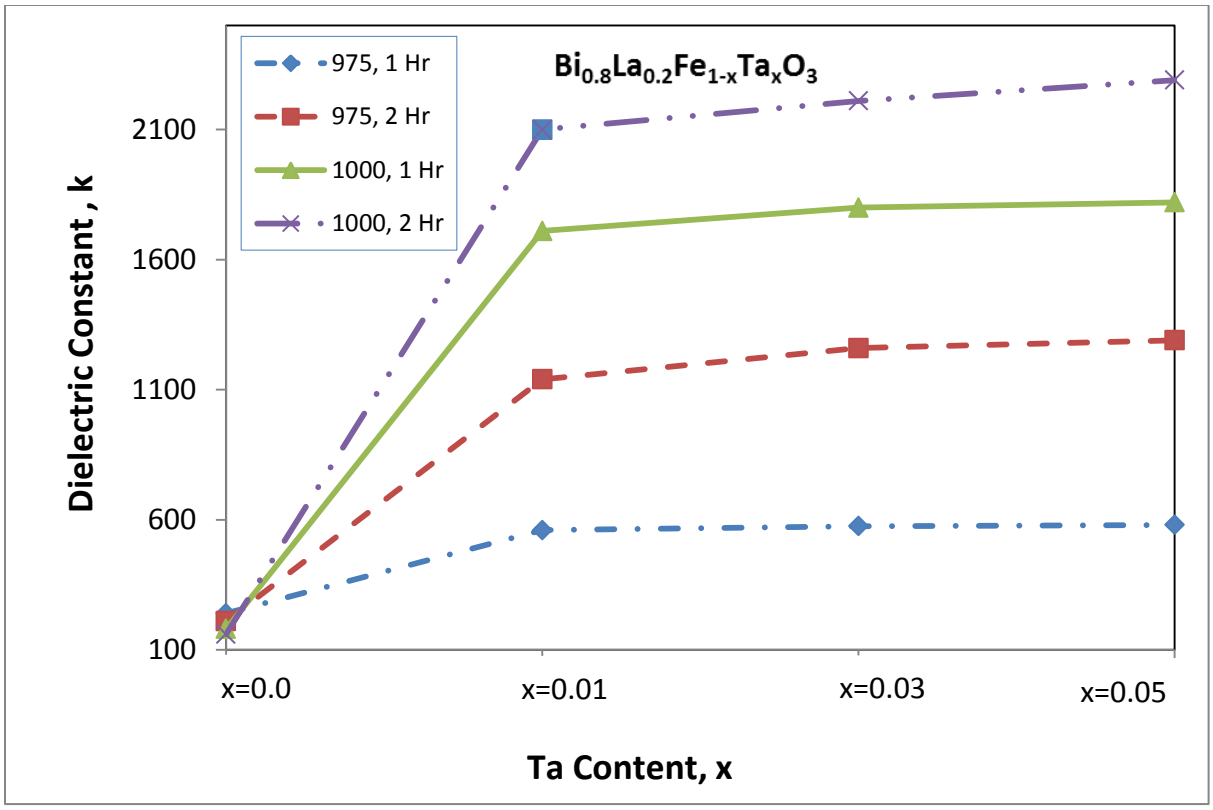

Figure 4.22: Variation of dielectric constant with Ta addition (x) for $Bi_{0.8}La_{0.2}Fe_{1-x}Ta_xO_3$ samples (x= 0.00, 0.01, 0.03, and 0.05) sintered at 975 and 1000°C for both 1 and 2 hours.

The data from figure 4.22 reveals that for each sintering condition there is a sharp drop in dielectric constant value for $Bi_{0.8}La_{0.2}FeO_3$ sample. In other words, addition of Ta to the $Bi_{0.8}La_{0.2}FeO_3$ ceramics results in a sharp rise in the dielectric constant. The main cause of poor dielectric properties for $Bi_{0.8}La_{0.2}FeO_3$ samples is excessive grain growth. Large grained samples have a small volume fraction of grain boundaries and hence provide less resistance to the flow of leakage current. The increase in dielectric properties for $Bi_{0.8}La_{0.2}Fe_{1-x}Ta_xO_3$ samples (x=0.01, 0.03, 0.05) may be attributed to the increase in resistivity of these samples due to large volume fraction of grain boundaries as a consequence of decrease in grain size [149].

As stated earlier, for each sintering condition the dielectric constant value increases with increasing tantalum doping. This is mainly due to the decrease in leakage current with increasing tantalum doping. It is well known that, in perovskite $BiFeO_3$ oxygen vacancies could be formed in the process of sintering due to Bi volatility and the transition from Fe^{3+} to Fe^{2+}. These

vacancies act as a source of leakage current and reduce the resistivity of the samples. Ta^{5+} ion play the role of donor in $BiFeO_3$ because it possess a higher valance then Fe^{3+}. The addition of Ta^{5+} in BFLO requires charge compensation which can be achieved by filling of oxygen vacancies [149, 150] Thus with increasing addition of Ta^{5+} the dielectric property of the samples increase due to decease in oxygen vacancies/leakage current.

However, for all compositions the best value of dielectric constant were obtained when they were sintered at 1000^{o}C for 2 hours because of attainment of best combination of grain size and %TD together with less leakage current. The variation of dielectric constant with frequency for $Bi_{0.8}La_{0.2}Fe_{1-x}Ta_xO_3$ samples (x=0.01, 0.03, and 0.05) sintered at 1000^{o}C for 2 hours are shown in Figure: 4.23. It is evident that the dielectric constant value decrease with increasing frequency for all these compositions. According to literature this variation of dielectric constant with frequency is expected. At higher frequencies the polarization fails to follow the frequency of the applied field and the loss increases. This phenomenon can be attributed to the Maxwell–Wagner-type contribution to the dielectric constant, which is also present in the temperature dependence of dielectric constant for $Bi_{0.8}La_{0.2}FeO_3$. This phenomenon is related to the space charge relaxation at the interface. The space charges are suggested to originate from V_O^{2+},V_{Bi}^{3-}, etc. At low frequencies, the space charges can follow the applied electric field and contribute to the dielectric constant. While at high frequencies, they do not have time to build up and undergo relaxation. Compared to $Bi_{0.8}La_{0.2}FeO_3$, the substitution of Ta^{5+} for Fe^{3+} in $Bi_{0.8}La_{0.2}Fe_{1-x}Ta_xO_3$ reduces the oxygen vacancies significantly because of the requirements of charge compensation, leading to the absence of the Maxwell–Wagner effect. [151]. The frequency dependence of dielectric constant for $Bi_{0.8}La_{0.2}Fe_{1-x}Ta_xO_3$ is weaker than that of $Bi_{0.8}La_{0.2}FeO_3$ and the dielectric loss of $Bi_{0.8}La_{0.2}Fe_{1-x}Ta_xO_3$ is smaller than that of $Bi_{0.8}La_{0.2}FeO_3$.

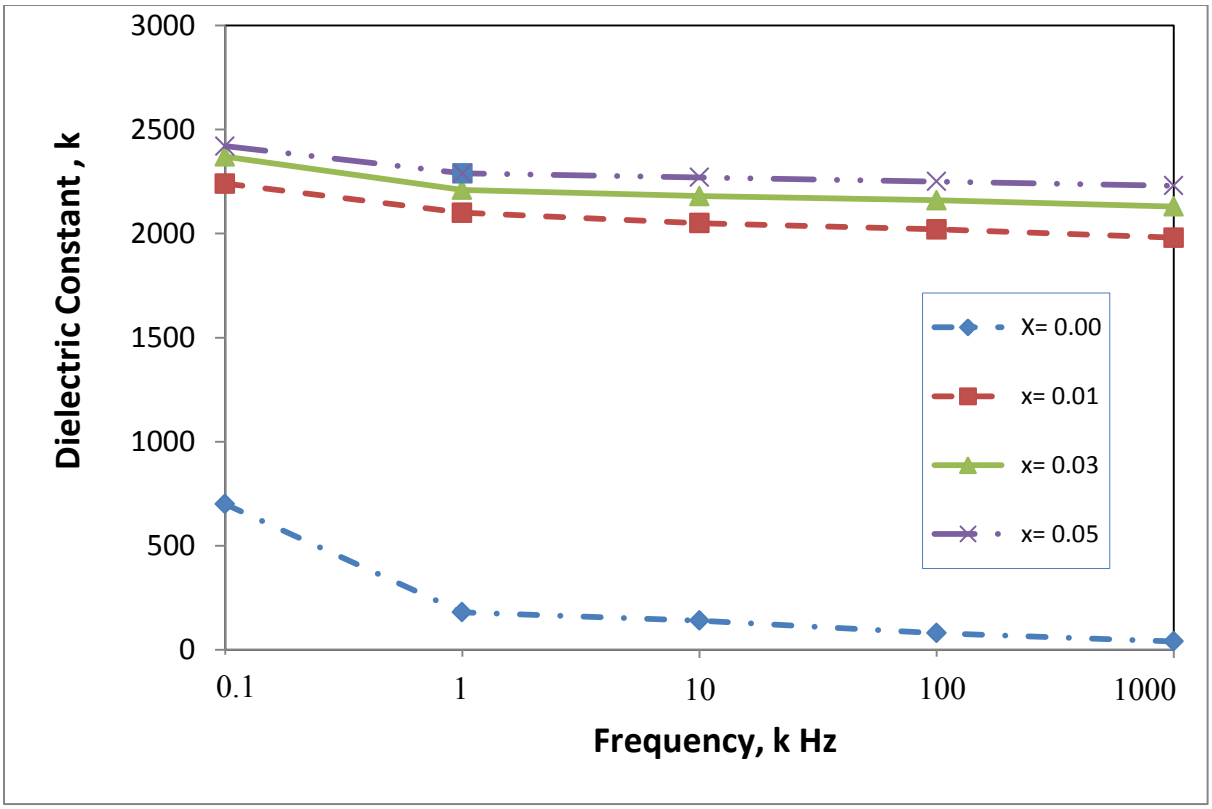

Figure 4.23: Variation of dielectric constant with frequency for $Bi_{0.8}La_{0.2}Fe_{1-x}Ta_xO_3$ samples (x= 0.00, 0.01, 0.03, and 0.05) samples sintered at 1000°C for 2 hours.

The variation of dielectric constant with temperature of these samples is shown in figure 4.23 for different frequencies. At higher temperatures a remarkable increase in k-value in $Bi_{0.8}La_{0.2}FeO_3$ sample occurs due to space charge polarization [1]. As discussed in the previous sections, the oxygen deficiency is an inherent problem with $BiFeO_3$. So, there is always some contribution of space charge polarization due to oxygen ion vacancies in all the measured samples over the entire temperature range. But at higher temperature this effect becomes more prominent due to a thermally activated process, in which the k-value starts increasing after a certain temperature. The rise in the value of the dielectric constant beyond this temperature range may be due to the space charge polarization [152]. However, in Ta-substituted samples (x = 0.01, 0.03, 0.05) such behaviour is not so remarkable. Therefore, stability of dielectric constant with temperature is considerably improved with the increase in Ta content. This indicates that the oxygen vacancy in codoped $BiFeO_3$ was controlled by tantalum doping and thereby improved the resistivity.

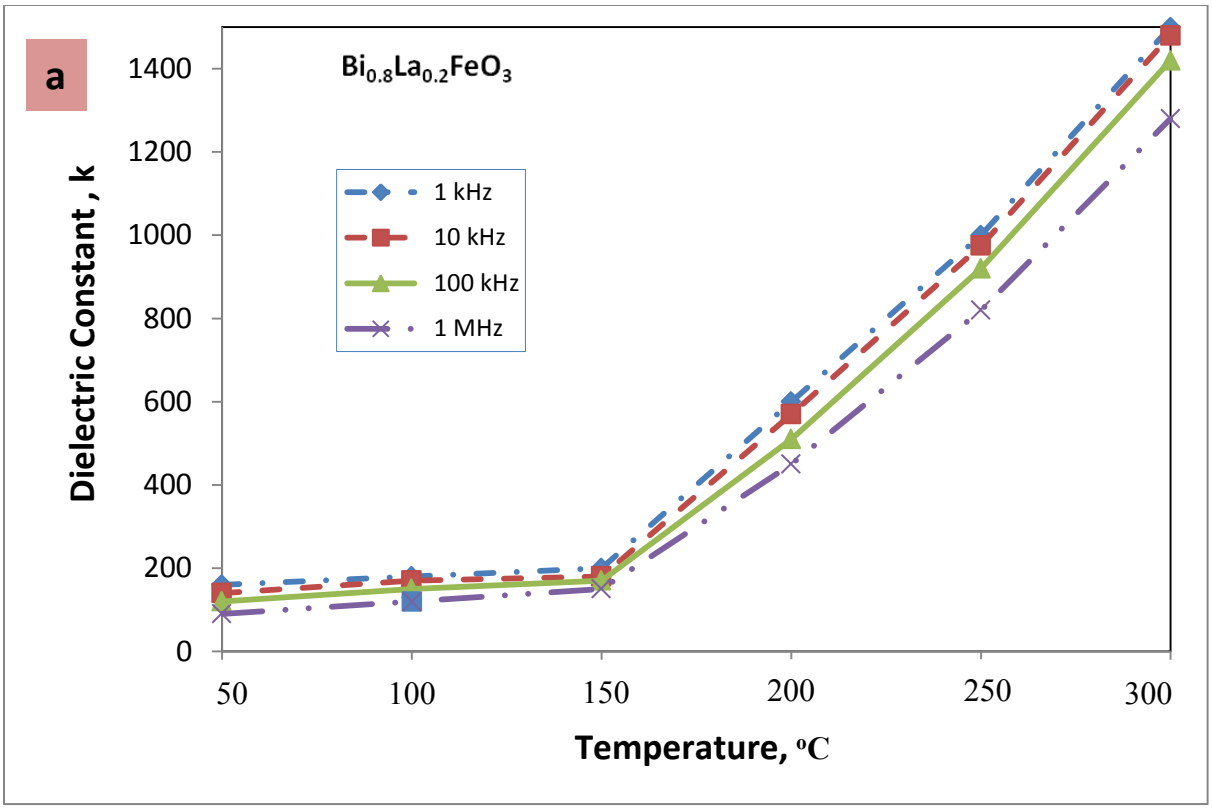
a
Bi0.8La0.2FeO3
Dielectric Constant , k
1400
1200
1000
800
600
400
200
0
1 kHz
10 kHz
100 kHz
1 MHz
50
100
150
200
250
300
Temperature, °C

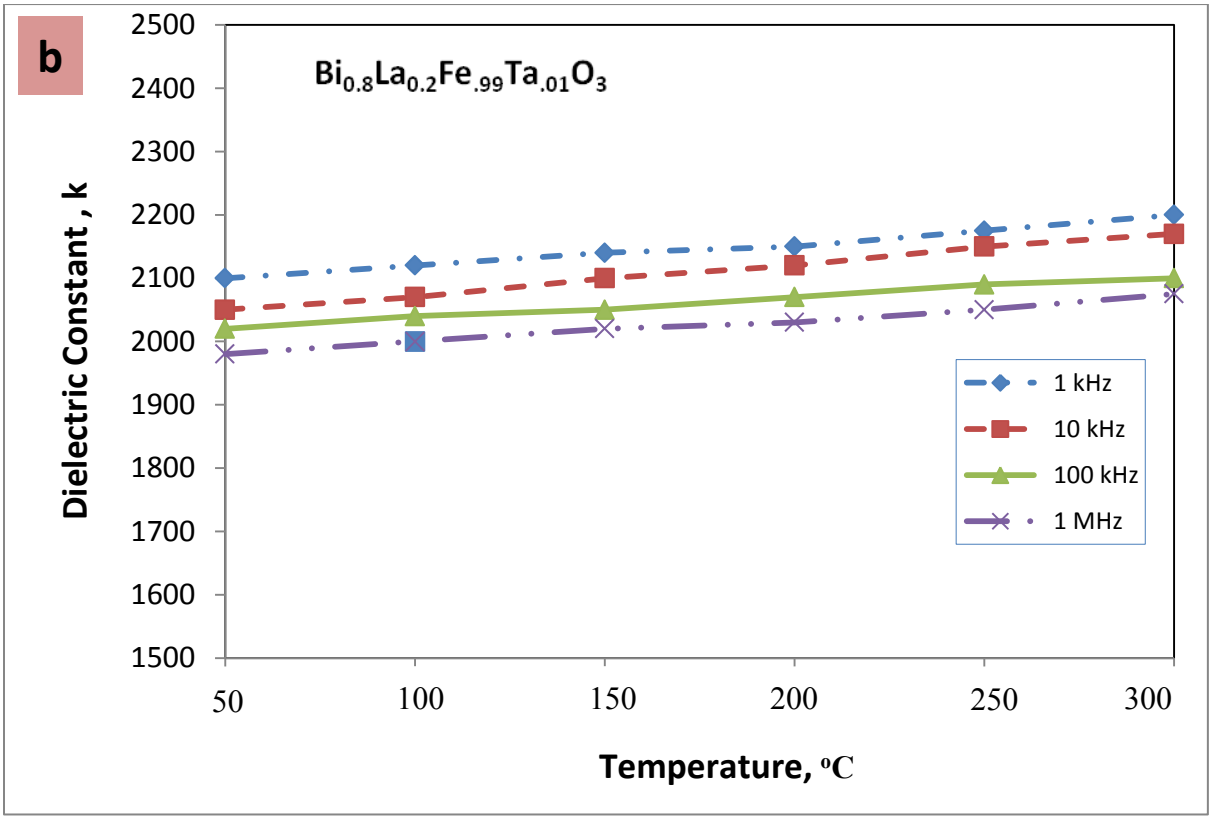
b
Bi0.8La0.2Fe.99Ta.01O3
Dielectric Constant , k
2500
2400
2300
2200
2100
2000
1900
1800
1700
1600
1500
1 kHz
10 kHz
100 kHz
1 MHz
50
100
150
200
250
300
Temperature, °C

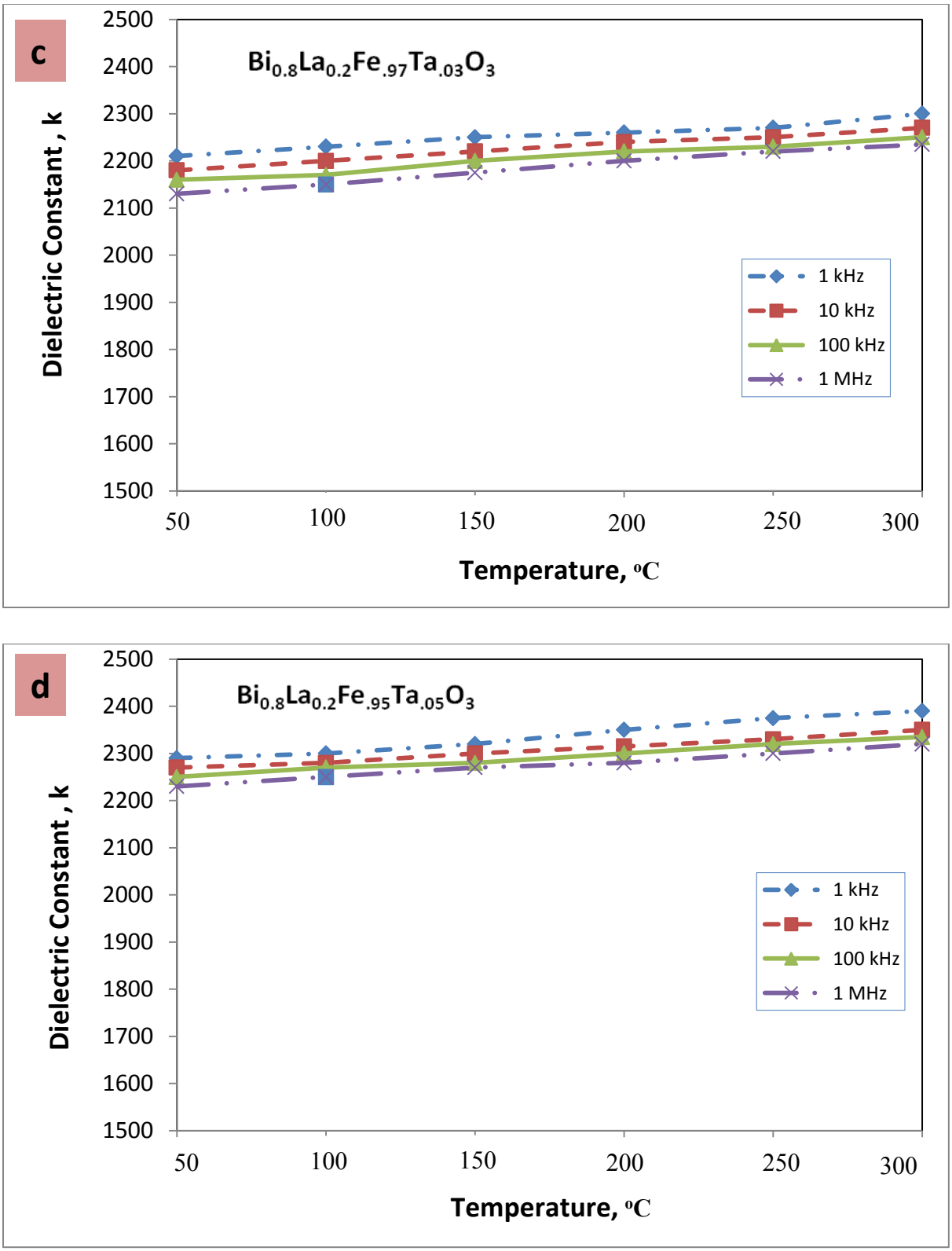

Figure 4.24: Variation of dielectric constant with temperature for $Bi_{0.8}La_{0.2}Fe_{1-x}Ta_xO_3$ (a) x= 0.00, (b) 0.01, (c) 0.03 and (d) 0.05samples sintered at 1000°C for 2 hours.

4.6 DTA analysis

Compared to other multiferroics, pure BFO exhibits a higher ferroelectric Curie temperature (T_C~830^{o}C). It has been reported that, rhombohedral–orthorhombic transition occurs at this Curie temperature. This transition is accompanied by a peak in the dielectric constant; this has been taken as an indication of a ferroelectric–paraelectric transition [153]. This is an attractive feature of dielectric property of BFO, which allows its usage in electronic devices up to very high temperature. To determine the ferroelectric Curie temperature of our doped samples DTA (200-1000^{o}C) was performed. The DTA result of the samples sintered at 1000^{o}C for 2 hours are shown in figure: 4.25.

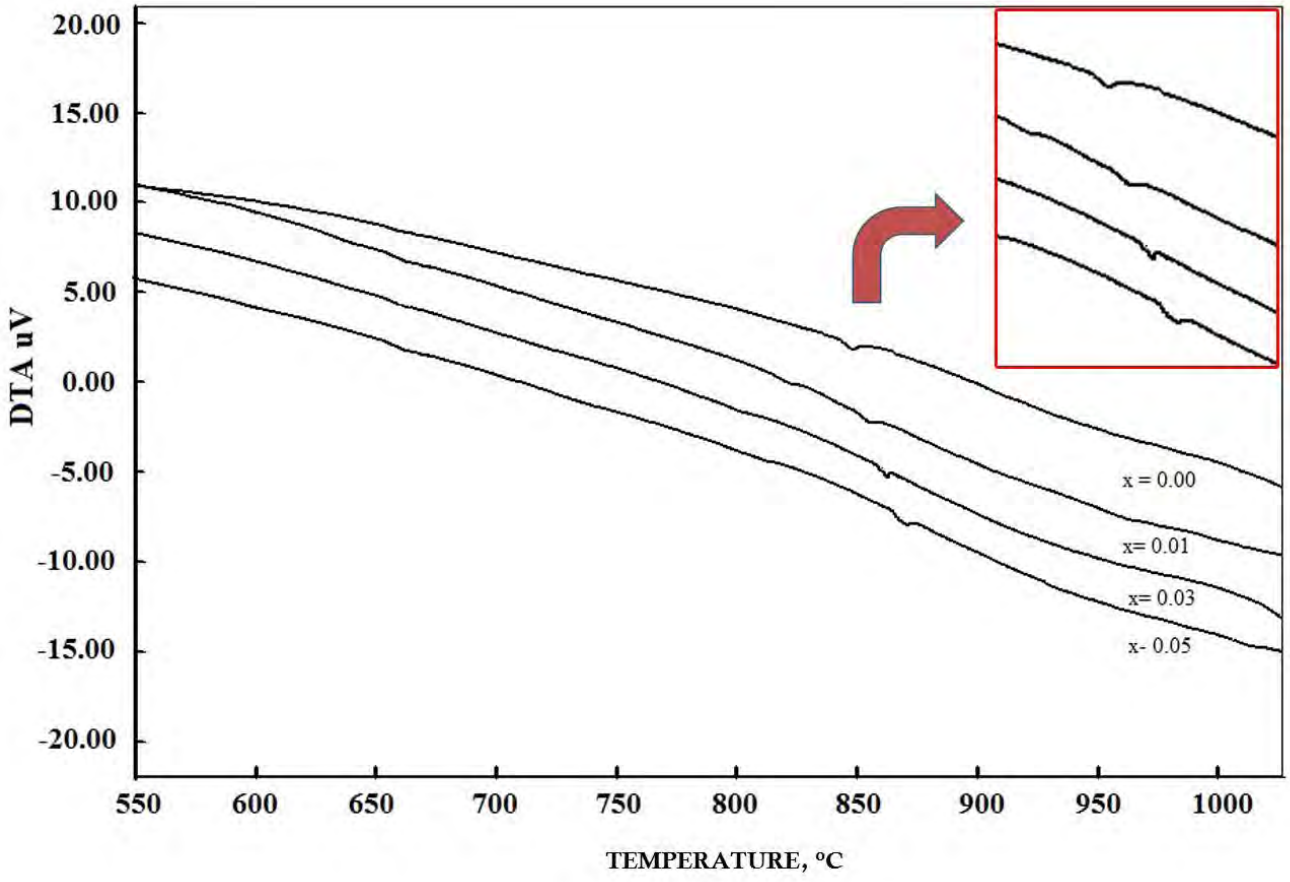

Figure 4.25: DTA analysis for $Bi_{0.8}La_{0.2}Fe_{1-x}Ta_xO_3$ samples (x= 0.00, 0.01, 0.03, 0.05) sintered at 1000^{o}C for 2 hours.

For the $Bi_{0.8}La_{0.2}FeO_3$ compound, a peak obtained at 840^{o}C is attributed to the ferroelectric transition (T_C) in this compound. The peak is shifted towards higher temperature in the Ta-

substituted compounds and reaches 870^{o}C for x=0.05, exhibiting ferroelectric characteristics over a wide temperature range. This increase in T_C can be due to the decrease of pressure with increase in the cell volume [154]. In $BaTiO_3$ the various transition temperatures shift down on compression [155]. Similarly, lowering of ferroelectric transition temperature is observed when doped with smaller atoms.

According to literature, at Curie temperature there is a first-order transition to a high-temperature β phase that is accompanied by a sudden volume contraction [94,95]. Although there is disagreement about the exact symmetry of the β phase above Curie point, most reports agree that it is centrosymmetric, [97-102] so it is probably a safe bet that the α–β transition at Curie temperature is indeed the ferroelectric–paraelectric transition. Palai et al.[49] propose that the symmetry of the β phase is orthorhombic, although their data does not allow establishing the exact space group with certainty. Some authors have argued that the β phase may be tetragonal or pseudo tetragonal,[98] but that is impossible, since the domain structure rules out a tetragonal symmetry and the perovskite a, b, c lattice constants are each quite different.[49,72] It was also proposed that this phase may instead be monoclinic;[98,99] the measured monoclinic angle was nevertheless initially quoted as 90^{o} within experimental error,[98] so that the β phase was in effect ‗metrically orthorhombic'' (i.e., the angles may be 90^{o}, but internal ion positions in each unit cell do not satisfy orthorhombic constraints). More recently, however, Haumont et al. [99] have quoted a monoclinic angle of 90.018.On the other hand, the extra XRD lines used to infer monoclinic structure have not been not identified. Also, the domains studied optically do not reveal the many extra wall orientations that would exist if the symmetry were monoclinic instead of orthorhombic. So, till now all the arguments are in favor of the β phase being orthorhombic.

4.7 Complex initial permeability measurement

The complex initial permeability is given by $\mu_i^* = \mu_i' - i\mu_i''$, where μ_i' and μ_i'' are the real and imaginary parts of initial permeability, respectively. The real part of permeability, μ_i', describes the stored energy expressing the component of magnetic induction B in phase with

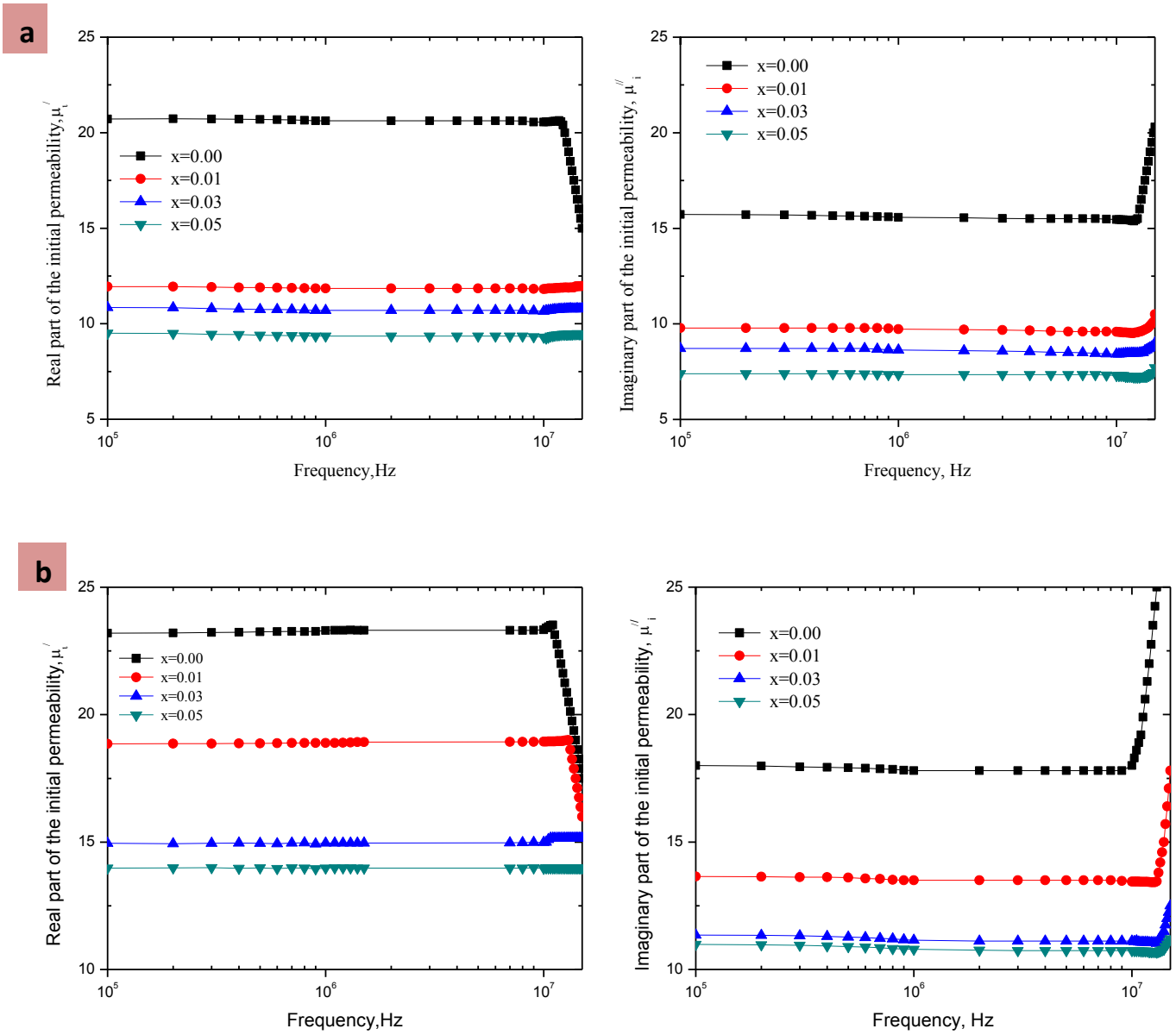

Figure 4.26: The variation of μ_i' and μ_i'' with frequency for $Bi_{0.8}La_{0.2}Fe_{1-x}Ta_xO_3$(x= 0.00, 0.01, 0.03, 0.05) samples sintered at (a) 975°C and (b) 1000°C for 2 hours.

alternating magnetic field H. The imaginary part of permeability, μ_i'', describes the dissipation of energy expressing the component of B at 90^o out of phase with the alternating magnetic field.

The variation of the complex permeability spectra for various $Bi_{0.8}La_{0.2}Fe_{1-x}Ta_xO_3$ (x= 0.00, 0.01, 0.03, 0.05) samples sintered at 975 and 1000^oC for 2 hours is shown in figure 4.26. The general characteristic of the permeability spectra is that μ_i' remains fairly constant in a certain frequency range, while at higher frequency it drops rapidly to a very small value and there is an increase in μ_i''. The appearance of μ_i'' is due to the lagging of the motion of the domain walls with the applied alternating magnetic field. This behavior resembles a typical relaxation character. Figure 4.26. (a) shows that for $Bi_{0.8}La_{0.2}Fe_{1-x}Ta_xO_3$ (x=0.01, 0.03, 0.05) ceramics the μ_i' remains almost constant with increase in frequency up to 15MHz. However, for $Bi_{0.8}La_{0.2}FeO_3$samples the μ_i' remains almost constant with increase in frequency up to 12 MHz and for further increase in frequency μ_i' decreases due to the domain wall relaxation. It is also observed that μ_i' decreases with increase in Ta addition because of decrease in density and grain size. At certain frequency μ_i' attains the highest value and after that decreases and μ_i'' increases rapidly as shown in figure 4.26 (a). The frequency at which the μ_i' attain highest value is known as the resonance frequency, fr, which is the limiting frequency of magnetic materials, below which the materials can be efficiently used. At 975^oC, fr is only obtained for $Bi_{0.8}La_{0.2}FeO_3$ which is approximately 12MHz.

As sintering temperature is increased from 975^oC to 1000^oC, fr is obtained for both $Bi_{0.8}La_{0.2}FeO_3$ and $Bi_{0.8}La_{0.2}Fe_{.99}Ta_{.01}O_3$ ceramics as shown in figure 4.26 (b). Moreover, fr shifted towards lower frequency with the addition of Ta content or increase in μ_i'. At 1000^oC, μ_i' for $Bi_{0.8}La_{0.2}FeO_3$increases to 23 from 21 at 975^oC and fr decreases to 10 MHz from 12 MHz and for $Bi_{0.8}La_{0.2}Fe_{0.99}Ta_{0.01}O_3$ μ_i' increases to 18 from 12 and a previously nonexistent fr appears at 14MHz. However, the μ_i' of $Bi_{0.8}La_{0.2}Fe_{0.97}Ta_{0.03}O_3$and $Bi_{0.8}La_{0.2}Fe_{0.95}Ta_{0.05}O_3$ samples still remains almost constant with increase in frequency up to 15MHz.It is observed that the fr and μ_i' are inversely proportional, which confirms Snoek's relation, μ_i'fr = constant [159]. As the average grain diameter is observed to decrease with increase in Ta substitution, the decrease in μ_i' with increase of Ta substitution is expected. Enlargement of average grain diameter enhances the number of domain walls in each grain. Any increase in the number of domain walls result in an increase in μ_i'. The domain wall motion is affected by the average grain size and enhances

with increase ingrain size. Larger grains tend to consist of a greater number of domain walls. The magnetization caused by domain wall movement requires less energy than that is required by domain rotation. As the number of walls increases with the grain sizes, the contribution of wall movement to magnetization is increased [156-158]. As Ta addition reduces grain size it reduces the number the domain walls hence in effect the contribution of wall movement to magnetization is decreased thus reducing μ_i'.

Comparing figure 4.26 (a) and (b) it is also observed that μ_i' increases with increase in sintering temperature. This is because the average grain diameter is increased with increase in sintering temperature. Therefore, the increase of μ_i' with increasing sintering temperature is also anticipated.

5. CONCLUSION

The objective of this thesis project was to examine the effects of codoping La and Ta on BFO hence developing a novel multiferroic material exhibiting both ferroelectric and ferromagnetic properties. This goal was successfully achieved.

Although BFO is considered a promising candidate for applications in magnetic storage devices, leakage current due to oxygen vacancies and other impurities is a major problem limiting its practical applications. It has been observed that doping with lone-pair active La^{3+} ions at Bi-sites and magnetic transition ion Ta^{5+} at Fe-sites increased its resistance by reducing the leakage current and enhanced the multiferroic properties relative to non-substituted BFO. Doping changes cycloid spin structure of BFO to a canted spin structure which destructs the spin cycloid, releases locked magnetization and enhances the magnetoelectric interaction hence resulting in significantly improved magnetic properties. This research revealed the following:

- $Bi_{0.8}La_{0.2}Fe_{1-x}Ta_xO_3$ (x = 0.0, 0.01, 0.03 and 0.05) ceramics were successfully prepared using solid state method which was confirmed by the XRD analysis that indicated formation of single phase distorted R3c structure.
- Percentage theoretical density as high as 97.6% was achieved for $Bi_{0.8}La_{0.2}FeO_3$ ceramics although this was associated with excessive grain growth. However, addition of Ta dramatically reduced the grain size and resulted in desirable multiferroic properties.
- Combination of good theoretical density (> 95%) and grain size (0.92-.98 μm) was obtained at a sintering temperature of 1000^{o}C for a holding time of 2 hours. Optimum multiferroic properties were obtained in this sintering zone.
- In contrast to pure BFO, La and Ta codoped BFO shows superior values of dielectric constant and magnetic permeability.
- The best values of dielectric constant (> 2000) at room temperature were attained for the Ta doped samples at grain sizes in the range of 0.92-0.98 μm which is in accordance to work reported by previous researchers.

- At higher temperatures a considerable increase in the dielectric constant of $Bi_{0.8}La_{0.2}FeO_3$ samples occurred due to space charge polarization. However, in Ta-substituted ceramics the stability of dielectric constant with temperature is considerably improved.
- DTA analysis revealed that the peak for ferroelectric transition (T_C) shifted towards higher temperatures for the Ta-substituted ceramics and reached 870^oC for x=0.05. Thus codoped BFO exhibited ferroelectric characteristics over a wider temperature range than pure BFO.
- The real part of initial permeability, μ_i', decreases with increasing Ta substitution due to decrease in grain size. Moreover, it is observed that μ_i' increases with sintering temperature.
- For samples sintered at 1000^oC for 2 hours, μ_i' of $Bi_{0.8}La_{0.2}Fe_{0.97}Ta_{0.03}O_3$ and $Bi_{0.8}La_{0.2}Fe_{0.95}Ta_{0.05}O_3$ ceramics remains almost constant with increase in frequency up to 15MHz. However, for $Bi_{0.8}La_{0.2}FeO_3$ and $Bi_{0.8}La_{0.2}Fe_{.99}Ta_{.01}O_3$, μ_i' remains constant up to resonance frequency, fr, i.e. 10 MHz and 14MHz respectively after which there is a sharp decrease in μ_i' and increase in μ_i'' due to domain wall relaxation.
- Moreover, it is observed that the fr and μ_i' are inversely proportional, thus confirming Snoek‘s relation.

6. SUGGESTION FOR FUTURE WORK

(i) Fabricating a solid solution of BFO with other ABO_3 perovskite materials, such as $BaTiO_3$.

(ii) Synthesizing $BiFeO_3$ nano particles with grain size below 62 nm to achieve ferromagnetism by destroying spiral spin structure.

(iii) Depositing ultra-thin $BiFeO_3$ single layer or multilayer films to enhance ferroelectric property.

References

[1] H. Singh and K. L. Yadav ―Dielectric, magnetic and magnetoelectric properties of La and Nb codoped bismuth ferrite,‖ Journal of Physics: Condensed Matter, Vol. 23, 2011, pp. 385901:1-6.

[2] Z. M. Tian, S. L. Yuan, X. L. Wang, X. F. Zheng, S. Y. Yin, C. H. Wang and L. Liu, ―Size effect on magnetic and ferroelectric properties in $Bi_2Fe_4O_9$ multiferroic ceramics,‖ Journal of Applied Physics, Vol. 106, 2009, pp. 103912: 1-4.

[3] Y. Lin, Q. Jiang, Y. Wang, C. Nan, L. Chen, and J. Yu ―Enhancement of ferromagnetic properties in $BiFeO_3$ polycrystalline ceramic by La doping,‖ Applied Physics Letters, Vol. 90, 2007, pp. 172507:1-3.

[4] S. Cheong and M. Mostovoy, ―Multiferroics: a magnetic twist for ferroelectricity,‖ Nature Materials, Vol.6, 2007, pp. 13-20.

[5] N. A. Hill, ―Why are there so few magnetic ferroelectrics?,‖ Journal of Physical Chemistry B, Vol. 104, 2000, pp. 6694–6709.

[6] Y. F. Cui, Y. G. Zhao, L. B. Luo, J. J. Yang, H. Chang, M. H. Zhu, D. Xie, and T. L. Ren, ―Dielectric, magnetic, and magnetoelectric properties of La and Ti codoped $BiFeO_3$,‖ Applied Physics Letters, Vol. 97,2010, pp. 222904: 1-3.

[7] A.K. Ghosh, H. Kevin, B. Chatterjee, G.D. Dwivedi, A. Barman, H.D. Yang and S. Chatterjee, ―Effect of Sr-doping on multiferroic properties of $Bi_{0.8}La_{0.2}Fe_{0.9}Mn_{0.1}O_3$‖, Solid State Communications, Vol. 152, Issue 6, 2009, pp. 557-560.

[8] G. Catala, and J.F. Scott, "Physics and applications of bismuth ferrite," Advanced Materials, Vol. 21, 2009, pp. 2463-2485.

[9] I. Sosnowska, T.P. Neumaier, and E. Steichele, ―Spiral magnetic ordering in bismuth ferrite,‖ Journal of Physics C: Solid State Physics, Vol. 15, 1982, pp. 4835.

[10] I. Sosnowska, W. Sch¨afer, W. Kockelmann, K.H. Andersen and I.O. Troyanchuk, ―Crystal structure and spiral magnetic ordering of BiFeO3 doped with manganese,‖ Applied Physics A, Vol. 74, 2002, pp. s1040-s1042.

[11] C. Ederer and N.A. Spaldin, ―Weak ferromagnetism and magnetoelectric coupling in bismuth ferrite,‖ Physics Review B, Vol. 71, 2005, pp. 060401.

[12] Y.K. Jun and S.H. Hong, ―Dielectric and magnetic properties in Co-and Nb-substituted $BiFeO_3$ ceramics,‖ Solid State Communication, Vol. 144, 2007, pp. 329-333.

[13] M. Kumar and K.L. Yadav, ―Rapid liquid phase sintered Mn doped $BiFeO_3$ ceramics with enhanced polarization and weak magnetization,‖ Applied Physics Letters, Vol. 91, 2007,pp. 242901- 242901.

[14] F. Chang, N. Zhang, F. Yang, S. Wang and G. Song, Journal of Physics D: Applied Physics, 2007, Vol. 40,pp. 7799.

[15] X. Qi, J. Dho, R. Tomov, M. G. Blamire, J. L. M. Driscoll, ―Greatly reduced leakage current and conduction mechanism in aliovalent-ion-doped $BiFeO_3$,‖ Applied Physics Letters, Vol. 86, 2005, pp. 062903-062903.

[16] Y. J. Zhang, H. G. Zhang, J. H. Yin, H. W. Zhang, J. L., Chen, W. Q. Wang and G. H. Wu, Structural and magnetic properties in $Bi_{1-x}R_xFeO_3$ (x=0–1, R=La, Nd, Sm, Eu and Tb) polycrystalline ceramics. Journal of Magnetism and Magnetic Materials, Vol. 322, 2010, pp. 2251-2255.

[17] Z. X. Cheng, X. L. Wang, H. Kimura, K. Ozawa, S. Dou, ―La and Nb codoped $BiFeO_3$ multiferroic thin films on $LaNiO_3$/Si and IrO_2/Si substrates,‖ Applied Physics Letters, Vol. 92, 2008, pp. 092902-092902.

[18] Z. Cheng, X. Wang, S. Dou, H. Kimura, K. Ozawa, ―Improved ferroelectric properties in multiferroic $BiFeO_3$ thin films through La and Nb codoping,‖ Physics Review B, Vol. 77, 2008, pp. 092101.

[19] M. Cazayous, D. Malka, D. Lebeugle, D. Colson, ―Electric field effect on BiFeO3 single crystal investigated by Raman spectroscopy,‖ Applied Physics Letters, Vol. 91, 2007, pp. 071910-071910.

[20] G. L. Yuan, K. Z. B. Kishi, J. M. Liu, S. W. Or, Y. P. Wang, Z. G. Liu, ―Multiferroic Properties of Single-Phase Bi0.85La0.15FeO3 Lead-Free Ceramics,‖ Journal of American Ceramics Society, Vol. 89, 2006, pp. 3136-3139.

[21] Y. H. Lin, Q. Jiang, Y. Wang, C. W. Nan, L. Chen and J. Yu, ―Enhancement of ferromagnetic properties in $BiFeO_3$ polycrystalline ceramic by La doping,‖ Applied Physics Letters, Vol. 90, 2007, pp. 172507-172507.

[22] M. Kumar and K. L. Yadav, ―Study of room temperature magnetoelectric coupling in Ti substituted bismuth ferrite system,‖ Journal of Applied Physics, Vol. 100, 2006, pp. 074111-074111.

[23] I. O. Troyanchuk, N. V. Tereshko, A. N. Chobot, M. V. Bushinsky and K. B¨arner, —Weak ferromagnetism in $BiFeO_3$ doped with titanium," Physica B, Vol. 404, 2009, pp. 4185-4189.

[24] J. Wang, J. B. Neaton, H. Zheng, V. Nagarajan, S. B. Ogale, B. Liu, D. Viehland, V. Vaithyanathan, D. G. Schlom, U. V. Waghmare, N. A. Spaldin, K. M. Rabe, M. Wuttig and R. Ramesh, —Epitaxial BiFeO3 multiferroic thin film heterostructures," Science, Vol. 299, 2003, pp. 1719-1722.

[25] D. Lebeugle, D. Colson, A. Forget, M. Viret, P. Bonville, J. F. Marucco and S. Fusil, —Very large spontaneous electric polarization in BiFeO3 single crystals at room temperature and its evolution under cycling fields," Applied Physics Letters, Vol. 91, 2007, pp. 022907-022907.

[26] D. Lebeugle, ‗Groupement de Recherche sur les Nouveaux Etats Electroniques de la Matiere: GdR NEEM'; Gif sur Yvette, November 2006.

[27] R. Lobo, R. L. Moreira, D. Lebeugle and D. Colson, —Infrared phonon dynamics of a multiferroic $BiFeO_3$ single crystal," Physics Review B, Vol. 76, 2007, pp. 172105.

[28] N. Jeon, D. Rout, I. W. Kim, and S.J. L. Kang, —Enhanced Multiferroic Properties of Single-phase $BiFeO_3$ Bulk Ceramics by Ho doping," Applied Physics Letter, Vol. 98, Issue 7, 2011, pp 072901-072903.

[29] D. Lebeugle, Ph.D. Thesis, Saclay Institute of Matter and Radiation, 2007.

[30] X. Qi, J. Dho, R. Tomov, M. G. Blamire and J. L. MacManus-Driscoll, —Greatly reduced leakage current and conduction mechanism in aliovalent-ion-doped $BiFeO_3$," Applied Physics Letters, Vol. 86, 2005, pp 062903:1-3.

[31] D. H. Wang, W. C. Goh, M. Ning, and C. K. Ong, —Effect of Ba doping on magnetic, ferroelectric, and magnetoelectric properties in mutiferroic $BiFeO_3$ at room temperature," Applied Physics Letters, Vol. 88, 2006, pp 212907: 1-3.

[32] Y. Lin, Q. Jiang, Y.Wang, C. Nan, L. Chen, and J. Yu, —Enhancement of ferromagnetic properties in $BiFeO_3$ polycrystalline ceramic by La doping," Applied Physics Letters, Vol. 90, 2007, pp 172507:1-3.

[33] Y. F. Cui, Y. G. Zhao, L. B. Luo, J. J. Yang, H. Chang, M. H. Zhu, D. Xie, and T. L. Ren, —Dielectric, magnetic, and magnetoelectric properties of La and Ti codoped BiFeO3," Applied Physics Letters, Vol. 97, 2010, pp.222904: 1-3.

[34] C. Lan, Y. Jiang and S. Yang, "Magnetic properties of La and (La, Zr) doped $BiFeO_3$ ceramics," Journal of Material Science, Vol. 46, 2011, pp 734–738.

[35] Reetu, A. Agarwal1, S. Sanghi, Ashima and N. Ahlawat, "Structural transformation and improved dielectric and magnetic properties in Ti-substituted $Bi_{0.8}La_{0.2}FeO_3$ multiferroics," Journal of Physics D: Applied Physics, Vol. 45, 2012, pp 165001:1-9.

[36] A. K. Ghosh, G. D. Chatterjee, B. Rana, A. Barman, S. Chatterjee and H. D. Yang., "Role of codoping on multiferroic properties at room temperature in $BiFeO_3$ ceramic", Solid State Communications, Vol. 166, 2013, pp 22–26.

[37] J. Li, K. Liu, J. Xu, L. Wang, L. Bian and F. Xu, "Structure-Dependent Electrical, Optical and magnetic properties of Mn-Doped BiFeO3 thin films prepared by the sol-gel process", Journal of Materials Science Research, Vol. 2, 2013, pp 75.

[38] Z. Cheng, X. Wang, and S. Dou, "Improved ferroelectric properties in multiferroic BiFeO3 thin films through La and Nb codoping," Physical Review B, Vol. 77, 2008, pp 092101: 1-4.

[39] L. Zhai, Y. G. Shi, S. L. Tang, L. Y. Lv and Y. W. Dou, "Large magnetic coercive field in Bi0.9La0.1Fe0.98Nb0.02O3 polycrystalline compound," Journal of Physics D: Applied Physics Vol. 42, 2009, pp 165004.

[40] B. F. Yu, M. Y. Li, J. Liu, D. Y. Guo, L. Pei, X. Z. Zhao, "Enhanced electrical properties in multiferroic BiFeO3 ceramics co-doped by La3+ and V5+," Journal of Physics D: Applied Physics, Vol. 41, 2008, pp 065003.

[41] L. E. Cross, "Ferroic Materials and Composites: Pass, Press, and Future" (1997).

[42] F. Duan and J. Guojun, "Introduction to Condensed Matter Physics," World Scientific (Vol. 1), Singapore, 2005.

[43] J. M. Yeomans, "Statistical Mechanics of Phase Transitions," Oxford University Press, 2002.

[44] M. E. Lines and A. M. Glass, "Principles and Applications of Ferroelectrics and Related Materials," Oxford University Press, 2004.

[45] C. Kittel, "Introduction to solid state physics," American Journal of Physics, Vol. 35, 1967, pp. 547-548.

[46] E. K. H Salje, "Phase Transitions in Ferroelastic and Co-elastic Crystals," Cambridge University Press, 1990.

[47] V. Muller, A. Fuith, J. Fousek, H. Warhanek and H. Beige, "Spontaneous strain in ferroelastic incommensurate [N(CH3)4]2CuCl4 crystals," Solid State Communications, Vol. 104, 1997, pp. 455-458.

[48] L. Jian and C. M. Wayman, "Compressive behavior and domain-related shape memory effect in LaNbO4 ceramics," Materials Letters, Vol. 26, 1996, pp 1-7.

[49] R. E. Newnham, "Molecular mechanisms in smart materials," MRS Bulletin, Vol. 22, 1997, pp. 20-34.

[50] Van E. Wood, A. E. Austin, "Magnetoelectric interaction phenomena in crystals," edited by A. J. Freeman and H. Schmid, Gordon and Breach Science Publishers, 1975.

[51] G. A. Smolenskii and I. E. Chupis, "Ferroelectromagnets," Soviet Physics Uspekhi, Vol. 25, 1982, pp 475.

[52] D.I. Khomskii, "Multiferroics: different ways to combine magnetism and ferroelectricity," Journal of Magnetism and Magnetic Materials, Vol. 306, 2006, pp 1-8.

[53] M. Fiebig, "Revival of the magnetoelectric effect," Journal of Physics D: Applied Physics, Vol 38, 2005, pp. R123.

[54] W. Eerenstein, N. D. Mathur, and J. F. Scott, "Multiferroic and magnetoelectric materials," Nature, Vol. 442, 2006, pp 759.

[55] J. P. Velev, S. S. Jaswal, and E. Y. Tsymbal, "Multi-ferroic and magnetoelectric materials and interfaces," Philosophical Transactions of the Royal Society A: Mathematical, Physical and Engineering Sciences, Vol. 369, 2011, pp 3069.

[56] W. Prellier, M. Singh, P. Murugavel, "The single-phase multiferroic oxides: from bulk to thin film," Journal of Physics: Condensed Matter, Vol. 17, 2005, pp. R803.

[57] Y. Tokura and N. Kida, "Dynamical magnetoelectric effects in multiferroic oxides," Philosophical Transactions of the Royal Society A: Mathematical, Physical and Engineering Sciences," Vol. 369, 2011, pp. 3679-3694.

[58] G. Lawes and G. Srinivasan, "Introduction to magnetoelectric coupling and multiferroic films," Journal of Physics D: Applied Physics, Vol. 44, 2011, pp. 243001.

[59] M. Fieberg, "Revival of the magnetoelectric effect", Journal of Physics D: Applied Physics, Vol. 38, 2005, pp. R123.

[60] W. Ehrenstein, N. Mazur, J. Scott, "Multiferroic and magnetoelectric materials", Nature, Vol. 442, 2006, pp. 759.

[61] R. Ramesh, N.A. Spaldin, "Multiferroics: progress and prospects in thin films", Nature Materials, Vol. 6, 2007, pp. 21-29.

[62] Special issue, Journal of Physics: Condensed Matter, Vol. 20, 2008, pp. 434201-434220.

[63] D.I.Khomskii, "Magnetism and ferroelectricity: why do they so seldom coexist?," Bulletin of American Physical Society C, Vol. 1, 2001, pp. 21002.

[64] B. B. Van. Aken, T. T. M. Palstra, A. Filippetti, and N. A. Spaldin, "The origin of ferroelectricity in magnetoelectric $YMnO_3$", Nature Materials, Vol. 3, 2004, pp 164-170.

[65] N. Hur, S. Park, P. A. Sharma, J. S. Ahn, S. Guha and S. W. Cheong, "Electric polarization reversal and memory in a multiferroic material induced by magnetic fields", Nature, Vol. 429, 2004, pp 392-395.

[66] H. Kastura, N. Nagaosa and A. V. Balatsky, "Spin current and magnetoelectric effect in noncollinear magnets," Physics Review Letters, Vol. 95, 2005, pp. 057205.

[67] T. Kimura, T. Goto, H. Shintani, K. Ishizaka, T. Arima, and Y. Tokura, "Magnetic control of ferroelectric polarization," Nature, Vol. 426, 2003, pp. 55-58.

[68] Y. J. Choi, H. T. Yi, S. Lee, Q. Huang, V. Kiryukhin and S. W. Cheong, "Ferroelectricity in an Ising Chain Magnet," Physics Review Letters, Vol. 100, 2008, pp. 047601.

[69] I. A. Sergienko, C. Şen, E. Dagotto, "Ferroelectricity in the Magnetic E-Phase of Orthorhombic Perovskites," Physics Review Letters, Vol. 97, 2006, pp. 227204.

[70] N. Lee, Y. J. Choi, M. Ramazanoglu, W. Ratcli , V. Kiryukhin, and S.-W. Cheong, "Mechanism of exchange striction of ferroelectricity inmultiferroic orthorhombic HoMnO single crystals," Physics Review B, Vol. 84, 2011, pp. 3020101.

[71] Y. F. Popov, A. M. Kadomtseva, G. P. Vorob'Ev and A. K. Zvezdin, "Discovery of the linear magnetoelectric effect in magnetic ferroelectric BiFeo3 in a strong magnetic field," Ferroelectrics, Vol. 162, 1994, pp. 135-140.

[72] R.D. Shannon, ―Revised Effective Ionic Radii and Systematic Studies of Interatomie Distances in Halides and Chaleogenides,‖ Acta Crystallographica, Vol. A32 1976, pp 751-767.

[73] T. Mizokawa, D.I. Khomskii and G.A. Sawatzky, ―Interplay between orbital ordering and lattice distortions in LaMnO3, YVO3, and YTiO3,‖ Physics Review B, Vol. 60, 1999, pp 7309.

[74] R.E. Cohen, H. Krakauer, Ferroelectrics, Vol.136, 1992, pp 95.

[75] P. Curie, ―Sur la syme´trie dans les phe´nomènes ***physiques***. Syme´trie d'un champ e´lectrique et d'un champ magne´tique‖, Journal de Physique, Vol. 3, 1894, pp 393-417.

[76] J. Valasek, ―Piezoelectric and allied phenomena in Rochelle salt‖, Physical Review, Vol. 15, 1920, pp 537-538.

[77] A. Perrier and A. J. Staring, Archives des Sciences Physiques et Naturelles (Geneva), Vol. 4, 1922, pp 373-382.

[78] A. Perrier and A. J. Staring, Archives des Sciences Physiques et Naturelles (Geneva), Vol. 5, 1923, pp 333.

[79] T. H. O‘Dell, ―The Electrodynamics of Magneto-electric Media‖, Publisher: North-Holland, Amsterdam, 1970.

[80] I.E. Dzyaloshinskii, Zh. Eksp. Teor. Fiz., Vol. 37, 1959, pp 88. [Soviet Physics ―JETP, Vol. 10, 1959, pp 628.]

[81] D.N. Astrov, Zh. Eksp. Teor. Fiz., Vol. 38, 1960, pp 984. [Soviet Physics — JETP, Vol. 11, 1960, pp 708.]

[82] E. Ascher, H. Rieder, H. Schmid and H. Stossel, ―Some Properties of Ferromagnetoelectric Nickel-Iodine Boracite‖, $Ni_3B_7O_{13}I$ Journal of Applied Physics, Vol. 37, 1966, pp 1404-1405.

[83] G. A. Smolensky, V. A. Isupov and A. I. Agronovskaya, Soviet Physics — Solid State, Vol. 1, 1959, pp 149- 150.

[84] G. A. Smolenskii and I. E. Chupis, Soviet Physics — Solid State, Vol. 4, 1962, 4, pp 807.

[85] H. Schmid, ―Multi-ferroic magnetoelectrics. Ferroelectrics‖, Vol. 162, 1994, pp 665.

[86] M. Fiebig, ―Revival of the magnetoelectric effect‖, Journal of Physics D: Applied Physics, Vol. 38, 2005, pp R123.

[87] W. Eerenstein, N.D. Mathur and J.F. Scott, "Multiferroic and magnetoelectric materials", Nature, Vol. 442, 2006, pp 759.

[88] J. Wang, J.B. Neaton, H. Zheng, V. Nagarajan, S.B. Ogale, B. Liu, D. Viehland, V. Vaithyanathan, D.G. Schlom, U.V. Waghmare, N.A. Spaldin, K.M. Rabe, M.Wuttig and R. Ramesh, "Epitaxial $BiFeO_3$ Multiferroic Thin Film Heterostructures", Science, Vol. 299, 2003, pp 1719-1722.

[89] A. Filippetti and N.A. Hill, "Coexistence of magnetism and ferroelectricity in perovkites," Physics Review B, Vol. 65, 2002, pp 195120.:

[90] V.S Filip'ev, I.P Smol'yaninov, E.G Fesenko and I.I Belyaev, Soviet Physics — Crystallogr., Vol. 5, 1960, pp 913.

[91] F. Kubel and H. Schmid, "Structure of a ferroelectric and ferroelastic monodomain crystal of the perovskite $BiFeO_3$," Acta Crystallographica B, Vol. 46, 1990, pp 698.

[92] A. Palewicza, I. Sosnowskaa, R. Przeniosłoa and A.W. Hewat, "$BiFeO_3$ Crystal Structure at Low Temperatures," Acta Physica Polonica A, Vol. 117, 2010, pp 296.

[93] R. D. Shannon, "Revised Effective Ionic Radii and Systematic Studies of Interatomic Distances in Halides and Chalcogenides," Acta Crystallographica A, Vol. 32, 1976, pp 751.

[94] R. Palai, R. S. Katiyar, H. Schmid, P. Tissot, S. J. Clark, J. Robertson, S. A. T. Redfern, G. Catalan and J. F. Scott, "β phase and γ-β metal-insulator transition in multiferroic $BiFeO_3$," Physics Review B, Vol. 77, 2008, pp 014110.

[95] M. Polomska, W. Kaczmarek and Z. Pajak, "Electric and magnetic properties of $(B1-xLax)FeO_3$ solid solutions," Physica Status Solidi, Vol. 23, 1974, pp 567-574.

[96] N. N. Krainik, N. P. Khuchua, A. A. Bierezhnoi, A. G. Tutov, A. J. Cherkashtschenko, Izvestiya Akademii Nauk SSR, Seriya Fizicheskaya,Vol. 29, 1965, pp 1026.

[97] R. Haumont, J. Kreisel, P. Bouvier and F. Hippert, "Spin-phonon coupling in multferroics," Physics Review B, Vol. 73, 2006, 73, pp 132101.

[98] I. A. Kornev, S. Lisenkov, R. Haumont, B. Dkhil and L. Bellaiche, "Finite- temperature properties of multiferroic $BiFeO_3$," Physics Review Letter, Vol. 99, 2007, pp 227602.

[99] R. Haumont, I. A. Kornev, S. Lisenkov, L. Bellaiche, J. Kreisel and B. Dkhil, ―Phase stability and structural temperature dependence in powdered multiferroic $BiFeO_3$," Physics Review B, Vol. 78, 2008, pp 134108.

[100] S.M. Selbach, T. Tybell, M.-A. Einarsrud and T. Grande, ―High-temperature semiconducting cubic phase of BiFe0.7Mn0.3O3+,"Advanced Materials, Vol. 20, 2008, pp 3692.

[101] D. C. Arnold, K. S. Knight, F. D. Morrison, P. Lightfoot, Physics Review Letter, Vol. 102, 2009, pp 027602.

[102] S. A. T. Redfern, J. N. Walsh, S. M. Clark, G. Catalan, J. F. Scott, arXiv: 0901.3748, 2009 (unpublished).

[103] J.R. Teague, R. Gerson and W. J. James, Solid State Communications, Vol. 8, 1970, pp. 1073.

[104]. F. Zavaliche, R.R. Das, D.M. Kim, C.B. Eom, S.Y. Yang, P. Shafer, and R. Ramesh, Applied Physics Letter, Vol. 87, 2005, pp 182912.

[105] N. N. Krainik, N. P. Khuchua, V. V. Zhdanova, V. A. Evseev, Soviet Physics — Solid State, Vol. 8, 1966, pp. 654.

[106] W. Kaczmarek, Z. Pajak, M. Polomska, Solid State Communication,Vol. 17, 1975, pp.807.

[107] S. Kamba, D. Nuzhnyy, M. Savinov, J. S ˇ ebek, J. Petzelt, J. Prokles˘ka, R.Haumont, J. Kreisel, Physics Review B, Vol. 75, 2007, pp.024403.

[108] M. Polomska, W. Kaczmarek, Z. Pajak, Physica Status Solidi, Vol. 23, 1974, pp.567.

[109] J.-P. Rivera, H. Schmid, Ferroelectrics, Vol. 204, 1997, pp.23.

[110] I. Sosnowska, T. Peterlin-Neumaier, E. Steichele, Journal of Physics C: Solid State Physics, Vol. 15, 1982, pp. 4835.

[111] P. Fischer, M. Polomska, I. Sosnowska, M. Szymanski, Journal of Physics C: Solid State Physics, Vol. 13, 1980, pp. 1931.

[112] D. Lebeugle, D. Colson, A. Forget, M. Viret, A.M. Bataille, A. Gukasov, Physical Review Letters, Vol. 100, 2008, pp. 227602.

[113] G. Catalan, G. and J.F. Scott, Advanced Materials, Vol. 21, 2009, pp. 2463 .

[114] W. Jie, R. Haumont, R. Jarrier, P. Berhtet, B. Dkhil, Applied Physics Letter, Vol. 96, 2010, pp. 102509.

[115] X. Qingyu, Z. Haifa, D. Wu, T. Qiu, and M.X. Xu, Applies Physics Letter, Vol. 95, 2009, pp. 112510.

[116] W. Yao, Q. Jiang, H. He, C.W. Nan, Applied Physics Letter, Vol. 88, 2006, pp. 142503.

[117] M. Kumar, K.L. Yadav, Applied Physics Letter, Vol. 91, 2007, pp. 112911.

[118] S.R. Shannigrahi, A. Huang, N. Chandrasekhar, D. Tripathy, A.O. Adeyeye, Applied Physics Letter, Vol. 90, 2007, pp. 022901.

[119] Z. Shan-Tao, Z. Yi Lu, D. Ming-Hui, C. Chao-Ling, L. Yan-Feng, Z. Zhi-Guo, M. Yong-Yuan, P. Nai-Ben, X. Q., Applied Physics Letter, Vol. 88, 2006, pp. 162901.

[120] Z. Yan, K.F.Wang, J.F. Qu, Y. Wang, Z.T. Song, and S.L. Feng, Applied Physics Letter, Vol. 91, 2007, pp. 082906.

[121] S. Karimi, I.M. Reaney, I. Levin, I. Sterianou, Applied Physics Letter, Vol. 94, 2009, pp. 112903.

[122] V.A. Khomchenko, V. V. Shvartsman, P. Borisov, W. Kleemann, D.A. Kiselev, I.K. Bdikin, J.M. Vieira, A.L. Kholkin, Acta Materialia, Vol. 57, 2009, pp. 5137 .

[123] Fujitsu website: http://www.fujitsu.com/my/news/pr/fmal20060808.html

[124] H. W. Jang, S. H. Baek, D. Ortiz, C. M. Folkman, C. B. Eom, Y. H. Chu, P. Shafer, R. Ramesh, V. Vaithyanathan, D. G. Schlom, Applied Physics Letter, Vol. 92, pp. 062910.

[125] X. J. Lou, C. X. Yang, T. A. Tang, Y. Y. Lin, M. Zhang, J. F. Scott, Applied Physics Letter, Vol. 90, 2007, pp. 262908.

[126] D. I. Woodward, I. M. Reaney, R. E. Eitel, C. A. Randall, Journal of Applied Physics, Vol. 94, 2003, pp. 3313.

[127] B. Noheda, D. E. Cox, G. Shirane, J. A. Gonzalo, L. E. Cross, S. E. Park, Applied Physics Letter, Vol. 94, 1999, pp. 2059.

[128] S. Fujino, M. Murakami, V. Anbusathaiah, S.-H. Lim, V. Nagarajan, C. J. Fennie, M. Wuttig, L. Salamanca-Riba, I. Takeuchi, Applied Physics Letter, Vol. 92, 2008, pp. 202904.

[129] H. Bea, M. Gajek, M. Bibes, A. Barthelemy, Journal of Physics: Condensed Matter, Vol. 20, 2008, pp. 434231.

[130] T. Zhao, A. Scholl, F. Zavaliche, K. Lee, M. Barry, A. Doran, M. P. Cruz, Y. H. Chu, C. Ederer, N. A. Spaldin, R. R. Das, D. M. Kim, S. H. Baek, C. B. Eom, R. Ramesh, Nature Materials, Vol. 5, 2006, pp. 823.

[131] S. Lee, W. Ratcliff, S.-W. Cheong, V. Kiryukhin, Applied Physics Letter, Vol. 92, 2008, pp. 192906.

[132] D. Lebeugle, D. Colson, A. Forget, M. Viret, A. M. Bataille, A. Gukasov, Physics Review Letter, Vol. 100, 2008, pp. 227602.

[133] J. Nogues, I. K. Schuller, Journal of Magnetism and Magnetic Materials, Vol. 192, 1999, pp. 203.

[134] P. Borisov, A. Hochstrat, X. Chen, W. Kleemann, C. H. Binek, Physics Review Letter, Vol. 94, 2005, pp. 117203.

[135] V. Laukhin, V. Skumryev, X. Martı ´, D. Hrabovsky, F. Sa´nchez, M. V. Garcı ´a-Cuenca, C. Ferrater,M. Varela, U. Lu¨ders, J. F. Bobo, J. Fontcuberta, Physics Review Letter, Vol. 97, 2006, pp. 227201.

[136] J. Dho, X. Qi, H. Kim, J. L. MacManus-Driscoll, M. G. Blamire, ―Large electric polarization and exchange bias in multiferroic BiFeO3", Advanced Materials, Vol. 18, 2006, pp. 1445.

[137] H. Be´a, M. Bibes, S. Cherifi, F. Nolting, B. Warot-Fonrose, S. Fusil, G. Herranz, C. Deranlot, E. Jacquet, K. Bouzehouane, A. Barthe´le´my, ―Tunnel magnetoresistance and robust room temperature exchange bias with multiferroic BiFeO3 epitaxial thin films", Applied Physics Letter, Vol. 89, 2006, pp. 242114.

[138] H. Béa, M. Bibes, F. Ott, B. Dupe´, X.-H. Zhu, S. Petit, S. Fusil, C. Deranlot, K. Bouzehouane, A. Barthélémy, ―Mechanisms of exchange bias with multiferroic BiFeO3 epitaxial thin films", Physics Review Letter, Vol. 100, 2008, pp. 017204.

[139] Y.-H. Chu, L. W. Martin, M. B. Holcomb, M. Gajek, S.-J. Han, Q. He, N. Balke, C.-H. Yang, D. Lee, W. Hu, Q. Zhan, P.-L. Yang, A. Fraile-Rodrı ´guez, A. Scholl, S. X. Wang, R. Ramesh, ―Electric-field control of local ferromagnetism using a magnetoelectric multiferroic" Nature Materials, Vol. 7, 2008, pp. 478-482.

[140] H. Bea, S. Fusil, K. Bouzehouane, M. Bibes, M. Sirena, G. Herranz, E. Jacquet, J.-P. Contour, A. Barthélémy, ―Ferroelectricity down to at least 2 nm in multiferroic BiFeO3 epitaxial thin films" Japanese Journal of Applied Physics, Vol. 45, 2006, pp. L187.

[141] M. Gajek, M. Bibes, S. Fusil, K. Bouzehouane, J. Fontcuberta, A. Barthélémy, A. Fert, ―Tunnel junctions with multiferroic barriers", Nature Materials, Vol. 6, 2007, pp. 296.

[142] M. Bibes, A. Barthélémy, ―Towards a magnetoelectric memory", Nature Materials, Vol. 7, 2008, pp. 425-426.

[143] Y. P. Wang, L. Zhou, M. F. Zhang, X. Y. Chen, J. M. Liu, and Z. G. Liu, ―Room-temperature saturated ferroelectric polarization in BiFeO3 ceramics synthesized by rapid liquid phase sintering" Applied Physics Letters, Vol. 84, 2004, pp. 1731-1733.

[144] M. I. Morozov, N. A. Lomanova, and V. V. Gusarov, ―Specific features of BiFeO 3 formation in a mixture of bismuth (III) and iron (III) oxides", Russian Journal of General Chemistry, Vol. 73, 2003, pp. 1676-1680.

[145] Z. Dai, Y. Akishige, ―Electrical properties of multiferroic BiFeO3 ceramics synthesized by spark plasma sintering" Physics D: Applied Physics , Vol. 43, 2010, pp. 445403

[146] C. Chung, J. Lin, J. Wu, ―Influence of Mn and Nb dopants on electric properties of chemical-solution-deposited BiFeO3 films", Applied Physics Letter, Vol. 88, 2006, pp. 242909-242909.

[147] P. Lawita, A. Watcharapasorn, S. Jiansirisomboon, ―Effect of Nd2O3 Dopant on Phase and Microstructure of Bismuth Ferrite Ceramics", Journal of the Microscopy Society of Thailand, Vol. 5 (1-2), 2012, pp. 71-74.

[148] Z. M. Tian, S. L. Yuan, X. L. Wang, X. F. Zheng, S. Y. Yin, C. H. Wang and L. Liu, Journal of Applied Physics, Vol. 106, 2009, pp. 103912: 1-4.

[149] M. Kumar and K. L. Yadav, ―Rapid liquid phase sintered Mn doped $BiFeO_3$ ceramics with enhanced polarization and weak magnetization", Applied Physics Letters, Vol. 91, 2007, pp. 242901-242901-3

[150] C. Chung, J. Lin, J. Wu, ―Influence of Mn and Nb dopants on electric properties of chemical-solution-deposited $BiFeO_3$ films", Applied Physics Letters, Vol. 88, 2006, pp. 242909.

[151] S. J. Kim, S. H. Han, H. G. Kim, A. Y. Kim, J. S. Kim, "Multiferroic Properties of Ti-doped $BiFeO_3$ Ceramics", Journal of the Korean Physical Society, Vol. 56, 2010, pp. 439-442.

[152] A.K. Jonscher, F. Meca and H. M. Millany, "Charge-carrier contributions to dielectric loss", Journal of Physics C: Solid State Physics, Vol. 12, 1979, pp. L293.

[153] G. Catalan, J. F. Scott, "Physics and Applications of Bismuth Ferrite", Advanced Materials, Vol. 21, 2009, pp. 2463–2485.

[154] R. Das, K. Mandal, "Magnetic, ferroelectric and magnetoelectric properties of Ba-doped BiFeO3", Journal of magnetism and magnetic materials, Vol. 324, 2012, pp. 1913-1918.

[155] T. Ishidate, S. Abe, "Elastic anomaly and phase transition of $BaTiO_3$", Physical Review Letters, Vol.78, 1997, pp. 12.

[156] A .K. M. A. Hossain, M. L. Rahman, "Enhancement of microstructure and initial permeability due to Cu substitution in $Ni_{0.50-x}Cu_xZn_{0.50}Fe_2O_4$ ferrites", Journal of Magnetism and Magnetic Materials, Vol. 323, 2011, pp. 1954–1962.

[157] A. K. M. A. Hossain, M. A. Rahman, S. F. U. Farhad, B. Vilquin, H. Tanaka, "Effect of Li substitution on the magnetic properties of $Li_xMg_{0.40}Ni_{0.60-2x}Fe_{2+x}O_4$ ferrites", Physica B, Vol. 406, 2011, pp. 1506–1512.

[158] A. K. M. A. Hossaina, M. M. A. Chowdhurya, B. Vilquinb, H. Tanakac, "Influence of Li substitution on structural and magnetic properties of $Li_xNi_{0.2}Mg_{0.8-2x}Fe_{2+x}O_4$", Materials Chemistry and Physics, Vol. 133, 2012, pp. 941– 945.

[159] J. L. Snoek, "Dispersion and absorption in magnetic ferrites at frequencies above one Mc/s", Physica, Volume 14, 1948, pp. 207-217.

[160] R. Mahbub, "The influence of dopants on $BaTiO_3$ ceramics dielectric properties", Undergraduate thesis, Bangladesh University of Engineering and Technology, 2012.

[161] A. Mousharraf, "Studying the effects of composition and sintering parameters on dielectric properties of tantalum oxide doped barium titanate", Master's thesis, Bangladesh University of Engineering and Technology, 2013.